

Infrared laser-absorption sensing for combustion gases



Christopher S. Goldenstein^{*[a](#)}, R.Mitchell Spearrin^b, Jay. B. Jeffries^c, Ronald K. Hanson^c

^a *Purdue University, West Lafayette, IN, USA*

^b *University of California Los Angeles, Los Angeles, CA, USA*

^c *Stanford University, Stanford, CA, USA*

ARTICLE INFO

Article History:

Received 25 July 2016

Accepted 15 December 2016

Available online xxx

Keywords:

Laser-absorption spectroscopy

Molecular spectroscopy

Combustion

Propulsion

ABSTRACT

Infrared laser-absorption spectroscopy (IR-LAS) sensors play an important role in diagnosing and characterizing a wide range of combustion systems. Of all the laser-diagnostic techniques, LAS is arguably the most versatile and quantitative, as it has been used extensively to provide quantitative, species-specific measurements of gas temperature, pressure, composition and velocity in both laboratory- and industrial-scale systems. Historically, most IR-LAS work has been conducted using tunable diode lasers; however, today's researchers have access to a wide range of light sources that provide unique sensing capabilities and convenient access to nearly the entire IR spectrum (≈ 0.8 to $16 \mu\text{m}$). In particular, the advent of room-temperature wavelength-tunable mid-infrared semiconductor lasers (e.g., interband- and quantum-cascade lasers) and hyperspectral light sources (e.g., MEMS VCSELs, Fourier-domain mode-locked lasers, dispersed supercontinuum, and frequency combs) has provided a number of unique capabilities that combustion researchers have exploited. The primary goals of this review paper are: (1) to document the recent development, application, and current capabilities of IR-LAS sensors for laboratory- and industrial-scale combustors and propulsion systems, (2) to elucidate the design and use of IR-LAS sensors for combustion gases through a discussion of the modern sensor-design process and state-of-the-art techniques, and (3) to highlight some of the remaining measurement opportunities, challenges, and needs. A thorough review and description of the fundamental spectroscopy governing the accuracy of such sensors, and recent findings and databases that enable improved modeling of molecular absorption spectra will also be provided.

© 2016 Elsevier Ltd. All rights reserved

Contents

1. Introduction	134
1.1. Role of IR-LAS in combustion.....	134
1.2. History of IR-LAS.....	135
1.3. Organization of paper.....	135
2. Fundamentals	136
3. Spectroscopic models and databases	137
3.1. Lineshape physics and models	137
3.1.1. Doppler broadening and the gaussian profile	137
3.1.2. Collisional broadening	138
3.1.3. Combined Doppler- and collisional-broadening and the Voigt profile	138
3.1.4. Dicke narrowing and the Rautian and Galatry profiles	138
3.1.5. Speed-dependent collisional broadening and the speed-dependent Voigt profile.....	139
3.1.6. Partially correlated quadratic-speed-dependent hard collision profile (pCqSDHC)	139
3.1.7. The impact approximation and the χ -Function	140
3.1.8. Line mixing	140
3.1.9. Results and discussion	140
3.2. Databases.....	141
3.2.1. Line-by-line data	141
3.2.2. Cross-section data.....	141
3.2.3. Uncatalogued data	142

* Corresponding author.

E-mail address: csgoldenstein@purdue.edu (C.S. Goldenstein).

4.	Techniques.....	142
4.1.	Scanned-wavelength direct-absorption spectroscopy	143
4.2.	Hyperspectral direct-absorption spectroscopy	143
4.3.	Wavelength-modulation spectroscopy.....	143
4.4.	Cavity-enhanced techniques	144
5.	Measurement challenges and solutions.....	145
5.1.	Solutions for nonuniform flows.....	145
5.1.1.	Single line-of-sight solutions	145
5.1.2.	Laser-absorption tomography	146
5.2.	Beam steering and emission.....	147
5.3.	Broad and blended spectra.....	147
5.4.	Breakdown of the impact approximation.....	148
5.5.	Non-zero WMS background	148
5.6.	1f-normalization with large absorbance	148
6.	Sources and hardware	148
6.1.	Near-infrared hardware	148
6.1.1.	Distributed-feedback (DFB) and distributed-Bragg reflector (DBR) tunable diode lasers.....	148
6.1.2.	Vertical cavity surface emitting lasers (VCSELs)	149
6.1.3.	Fourier-domain mode locked (FDML) lasers.....	149
6.1.4.	Dispersed supercontinuum sources	149
6.1.5.	Optical fibers	150
6.1.6.	Detectors.....	150
6.2.	Mid-infrared hardware	150
6.2.1.	Quantum cascade lasers (QCLs)	150
6.2.2.	Interband cascade lasers (ICLs).....	150
6.2.3.	Optical fibers	150
6.2.4.	Detectors.....	151
6.2.5.	Optical materials	151
6.3.	Emerging sources	152
6.3.1.	Chirped QCLs	152
6.3.2.	Frequency comb spectrometers	152
6.4.	Compact sensors	152
6.4.1.	Probe-based single-ended sensors.....	153
6.4.2.	Single-ended sensors using native surfaces.....	154
7.	Sensor-design process.....	154
7.1.	Identify measurement needs and challenges	154
7.2.	Selection of wavelength, hardware, and LAS technique	155
8.	Sensors for fundamental combustion chemistry studies	155
8.1.	Shock tubes	155
8.1.1.	Thermometry	155
8.1.2.	High-pressure studies and sensor development	156
8.1.3.	Fuel intermediates	156
8.1.4.	Cavity-enhanced studies.....	157
8.2.	Laboratory flames.....	157
9.	Sensors for power plants and gasifiers	157
9.1.	Large non-resonant transmission losses	158
9.2.	Collisional broadening in gases with unknown composition	158
10.	Sensors for gas turbines	159
10.1.	Lean-blowout control	159
10.2.	Gas-turbine combustors at elevated pressure	160
11.	Sensors for IC engines	160
11.1.	In-cylinder	160
11.2.	Engine intake and exhaust	161
12.	Sensors for scramjets	162
12.1.	Continuous-flow facilities.....	162
12.2.	Impulse facilities.....	163
12.3.	In-flight tests	164
13.	Sensors for detonation combustors.....	164
13.1.	Pulse-detonation combustors	165
13.2.	Rotating-detonation combustors	166
14.	Conclusions	168
14.1.	Key takeaways.....	168
14.1.1.	Techniques.....	168
14.1.2.	Mid-IR sensing	168
14.1.3.	Measurements of high-pressure gases	168
14.1.4.	Optical engineering	168
14.2.	Remaining needs and challenges	168

Nomenclature	
A	Integrated absorbance
ART	Algebraic-reconstruction tomography
ASE	Amplified spontaneous emission
c	Speed of light
CARS	Coherent anti-Stokes Raman scattering
CEAS	Cavity-enhanced absorption spectroscopy
CKD	Clough-Kneizys-Davies model
CRDS	Cavity ring-down spectroscopy
CST	Chemical-species tomography
DA	Direct absorption
DBR	Distributed-Bragg reflector
DCSCTF	Direct-connect supersonic combustion test facility
DDT	Deflagration-to-detonation transition
DFB	Distributed-feedback
DFG	Difference-frequency generation
DCS	Dual-comb spectroscopy
DSS	Dispersed supercontinuum source
E''	Lower-state energy
$E_{rupture}$	Modulus of rupture
EGR	Exhaust gas recirculation
f	Modulation frequency
f_r	Repetition rate
FDML	Fourier-domain mode-locked
FMS	Frequency-modulation spectroscopy
FTIR	Fourier-transform infrared spectroscopy
FWHM	Full-width at half-maximum
G	Gain of an optical cavity
\bar{g}	Mean relative speed of collision partners
GC	Gas chromatography
GP	Galaxy Profile
h	Planck's constant
HCCI	Homogeneous-charge compression ignition
HWHM	Half-width at half-maximum
I_o	Incident light intensity
I_t	Transmitted light intensity
ICAS	Intra-cavity absorption spectroscopy
ICOS	Integrated-cavity-output spectroscopy
ICL	Interband-cascade laser
IR-LAS	Infrared laser-absorption spectroscopy
k	Boltzmann constant
k_v	Spectral absorption coefficient
L	Path length through absorbing gas
LAT	Laser-absorption tomography
LBO	Lean blowout
LOS	Line-of-sight
M	Molecular weight
MEMS	Micro-electro-mechanical systems
MMF	Multi-mode fiber
MS	Mass spectrometry
n	Number density
n_γ	Collisional-broadening temperature exponent
$n_{refractive}$	Refractive index
N_i	Column density of absorbing species
P	Gas pressure
pCqSDHC	Partially correlated quadratic-speed-dependent hard-collision profile
PDE	Pulse-detonation engine
PIV	Particle-image velocimetry
PLIF	Planar laser-induced fluorescence
Q	Internal partition function
QCL	Quantum-cascade laser
qSDVP	Quadratic speed-dependent Voigt profile
R	Two-color ratio of integrated absorbance
R_M	Mirror reflectivity
RAM	Residual-amplitude modulation
RDE	Rotating-detonation engine
RP	Rautian profile
S	Transition linestrength
SMF	Single-mode fiber
SNR	Signal-to-noise ratio
SOA	Semiconductor optical amplifier
STP	Standard temperature and pressure
t_{coll}	Collision duration
T	Temperature
T_o	Reference temperature
T_{melt}	Melting temperature
\overline{T}_{n_i}	Species-weighted path-average temperature
TDL	Tunable diode laser
TDLAS	Tunable diode-laser absorption spectroscopy
TDLAT	Tunable diode-laser absorption tomography
TDM	Time-division multiplexed
U	Flow velocity
UVaSCF	Univ. of VA supersonic combustion facility
VCSEL	Vertical-cavity surface emitting laser
VP	Voigt profile
WMS	Wavelength-modulation spectroscopy
α	Absorbance
α_{CEAS}	Cavity-enhanced absorbance
α_{SP}	Single-pass absorbance
β	Frequency of velocity-changing collisions
γ_k	Collisional-broadening coefficient
$\gamma_{k,2}$	Speed-dependent collisional-broadening coefficient
Δf_r	Difference in repetition rate
Δv	Doppler shift
Δv_c	Collisional-broadening FWHM
$\Delta v_{c,2}$	Speed-dependent collisional-broadening FWHM
Δv_D	Doppler-broadening FWHM
Δv_{Diff}	Difference in Doppler shifted frequencies
θ	Angle of LOS relative to flow
λ_{low}	Cut-on wavelength
λ_{high}	Cut-off wavelength
v	Optical frequency
v_o	Linecenter frequency
σ_{Abs}	Absorption cross section
τ	Characteristic decay time
ϕ	Lineshape function
Φ	Equivalence ratio
X_{Abs}	Mole fraction of absorbing species

1. Introduction

1.1. Role of IR-LAS in combustion

Over the last 40+ years, a wide range of laser diagnostics have been developed and deployed for characterizing combustion via measurements of gas temperature, pressure, velocity, and composition. The development and application of these measurement methods has been highlighted in diagnostics colloquia during the past twenty biennial International Combustion Symposia (published in the Proceedings of the Combustion Institute), as well as in several excellent review articles and text books. For example, applications of laser diagnostics have been an important part of two Hottel papers at the International Combustion Symposium (1998 by Wolf-rum [1] and 2010 by Hanson [2]) as well as numerous other reviews such as those by Allen [3], Werle [4], Lackner [5], and Schulz et al. [6], and most recently, Bolshov et al. [7]. Several books have also been devoted to this subject. For example, Eckbreth [8] describes the

early history and the basic fundamental science of laser-diagnostic techniques, Kohse and Jeffries [9] provide a review of practical applications, and most recently, Hanson, Spearrin, and Goldenstein [10] provide a thorough description of the fundamental spectroscopy and physics needed by researchers and students to apply laser-based diagnostics to their work. This review will focus on documenting the status of infrared laser-absorption spectroscopy (IR-LAS) sensors, and the role they play in studying combustion science and characterizing combustion-based systems.

There are a wide variety of optical and non-optical diagnostics techniques that complement and compete with IR-LAS sensors used for combustion applications. The full arsenal of optical diagnostics (i.e., absorption, emission, laser-induced fluorescence, Raman, and laser-induced incandescence), as well as non-optical diagnostics (pressure transducers, thermocouples, gas chromatography and mass spectroscopy) are all quite useful for studying combustion. The primary advantage of IR-LAS is its ability to provide high-bandwidth, species-specific, *in situ* measurements of thermodynamic conditions (e.g., temperature, pressure) and a wide range of molecular species. Further, while the spatial resolution of IR-LAS is typically limited by its path-integrated nature, it is one of the most quantitative and broadly applicable laser-diagnostic techniques. Its comparatively simple signal interpretation enables quantitative measurements and it can be applied to virtually all temperatures and pressures. However, for many combustion applications, capturing the spatially-resolved structures in the flow field is needed, and planar laser-induced fluorescence (PLIF) and other pulsed imaging diagnostics are naturally preferred. Similarly, coherent anti-Stokes Raman scattering remains the preferred technique for providing point measurements of temperature and species.

From a practical standpoint, the costs of diode, quantum-cascade, and interband-cascade lasers that are now used routinely in IR-LAS are much less than that of the systems needed for laser-based imaging diagnostics. Similarly the acquisition and operational costs of laser detectors are much less than the cameras needed for imaging. The lasers used for IR-LAS are also smaller, more robust, and consume less power compared to current laser-based imaging systems. At the same time, the researcher developing sensors for combustion control and monitoring should not lose sight of the even lower operation and maintenance costs of thermocouples, pressure sensors, or optical emission detectors. A goal of this manuscript is to highlight the current state-of-the-art in applying IR-LAS to combustion systems in order to help the reader chose the most appropriate diagnostic suite for an application. First, we will review some of the early milestones that have shaped the development of IR-LAS.

1.2. History of IR-LAS

Soon after the laser was invented, Sulzmann [12] recognized the value of laser-absorption measurements of specific species in combustion gases, and the first applications using tunable diode lasers (TDLs) soon followed. In the late 1970s, TDLs and infrared detectors required cryogenic cooling and dispersive optics were required to select a single mode from the multi-mode laser output. To our knowledge, the first application of TDLs for spectrally resolved direct-absorption sensing in flames was reported by Hanson in 1977 [13]. These methods were quickly extended to shock-heated gases [14] and two-color thermometry in flame gases [15]. Not long after, frequency- and wavelength-modulation spectroscopy (FMS and WMS) were developed to increase the sensitivity of TDL absorption measurements [16–23].

Ironically, the first IR-LAS measurements were conducted in the mid-infrared (mid-IR), although the associated hardware limitations at the time severely complicated or precluded measurements outside of the laboratory. This began to change in the mid 1980s, when the telecommunication industry began producing large numbers of

AlGaAs and InGaAsP diode lasers that could be operated at room temperature. In 1988, Cassidy leveraged these advancements and used a fiber-coupled room-temperature TDL near 1.3 μm for trace-gas sensing via WMS [24]. In 1991, room temperature TDLs were first applied to gasdynamic applications via the development of the first diode-laser-based mass flux sensor based on spectrally resolved O₂ absorption [25], a technique which would be used in flight nearly 30 years later [26–28]. In 1993 Arroyo and Hanson [29] became the first to use telecommunication-grade TDLs near 1.4 μm for two-color thermometry and H₂O sensing in flames. Subsequent advancements leveraging telecommunication technology led to wavelength-multiplexed and fiber-coupled sensors for multi-parameter sensing [30,31], and the first TDLAS sensor for closed-loop combustor control [32]. Even though the TDL industry was in its infancy, there were many early applications to combusting flows and the reader is referred to several excellent reviews by Allen [3], Werle [4], and Wolfrum [1].

Research in the 2000s focused on improving the robustness of LAS sensors for field measurements via increased spectral information and use of improved WMS techniques, and these trends continue today. The enhanced wavelength tuning capabilities of VCSELs were exploited for the first high-pressure measurements of O₂ [33], as well as cesium spectra for temperature, pressure, and velocity measurements in detonation flows at high rates [34,35]. Soon after, Fourier-domain mode-locked (FDML) lasers were used to acquire even greater spectral information of H₂O near 1.4 μm for thermometry and H₂O sensing in a variety of combustion flows [36–38]. Around the same time, TDL-based sensors for combustion and propulsion applications shifted towards WMS owing to the development of improved, calibration-free WMS models [39–41] suitable for large modulation depths and the higher-order intensity modulation accompanying it, as well as 1/f-normalization. These methods were first applied to TDLAS sensors for temperature and H₂O sensing in an IC-engine [42] and a model-scramjet combustor [43].

Today researchers developing IR-LAS techniques and sensors have never had more design freedom. Nearly any wavelength in the IR can be accessed by single-mode, room-temperature lasers enabling sensitive monitoring of most molecular species of interest to combustion. Fig. 1 shows the intensity of various IR absorption transitions for a few combustion species at 300 and 1500 K. Unrestricted access to the IR spectrum has provided unprecedented opportunities for the development of LAS sensors that are tailored for unique conditions to optimize signal strength and temperature sensitivity, and minimize interfering absorption. These compact, solid-state laser sources include diode lasers (TDLs, visible to ≈3 μm), interband cascade lasers (ICLs, 3 to ≈6 μm), and quantum cascade lasers (QCLs, 4 to 20 μm), all of which provide sufficient power to be sensitively monitored by compact room temperature or thermoelectric-cooled detectors. In addition, a wide variety of hyperspectral sources continue to be developed, including MEMS VCSELs, FDML, dispersed supercontinuum, frequency combs, and external-cavity TDLs and QCLs. With these tools, there are few molecules that cannot be measured, which has taken us to an exciting time focused not only on the fundamental development of new LAS techniques, but on the transitioning of new LAS sensors into the field.

1.3. Organization of paper

The goals of this review are: (1) to thoroughly explain the underlying fundamentals of IR absorption spectroscopy and the most widely used IR-LAS techniques, (2) to document the recent development, application, and current capabilities of IR-LAS sensors for laboratory- and industrial-scale combustors and propulsion systems, (3) to elucidate the design and use of IR-LAS sensors for combustion gases through a discussion of the modern sensor-design process and

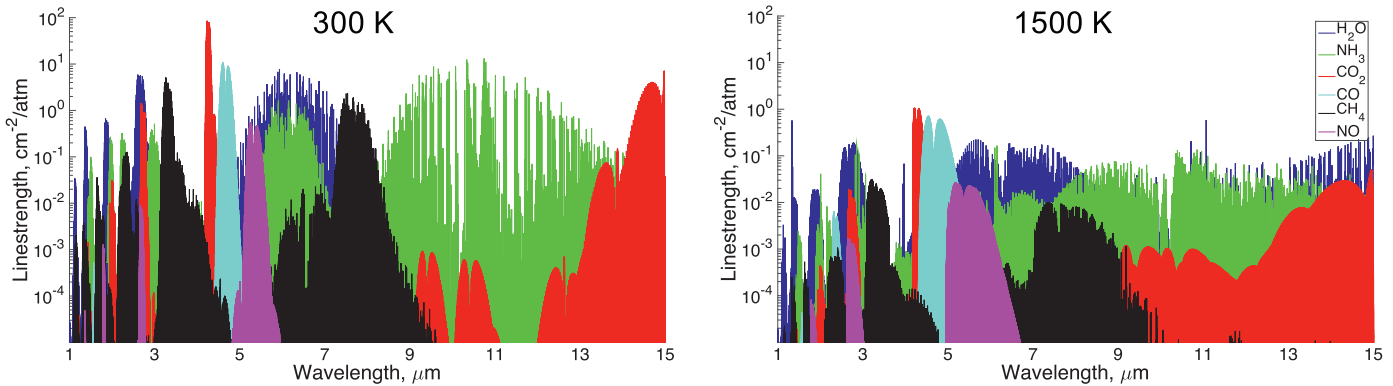


Fig. 1. Linestrengths (i.e., absorption strength) of several molecular species of interest to combustion systems. Calculations performed using the HITRAN2012 database [11] with some erroneous linestrengths removed.

state-of-the-art techniques, and (4) to highlight some of the remaining measurement opportunities, challenges, and needs facing researchers today. We begin this paper by reviewing the basic fundamentals of IR-LAS and follow with a comprehensive discussion of the various absorption-spectroscopy models and databases available to researchers today. Next, we discuss three of the most widely used IR-LAS techniques: direct absorption (DA), wavelength-modulation spectroscopy (WMS), and cavity-enhanced absorption spectroscopy (CEAS), where we consider fixed- and scanned-wavelength variants of these methods. We then discuss the optical hardware (i.e., lasers, fibers, IR materials etc.) available today, and the role they play in various IR-LAS techniques. Next, we provide a high-level discussion of the sensor-design process before we go on to review and highlight some of the most impressive examples of IR-LAS applied to studies of combustion science and combustion-based systems; sensors for: flames, shock tubes, power plants, gasifiers, gas turbines, internal combustion engines, scramjets, and detonation combustors will all be discussed. Our review is primarily limited to work done in the last 15 years (to avoid repeating the excellent, earlier reviews), with particular emphasis on the last 5 years. Further, our focus is on *in situ* IR-LAS sensing due to its non-intrusive nature and greater time resolution (compared to sampling-based methods). Lastly, we conclude with a brief discussion of key takeaways, and the remaining opportunities, challenges, and needs in IR-LAS research that are pertinent to combustion studies.

2. Fundamentals

The fundamentals of LAS are described to establish the conventions and units used throughout this manuscript and facilitate the discussion of more complex theory and diagnostic techniques that follow.

Atoms and molecules with a dipole moment can absorb and emit radiation. In the infrared, absorption and emission can occur when the photon energy is equal to (i.e., resonant with) to the spacing between two discrete *ro-vibrational* states and the amount of absorbed or emitted radiation is proportional to the number density in the absorbing or emitting states, respectively. This leads to discrete absorption or emission *transitions* within a given vibrational band (a group of transitions corresponding to a specific change in vibrational energy) and each individual transition within that band corresponds to a unique change in rotational energy. In reality, these discrete transitions are *broadened* by several mechanisms and a line-shape model is required to describe the distribution (in energy/wavelength/frequency space) over which a given transition absorbs or emits light. These concepts are illustrated in Fig. 2.

For a monochromatic light source, the light intensity transmitted through a uniform, absorbing gas is given by Beer's Law in the

following form:

$$I_t = I_0 \exp(-k_v L) \quad (1)$$

where I_0 and I_t are the incident and transmitted light intensities, k_v [cm^{-1}] is the spectral absorption coefficient per unit length at optical frequency v [cm^{-1}], and L [cm] is the path length through the absorbing gas. This formulation is valid for all cases where k_v is constant along the measurement path (e.g., uniform gas properties and negligible absorption-induced population transfer). In this case, the absorbance ($\alpha = k_v L$) can be related to gas properties using

$$\alpha(v) = \sum_j S_j(T) P \chi_{\text{Abs}} \phi_j(v, T, P, \chi) L \quad (2)$$

where $S(T)$ [$\text{cm}^{-2}\text{-atm}^{-1}$] is the linestrength as a function of temperature T [K], P [atm] is the gas pressure, ϕ [cm] is the lineshape function, and j denotes a specific absorption transition. In combustion gases, the lineshape function is usually modeled by the Voigt Profile (VP) owing to it accounting for both Doppler and collisional broadening. However, in certain cases (discussed in Section 3) the VP can lead to substantial errors, thereby motivating the use of more advanced lineshape models.

Typically ϕ is defined according to Eq. (3) such that the integrated absorbance, A , is given by Eq. (4). When individual transitions can be resolved, the integrated absorbance can be measured and used to calculate gas properties, thereby avoiding the need for *a priori* knowledge of line broadening.

$$\int_{-\infty}^{+\infty} \phi d\nu = 1 \quad (3)$$

$$A_j = S_j(T) P \chi_{\text{Abs}} L \quad (4)$$

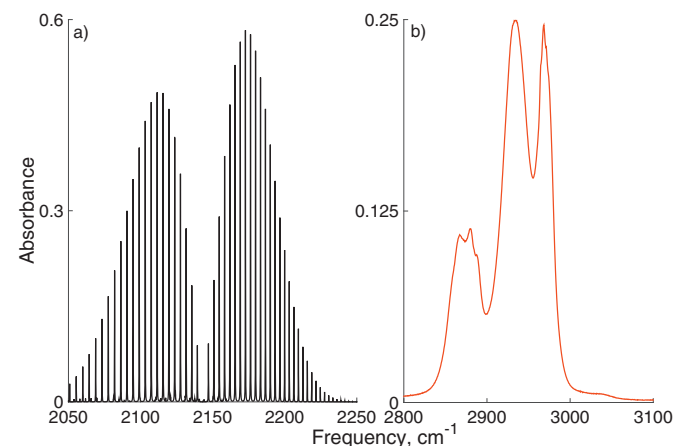


Fig. 2. Simulated absorbance spectra of CO near $4.7 \mu\text{m}$ [11] (a) and heptane near $3.4 \mu\text{m}$ [44] (b) at 1 atm, 298 K , 1% absorber by mole in air, across a 1 cm path.

For a gas in thermal equilibrium, the transition linestrength, $S(T)$, is given by:

$$S(T) = S(T_0) \frac{Q(T_0) T_0}{Q(T) T} \exp\left[-\frac{\hbar c E''}{k}\left(\frac{1}{T} - \frac{1}{T_0}\right)\right] \\ \left[1 - \exp\left(-\frac{\hbar c v_o}{k T}\right)\right] \left[1 - \exp\left(-\frac{\hbar c v_o}{k T_0}\right)\right]^{-1} \quad (5)$$

where T_0 is the reference temperature (296 K), Q is the internal partition function of the absorbing species, \hbar [J-s] is Planck's constant, k [J-K⁻¹] is the Boltzmann constant, c [cm s⁻¹] is the speed of light, E'' [cm⁻¹] is the lower-state energy of the transition, and v_o [cm⁻¹] is the transition linecenter frequency.

The measured integrated absorbance of a transition can be used to calculate the mole fraction of the absorbing species (with temperature, pressure, and path length known) and the gas temperature can be calculated directly from a measured two-color ratio of integrated areas using Eq. (6) [10].

$$T = \frac{\frac{\hbar c}{k} (E''_2 - E''_1)}{\ln R + \ln \frac{S_2(T_0)}{S_1(T_0)} + \frac{\hbar c}{k} \frac{E''_2 - E''_1}{T_0}} \quad (6)$$

Here R is the two-color ratio of integrated areas for transitions 1 and 2. Note that Eq. (6) depends only on R and spectroscopic parameters and is independent of pressure, mole fraction, and path length.

In addition, the velocity of a gaseous flow along a line-of-sight can be determined by measuring the Doppler-shifted absorption. For a single line-of-sight angled relative to the flow direction, the velocity of the gas, U , can be calculated using Eq. (7):

$$U = \frac{\Delta v}{v_o} \frac{c}{\cos(\theta)} \quad (7)$$

where θ is the angle of the line-of-sight relative to the flow direction and Δv is the measured Doppler-shift of the transition. In practice, this is typically done using two laser beams, e.g., angled at 45° and 135° relative to the flow (i.e., one directed upstream and one downstream), to enable use of the differential Doppler-shift (Δv_{Diff}). In this case, the flow velocity can be calculated using Eq. (8).

$$U = \frac{\Delta v_{Diff}}{v_o} \frac{c}{2 \sin(45^\circ)} \quad (8)$$

For molecules with unresolved rotational spectra (e.g., large hydrocarbons such as heptane) it is more convenient to use Eq. (9) to relate the absorbance to gas properties.

$$\alpha(v) = n \chi_{Abs} \sigma_{Abs}(v, T, P, \chi) L \quad (9)$$

Here n [molecules-cm⁻³] is the number density of the gas and σ [cm²-molecule⁻¹] is the absorption cross section of the absorbing species. The key difference between Eq. (2) and (9) is that Eq. (2) calculates the spectral absorbance by modeling the contribution of each individual absorption transition whereas Eq. (9) avoids this complexity via use of an absorption cross section which quantifies how much light a molecule absorbs at a given wavelength and thermodynamic conditions. While the latter approach is less complex, it relies on a lookup table (typically obtained from experiments) that cannot be extrapolated beyond the thermodynamic conditions for which the cross sections were obtained. In comparison, the former approach can be used to calculate the absorbance at an arbitrary thermodynamic condition as long as the fundamental spectroscopic parameters for the active transitions (e.g., linestrength, collisional-broadening coefficients) are available. Fig. 2 shows simulated absorbance spectra of the fundamental vibration band of CO (a) and the C-H stretch of heptane (b). The discrete absorbance spectrum of CO's fundamental vibration band was calculated using Eq. (2) and line-by-line parameters [11]. The absorbance spectrum of heptane's C-H stretch absorption band was calculated using Eq. (9) and the absorption cross section measured by Klingbeil et al. [44].

3. Spectroscopic models and databases

Accurate IR-LAS measurements of gas properties (temperature, pressure, composition, velocity) require an accurate spectroscopic model to convert the measured spectrum to the gas properties of interest. The absorption spectra of combustion gases are frequently challenging to model given that multi-component gases at high-temperatures and -pressures are frequently of interest. Elevated temperatures and pressures complicate the spectrum via the activation of high- E'' transitions and increased collision broadening, respectively, and multi-component gases complicate the calculation of lineshapes via species-specific collision broadening. Further, the large range of thermodynamic conditions, and the often extreme temperatures and pressures of interest, often preclude the use of empirically derived absorption cross-section data. As a result, line-by-line simulations are often the most suitable method for modeling absorption spectra.

Line-by-line simulations of absorption spectra require (1) a spectroscopic model and (2) spectroscopic parameters that describe how the line positions, strengths, and shapes depend on gas properties. Since the determination of linestrengths is relatively straightforward and most LAS techniques do not require precise knowledge of absolute line positions, this section will focus on discussing lineshape-physics and -models that are most appropriate for combustion gases due to their greater complexity. Our discussion will focus on models that are applicable to cases where the assumption of isolated lines (i.e., no line mixing) and the impact approximation are valid; however, both of these complexities will be discussed. This section will then conclude with a discussion on the status and availability of various spectroscopic databases with particular attention to those that are most relevant to gases at elevated temperatures and pressures.

3.1. Lineshape physics and models

In the vast majority of combustion applications, researchers have used the Voigt profile to model absorption lineshapes owing to its relative simplicity and, typically, high accuracy, yielding residuals within 2% of measured lineshapes at number densities near STP (standard temperature and pressure). However, many researchers have shown that the Voigt profile can lead to gull-wing shaped residuals (between measured and model spectra, shown later in Fig. 4a) on the order of 1–10% of the peak absorbance at low to moderate number densities (i.e., when collisional narrowing or speed-dependent broadening can be significant). Furthermore, it is also well known that the Voigt and Lorentzian profiles breakdown at high number densities due to line mixing and a breakdown of the impact approximation.

This section will discuss the underlying collision physics responsible for these complexities, the lineshape models that address them, and will point the reader to the relevant literature. Particular attention will be paid to H₂O and CO₂, however, more generally these molecules can be thought of as ambassadors for other molecules with large or small rotational-energy-level spacing, respectively. Table 1 introduces a few of these processes and points out the somewhat fortuitous nature of how molecules with large rotational-energy level spacing are prone to only Dicke narrowing and speed-dependent broadening complications, whereas molecules with small rotational-energy-level spacing are prone to only line mixing and the breakdown of the impact approximation. Table 2 illustrates the parameters needed by each lineshape model discussed in this section.

3.1.1. Doppler broadening and the gaussian profile

Doppler broadening occurs when molecules in the absorbing state have a velocity component in the same (or opposite) direction of the photon propagation. The absorbing molecules then see a

Table 1

Importance of various collisional-processes and -approximations influencing IR spectra of H₂O and CO₂.

Process	H ₂ O	CO ₂
Dicke narrowing	High	Low
Speed-dependent broadening	High	Low
Impact approximation	Low	High
Line mixing	Low	High

Table 2

Collisional-broadening and -narrowing parameters required for different lineshape models.

Lineshape	ν_D	β	ν_c	$\nu_{c,2}$
Gaussian	X			
Lorentzian			X	
Voigt	X		X	
Galatry	X	X	X	
Rautian	X	X	X	
qSD-Voigt	X		X	X

Doppler-shifted frequency will absorb radiation when the Doppler-shifted frequency is resonant with the absorption transition. Since the absorbers are distributed across a range of velocities (i.e., they may belong to different velocity classes), Doppler broadening is said to be *heterogeneous*. In the absence of other broadening mechanisms, the absorption lineshape of gases following a Maxwellian velocity-distribution function (VDF) is given by the Gaussian profile, ϕ_D :

$$\phi_D(\nu) = \frac{2}{\Delta\nu_D} \left(\frac{\ln 2}{\pi} \right)^{1/2} \exp \left[-4\ln 2 \left(\frac{\nu - \nu_0}{\Delta\nu_D} \right)^2 \right] \quad (10)$$

where the Doppler full-width at half-maximum (FWHM), $\Delta\nu_D$, is given by Eq. (11).

$$\Delta\nu_D = 7.1623 \times 10^{-7} \nu_0 \sqrt{T/M} \quad (11)$$

Here, M is the molecular weight of the absorbing species in g/mol and T is in K. Eq. (11) indicates that the Doppler FWHM scales linearly with the transition linecenter frequency and with $\sqrt{T/M}$ indicating that Doppler broadening is largest for high-frequency transitions, light-weight absorbers, and high temperatures.

3.1.2. Collisional broadening

Collisional broadening of a rovibrational absorption transition occurs when: (1) inelastic collisions reduce a molecule's lifetime in the absorbing state, (2) elastic dephasing collisions perturb the molecular rotation and/or vibration, or (3) elastic angular-momentum altering collisions re-orient the angular momentum vector of the dipole [45]. Collisional broadening is typically modeled as *homogeneous*, meaning the broadening process is independent of the absorber's speed. In this case, collisional broadening is accurately described by a Lorentzian profile, ϕ_L , and an ensemble-averaged collisional FWHM, $\Delta\nu_c$, given by Eq. (12) and (13), respectively.

$$\phi_L(\nu) = \frac{1}{2\pi} \frac{\Delta\nu_c}{(\nu - \nu_0)^2 + \left(\frac{\Delta\nu_c}{2} \right)^2} \quad (12)$$

$$\Delta\nu_c = 2P \sum_k \chi_k \gamma_k(T) \quad (13)$$

Here γ_k is the temperature-dependent ensemble-averaged collisional-broadening coefficient of perturbing-species k .

The temperature-dependence of γ_k is usually modeled via a power-law, Eq. (14).

$$\gamma_k(T) = \gamma_k(T_0)(T_0/T)^{n_\gamma} \quad (14)$$

Here n_γ is the collisional-broadening temperature exponent. It should be noted that the accuracy of Eq. (14) can break down over a large temperature range, particularly when the parameters are used beyond the temperature domain for which they were obtained. In our experience, usually a single value of n_γ is sufficient for temperatures from 300 to 1200 K, however, for greater accuracy we recommend using multiple values of n_γ , one for temperatures from 300 to 900 K and another for temperatures greater than 900 K, however, these are not steadfast rules.

3.1.3. Combined Doppler- and collisional-broadening and the Voigt profile

The Voigt profile (VP) is given by a convolution of the Gaussian and Lorentzian profiles and, therefore, accounts for both Doppler and collisional broadening. To date, the Voigt profile remains the lineshape of choice for most spectroscopic databases (e.g., HITRAN [11] and HITEMP [47]) owing to its wide applicability and balance between simplicity and accuracy. In practice, the Voigt profile is typically calculated using numerical approximations due to the computational cost of evaluating it directly. For example, algorithms developed by Humlicek [48] (later enhanced by Kuntz [49] and corrected by Ruyten [50]) and that of McClean et al. [51] are some of the most widely used approximations. The Voigt profile reduces to the Gaussian and Lorentzian profiles when $\Delta\nu_D$ or $\Delta\nu_c$ equal 0, respectively. However, numerical approximations can breakdown in these limits, therefore the user should be cautious.

To illustrate the lineshape profiles discussed thus far, Fig. 3 shows Gaussian, Lorentzian, and Voigt Profiles with $\Delta\nu_D = \Delta\nu_c = 0.04 \text{ cm}^{-1}$ (i.e., representative values of near-IR H₂O transitions dilute in air at 1 atm and 1000 K). Despite having equal FWHM, the Gaussian profile exhibits a considerably larger peak absorbance compared to the Lorentzian profile, thereby highlighting the non-equal nature of these broadening mechanisms. Furthermore, the FWHM of the Voigt profile is 0.066 cm^{-1} (i.e., representative of the convolution of Gaussian and Lorentzian distributions and, thus, is not equal to the sum of Doppler and collisional FWHM).

3.1.4. Dicke narrowing and the Rautian and Galatry profiles

At number densities near STP, Dicke narrowing may lead to a narrowed lineshape, typically observed as gull-wing residuals between a measured spectrum and its best-fit Voigt lineshape (see Fig. 4a). Dicke narrowing [52] refers to a collision-induced reduction of the Doppler width (compared to that predicted by Eq. (11)) that occurs when collisions confine the translational motion of the absorbers. It is most noticeable for high- J transitions of molecules with large

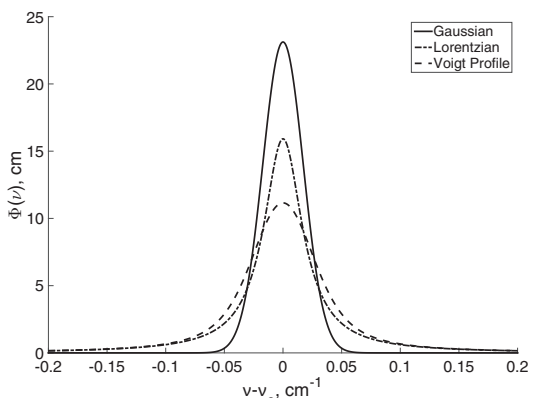


Fig. 3. Simulated Gaussian, Lorentzian, and Voigt profiles with $\Delta\nu_D = \Delta\nu_c = 0.04 \text{ cm}^{-1}$.

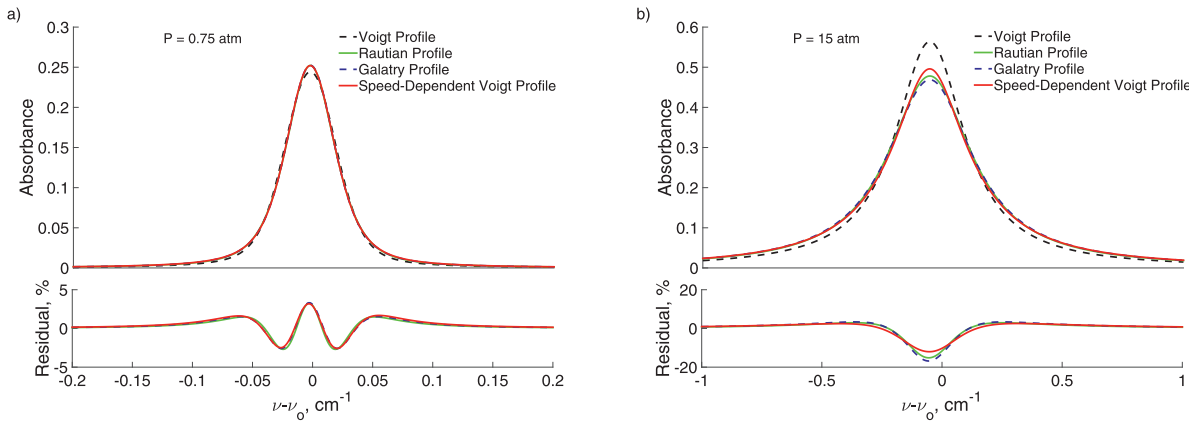


Fig. 4. Best-fit lineshapes for H_2O transition near 7471.6 cm^{-1} ($J''=16$) in N_2 at 1100 K , 0.75 atm (a) and simulated lineshapes (using best-fit parameters) at 1100 K and 15 atm (b). Lineshape parameters were taken from [46]. The residual is between the Voigt profile and all other lineshapes (quoted as percent of peak absorbance).

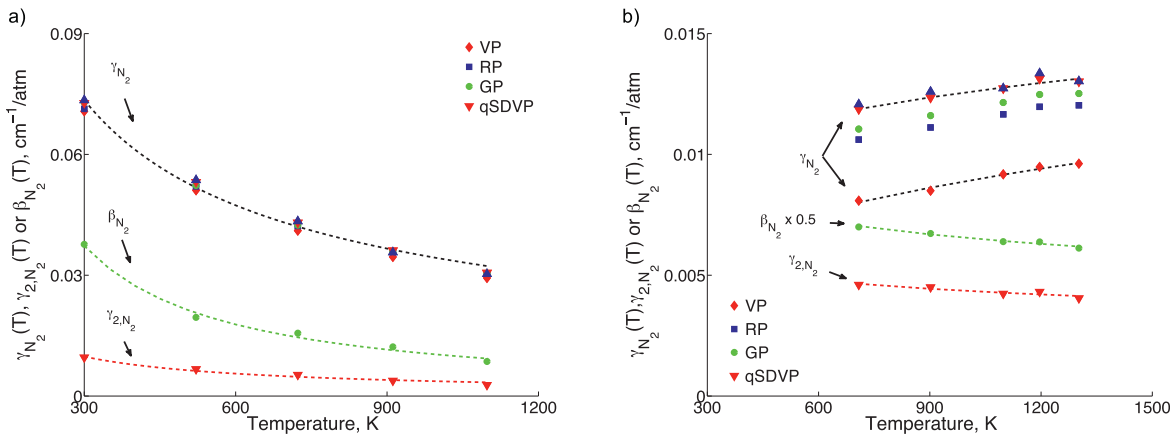


Fig. 5. Best-fit lineshape parameters as a function of temperature for an H_2O transition near 7413.02 cm^{-1} with $J''=8$ (a) and near 7471.6 cm^{-1} with $J''=16$ (b). The results highlight the importance of using more advanced lineshape models for high- J / H_2O transitions influenced by line-narrowing processes. Figures adapted from [46].

rotational-energy-level spacing (e.g., H_2O , HCl , HF), since collisional-broadening of such transitions is relatively weak. Further, it is usually more pronounced at number densities where the mean free path is comparable to the wavelength divided by 2π , and when the mass of the collision partner is much greater than that of the absorber.

The Rautian [53] (RP) and Galatry [54] (GP) profiles address Dicke narrowing using hard- and soft-collision models, respectively, via a parameter, z , that is related to the frequency of velocity-changing collisions, β , according to:

$$z = P \sum_k \chi_k \beta_k(T) / \Delta\nu'_D \quad (15)$$

Here, $\Delta\nu'_D = \Delta\nu_D / 2\sqrt{\ln 2}$ is the $1/e$ Doppler HWHM. While β is lineshape specific, due to the use of different collision models, it has been shown that the Rautian Profile is nearly identical to the Galatry Profile when $\beta_{\text{Rautian}} = 3/4\beta_{\text{Galatry}}$ (see [55] and Fig. 4a). Similar to the collisional-broadening coefficient, the temperature dependence of β_k is typically modeled using the power law. When $\beta=0$, the Rautian and Galatry profiles both reduce to the Voigt profile.

3.1.5. Speed-dependent collisional broadening and the speed-dependent Voigt profile

Like Dicke narrowing, speed-dependent collisional broadening tends to narrow the absorption lineshape leading to gull-wing shaped residuals (when compared to the Voigt profile, see Fig. 4a)

and is also most noticeable for high- J transitions of molecules with large rotational-energy-level spacing at number densities near STP. Speed-dependent collisional broadening (i.e., heterogeneous or non-Lorentzian collisional broadening) refers to cases where the efficiency of collisional broadening depends on the absorber's speed. Rigorously speaking, this is likely always the case since the absorber's speed alters the amount of kinetic energy available for promoting rotationally inelastic collisions and altering the trajectory of collisions; however, ignoring this complexity is surprisingly accurate in the majority of cases relevant to combustion.

Several lineshape models have been developed to address speed-dependent broadening (see [55] and the references therein), among the most popular is the quadratic-speed-dependent Voigt profile (qSDVP) [56–58] which addresses speed-dependent collisional broadening via a speed-dependent collisional-broadening coefficient, $\gamma_{k,2}$, and corresponding collisional FWHM, $\Delta\nu_{c,2}$. In the event that $\Delta\nu_{c,2} = \gamma_{k,2} = 0$ (i.e., the speed dependence of broadening is negligible), the speed-dependent Voigt profile reduces to the standard Voigt profile. Currently, very little temperature-dependent experimental data exists for, $\gamma_{k,2}$, however the power-law model has been suggested [55] and demonstrated [46] (see Fig. 5) as a suitable model for the temperature-dependence of $\gamma_{k,2}$, albeit over only a moderate temperature range.

3.1.6. Partially correlated quadratic-speed-dependent hard collision profile (pCQSDHC)

To provide the utmost accuracy in modeling the lineshapes of isolated transitions, the IUPAC has recommended that the pCQSDHC

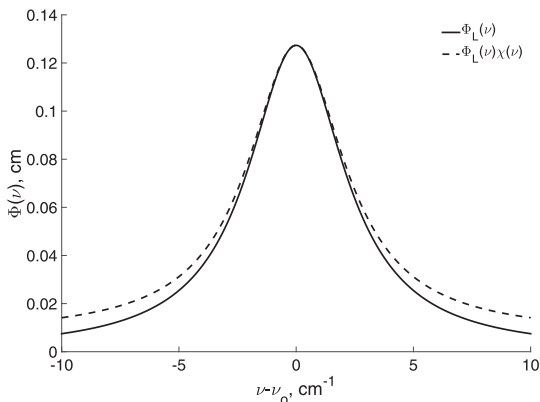


Fig. 6. Simulated Lorentzian profile and that corrected with χ -Function for an absorption transition with $\gamma = 0.05 \text{ cm}^{-1}/\text{atm}$ at 50 atm.

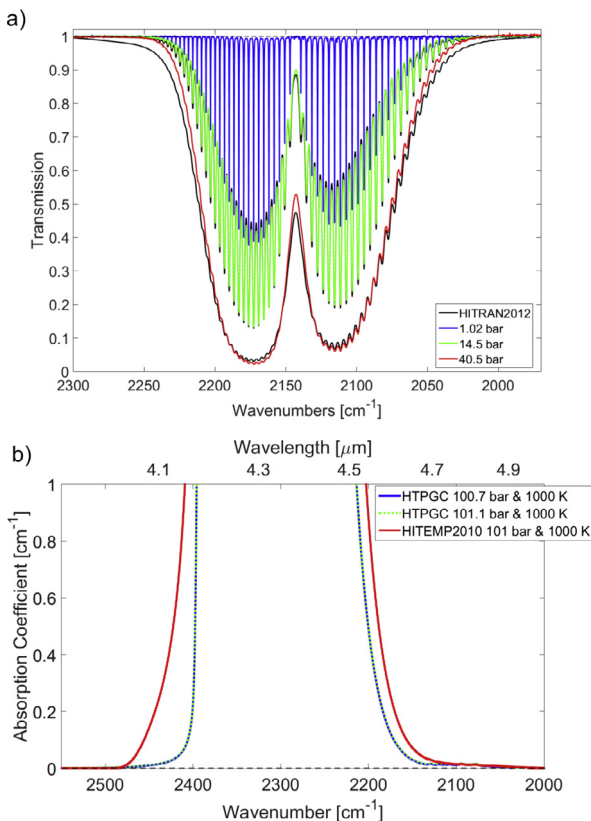


Fig. 7. FTIR measurements of fundamental vibration bands of 1% CO in N₂ (a) and 5% CO₂ in N₂ (b) compared with simulated spectra calculated using HITRAN 2012 [11] and the Voigt Profile. HTPGC refers to experimental measurements acquired in the high temperature and pressure gas cell. Figures adapted from [67].

profile be used in future databases [59]. This lineshape model [55] accounts for Doppler broadening, speed-dependent collision broadening (via a quadratic speed-dependence model) and pressure shifting, Dicke narrowing (via a hard collision model), and recognizes that velocity- and state-changing collisions are correlated. As such, 7 parameters are required to simulate the pCqSDHC; however, it reduces to simpler lineshape models (e.g., speed-dependent Voigt, Voigt, Lorentzian etc.) when specific parameters are set to zero. While this model has been shown to provide extreme accuracy (lineshape residuals near 0.01% of the peak absorbance [60]), the large number of free parameters and, correlation between several of them, currently mandates the use of multi-spectrum fitting (over a range of pressures) to high-fidelity data (SNR >> 1000) in order to obtain reliable lineshape parameters. That said, most absorption data acquired in

even remotely hostile combustion applications are not suitable for use with the pCqSDHC; however, the pCqSDHC will enable the development of improved databases and models (e.g., through controlled laboratory measurements) that will improve our ability to model absorption spectra in combustion gases at pressures of interest.

3.1.7. The impact approximation and the χ -Function

At high number densities, the impact approximation can breakdown leading to elevated absorption in the transition wings (compared to that predicted by Lorentzian-based lineshape models, see Fig. 6). The impact approximation assumes that collisions are instantaneous. Hartmann et al. [61] suggests that the impact approximation is valid when $2\pi c|\nu - \nu_0|t_{coll} \ll 1$ where the collision duration $t_{coll} = 1/\bar{g}\sqrt{\frac{\Delta\nu_c}{n}}c\bar{g}$ where \bar{g} is the mean relative speed of collision partners. This corresponds to number densities $<\approx 5$ amagat, depending on species [61].

Several researchers have developed and investigated methods for addressing the breakdown of the impact approximation. The most widely used is the CKD model developed by Clough et al. [62] which uses an empirical frequency-dependent correction factor, known as the χ -Function, to correct the Lorentzian (or Voigt) lineshape according to $\phi(\nu) = \phi_L(\nu)\chi(\nu)$ where $\chi = 1 - (1 - \chi')\frac{(\nu \pm \nu_0)^2}{25^2}$ for $|\nu \pm \nu_0| \leq 25 \text{ cm}^{-1}$ and $\chi = \chi'$ for $|\nu \pm \nu_0| \geq 25 \text{ cm}^{-1}$ with $\chi' = C \exp(-z^2)$ and $C = 6.65$ and $z = |\nu \pm \nu_0|/75$. However, several researchers have suggested C is temperature dependent [61], and Rieker et al. [63] showed that $C = 2.5$ was more accurate for H₂O spectra near 7204 cm⁻¹ at 700 K. It should be noted that the CKD model is not normalized to an area of 1 and, therefore, Eq. (3) is not applicable.

3.1.8. Line mixing

At high number densities, line mixing may also need to be accounted for to accurately model infrared absorption spectra. *Line mixing* (i.e., collisional coupling or collisional interference and not to be confused with *line blending* or *overlapping*) occurs when inelastic collisions transfer molecules between the two upper states and two lower-states of two absorption transitions. This process transfers absorption intensity (i.e., population) from the far wings of each transition into the region between transitions. In other words, collisions transfer absorbers from weakly absorbing regions to strongly absorbing regions leading to a narrowing of spectral structure [64] (see Fig. 7). The absorption spectrum can no longer be described as the sum of that of individual transitions using Eq. (2), and models that account for this process are needed. Unlike Dicke narrowing and speed-dependent broadening, line mixing is most pronounced when the spacing between rotational-energy-levels is small such that molecules can easily be shuffled between levels. As a result, line mixing is much more problematic for CO₂ and CO compared to H₂O. For example, Farooq et al. [65] showed significant line mixing effects at only 10 amagat for CO₂ transitions near 2.7 μm, while Nagali [66] suggests that line mixing for H₂O is not significant below 50 amagat using relations put forth by Hartmann et al. [61].

3.1.9. Results and discussion

Numerous researchers [46,58,68–76] have shown that using lineshape models that account for Dicke narrowing and/or speed-dependent collisional broadening at number densities comparable to STP can reduce mildly inaccurate lineshape residuals (i.e., 1–5% error) of the Voigt profile by ≈ 1 order of magnitude, typically leading to residuals below 0.1% of the peak absorbance. While these modest gains in accuracy may seem insignificant from the standpoint of practical sensing in combustion, using such lineshape models (when appropriate) to develop an empirically derived collisional-broadening database can translate into large gains in accuracy at higher pressures. For example, the recent study by Goldenstein et al.

[76] showed that simulations performed using N₂-broadening coefficients derived from least-squares fitting the Voigt profile to H₂O spectra at low pressures (i.e., 0.1 to 1 atm) overpredicted the peak absorbance of several high-*J* H₂O lines in N₂ by $\approx 30\%$ at 15 atm and 1500 K. In comparison, simulations performed using N₂-broadening coefficients derived from Galatry-profile fits to low-pressure spectra matched the measured spectra at 15 atm within 5% of the peak absorbance. This being said, it is particularly important to use more sophisticated lineshape profiles when the best-fit parameters will be used to simulate spectra at temperatures and pressures outside the domain from which they were obtained.

Fig. 4a shows simulated lineshapes of the H₂O transition near 7471.6 cm⁻¹ using empirically derived lineshape parameters for Voigt, Rautian, Galatry, and speed-dependent Voigt profiles. The more advanced lineshape profiles exhibit a strikingly similar shape which leads to controversy regarding the underlying physics that is primarily responsible for the gull-wing residuals of the Voigt profile (Dicke narrowing or speed-dependent broadening). However, a growing body of literature (see [46] and the references therein) showing transition-specific Dicke narrowing parameters suggests that speed-dependent broadening may be the primary mechanism, since Dicke narrowing is a species-specific process and should not be transition-specific [75]. The recent study by Goldenstein and Hanson [46] shows that the speed-dependent Voigt profile yields similar improvements at high temperatures, however, with best-fit lineshape parameters that exhibit a much more physical behavior than those of the Rautian and Galatry profiles, further supporting this theory that the speed-dependent Voigt profile is a more physical model. Regardless, further studies over a broad range of temperatures and pressures are needed to confirm this theory, and if possible, lineshape models that account for both Dicke narrowing and speed-dependent broadening (e.g., the pCqSDHC [55,59]) need to be studied.

Several researchers have studied the influence of the impact approximation and line mixing on IR-absorption spectra of H₂O [61,63,66,77] and CO₂ [65,67,78–80], and some studies have been conducted at high temperatures [61,63,66,67,77,78,80]. Regarding H₂O, Nagali and Hanson [77] acquired TDLAS measurements of H₂O absorption spectra near 7117 cm⁻¹ in an N₂ bath at number densities up to 18 amagat. The authors found that simulations performed with the Voigt profile and additive approximation agreed with measured spectra (within an uncertainty of $\approx 5\%$) in a 2 cm⁻¹ region around the transition linecenter. Later these authors investigated the transition near 7185 cm⁻¹ at similar conditions, and found that if the χ -Function was used to model the wings of a strong neighboring transition, simulations performed with the Voigt profile agreed with measurements. As a result, the authors concluded that line mixing was not significant (for the H₂O transitions studied) at up to 18 amagat. Furthermore, Nagali [66] later estimated that line mixing is not significant for H₂O below 50 amagat using the relations put forth by Hartmann [61] who states that the spacing between strongly coupled H₂O transitions in the P and R-branch is typically 10 cm⁻¹. However, experimental results for a wide range of transitions remain needed to validate this prediction.

In comparison to H₂O, line mixing is much more significant for CO₂. Farooq et al. [65] acquired FTIR measurements of the $\nu_1 + \nu_3$ CO₂ band near 2.7 μm at room temperature and up to 30 bar, and showed that a spectroscopic model developed by Niro et al. [81] (which accounts for line mixing) significantly improved the accuracy of the modeled spectra in the band center and wings compared to that calculated using the Lorentzian and χ -Function. More recently, Christiansen et al. [67] acquired FTIR measurements of CO₂ absorption near 2, 2.7 and 4.2 μm at high-temperatures and -pressures (see **Fig. 7**). Measured spectra of the ν_3 fundamental band at 100 bar and 1000 K are reported,

and simulations with the Voigt profile and HITRAN2012 database [11] were shown to significantly overpredict the absorption in the band wings, perhaps due to line-mixing effects. In addition, Christiansen et al. [67] show similar results for the CO fundamental vibration band at 40.5 bar and 296 K. Several authors have developed empirical corrections to improve the modeling of high-pressure CO₂ absorption spectra beyond that of the Voigt profile [78,82–85]. However, significant experimental research remains needed to evaluate the accuracy of these models.

3.2. Databases

3.2.1. Line-by-line data

For relatively small combustion species, with approximately 8 atoms or less, spectroscopic parameters in the infrared are mostly catalogued on a line-by-line basis by a few well-established databases, namely HITRAN/HITEMP [11,47], GEISA [87], and CDSD [88], with the latter database for carbon dioxide only. These databases are updated every few years and combine data collected from numerous laboratories with theoretical models to compile parameters for collisional broadening, intensity/linestrength, and pressure shift used, amongst other purposes, for predictive modeling of absorption spectra as described in the previous section. Pressure broadening and shift parameters are generally limited to collisions with nitrogen, air, or the absorbing species (i.e., self). The line-by-line databases cover most products and intermediates of combustion due to their small size, but the number of lines within the databases for each species varies considerably (e.g. $\approx 170,000$ lines for CO₂, $\approx 12,000$ lines for C₂H₂ in HITRAN) based on the relative number of active vibrational modes, the linestrength cutoff implemented in models, and the degree of investigation.

It should be noted that most spectroscopic databases have been constructed with low-temperature data and applications (e.g., atmospheric sensing) in mind, and combustion scientists must be cautious when utilizing these basic data for high-temperature simulations. Limitations of spectral modeling at combustion temperatures using data acquired at lower temperatures is largely due to insufficiency of the power law for modeling the temperature-dependence of collisional-broadening and pressure-shift as mentioned in **Section 3.1.2**. The Carbon Dioxide Spectroscopic Databank (CDSD) and HITEMP are notable exceptions, with line lists for five key combustion species (H₂O, CO₂, CO, NO, OH) created to more accurately represent high-temperature spectra at 1000 K or above. While managed independently, the current version of HITEMP (2010) incorporates parameters of CDSD-1000 [88]. More recently, the CDSD, managed by Tashkun et al., released CDSD-4000 [89], a line list developed for the temperature range of 2500 to 5000 K. Another high-temperature, species-specific line list is the BT2 water database developed by Barber et al. [90], which was used to inform HITEMP2010.

3.2.2. Cross-section data

For larger combustion species, such as fuels and larger fuel intermediates ($\approx \text{C}_3$ or higher), the high number of vibrational modes and corresponding infrared-active bands yield more daunting spectra to model on a line-by-line basis. This is exacerbated by the increased difficulty to experimentally investigate individual rovibrational transitions due to the more crowded and blended spectra, even at very low pressures. As such, spectroscopic data for these larger molecules are more commonly documented in a cross-section format at a given condition (temperature, pressure, composition). The absorption cross-section is most often resolved as a function of wavelength using a Fourier-Transform Infrared (FTIR) spectrometer. Two of the most comprehensive efforts to collect and aggregate infrared cross-section

data have been led by the Pacific Northwest National Lab (PNNL) [91] and the National Institute of Standard and Technology (NIST) [92] with each database containing hundreds of species and thousands of spectra. The majority of these spectra are collected at or very near room temperature, with the PNNL database offering spectra up to 50° C, and use nitrogen as the balance gas for various concentrations of the absorber. Due to the limited temperature range of the cross-section data in PNNL and NIST, the spectra for various fuels of interest to combustion must be cautiously used with regards to wavelength selection for high-temperature sensing applications. Yet another option, however, is to use uncatalogued data published by a wide range of researchers, some of which is discussed in the next section.

3.2.3. Uncatalogued data

Efforts to aggregate and standardize the format of spectroscopic data on a line-by-line or cross-section basis inherently require limitations of scope that leave an enormous amount of published spectroscopic data without centralized access. A significant portion of this uncatalogued data has been produced for combustion sensing purposes and falls into two primary categories: (1) high-temperature data, and (2) data collected with combustion species (e.g. CO₂, H₂O) as bath gas. Errors associated with extrapolating spectroscopic parameters (e.g., collisional-broadening coefficients) to high temperatures and the need to interrogate high- E'' transitions have motivated the development of the former, while collision-partner-specific collision broadening has motivated the latter. Fig. 8, reprinted from Sur et al. [86], highlights the impact of balance gas composition on the observed absorption spectra for NH₃ at slightly elevated temperatures, representative of combustion exhaust. CO₂ and H₂O have been observed to have collisional broadening coefficients that are much more than twice that of nitrogen or air, such that a gas mixture with only perhaps 5–10% of these combustion species can significantly alter the lineshape and peak absorption for a given transition. While documenting all such relevant but uncatalogued infrared data is beyond the scope of this paper, we note some recent contributions (either at high temperature or with combustion species as balance gas) that have been made for a number of molecules found in combustion flows including: H₂O [46,76,90,93–98], HCl [99,100], CO₂ [101–104], CO [105–107], CH₄ [108–110], C₂H₄ [111], C₃H₆ [112,113], iC₄H₈ [114], NO [115], NO₂ [116], N₂O [117], and NH₃ [86,118–120]. In addition, temperature-, pressure-, and bath-gas-dependent cross sections for a large number of hydrocarbons at elevated temperatures have been published [112,121–124]. It should be noted that

recent efforts have been taken to integrate and centralize spectroscopic data at the simulation and visualization level such that many data-types and databases (line-by-line, cross-section, etc.) may be readily utilized together for spectral modeling [125]. This approach provides for opportunity to integrate current uncatalogued data and future data that may not fit into the more focused scope of existing databases.

4. Techniques

This section discusses the fundamentals of the most common LAS techniques; recent applications of these techniques are discussed in Sections 8 through 13. Specifically, two categories of LAS techniques will be discussed: direct absorption and wavelength-modulation spectroscopy and these techniques will be further broken into the subcategories: fixed wavelength or scanned wavelength. In the former, the laser's wavelength is resonant with an absorption transition of interest and constant in time (for DA) or sinusoidally modulated about a fixed wavelength (for WMS). In the latter, the laser's wavelength is scanned across a portion of the absorption spectrum of interest, and in WMS, this wavelength scanning is accompanied by simultaneous sinusoidal wavelength modulation performed at a much higher frequency (typically 50 to 100 times greater than scan rate). In addition, a variety of hyperspectral direct-absorption techniques have emerged in the last 15 years and, due to their unique abilities, will be discussed separately from conventional scanned-wavelength DA.

Fixed-wavelength techniques are inherently less robust due to their limited spectral information and, as a result, are typically only used when extreme time resolution (order of MHz) is required and non-absorbing transmission losses are negligible or can be corrected for (e.g., with use of a non-resonant laser [126]). Fixed-wavelength direct absorption has been used extensively and effectively in shock-tube studies of chemical kinetics [2,127], and some work has been done in IC-engines [128] and pulse-detonation combustors [108,126].

Currently, the majority of laser-absorption sensor development for combustion flows revolves around advancing the state of scanned-wavelength techniques due to their (1) increased robustness and versatility, (2) increased potential for monitoring practical combustion systems, and consequently, (3) their increased complexity (compared to fixed-wavelength techniques). As a result, this section will focus on describing the fundamentals of the various LAS techniques, as well as, their application to cavity-enhanced configurations.

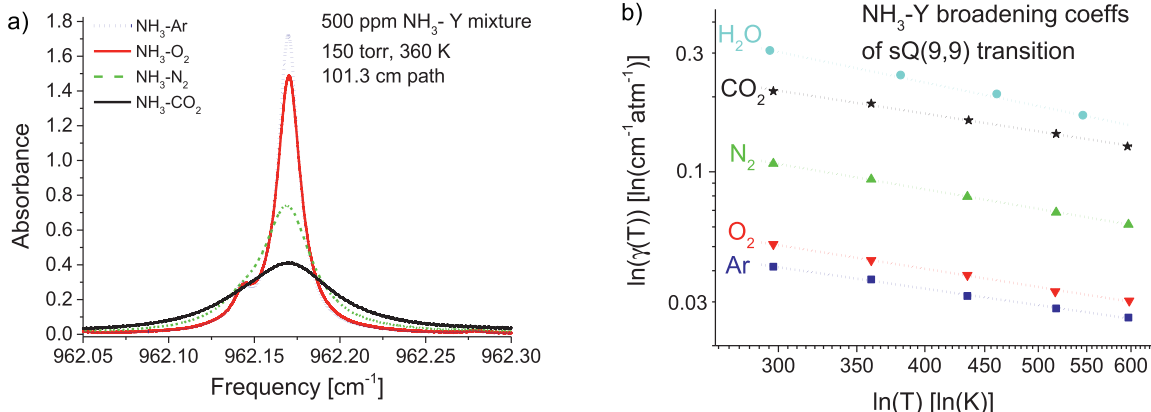


Fig. 8. Measured absorption spectra of NH₃ near 962.17 cm⁻¹ for different bath gases (a) and corresponding best-fit collisional-broadening coefficients of bath gas as a function of temperature (b). Results adapted from Sur et al. [86].

4.1. Scanned-wavelength direct-absorption spectroscopy

Scanned-wavelength direct absorption (scanned-DA) was first applied to combustion gases in the late 1970s [13–15], and due to its wide applicability, ease of operation, and relatively simple data interpretation, continues to be widely used to study combustion when SNR-levels permit [106,129–131]. Modern scanned-DA is typically performed with distributed-feedback diode, interband-, or quantum-cascade lasers. In this case, the laser's wavelength is scanned (via injection-current tuning) across one or a few absorption transitions to resolve the absorption spectrum of interest (see Fig. 9a). Gas properties are then calculated from the absorbance at a given wavelength or, more typically, from the integrated absorbance using Eq. (2) or (4), respectively. In harsh combustion environments, scanned-DA can suffer from low SNR, particularly in cases of low-absorbance ($\alpha < 0.01$). To overcome this, numerous researchers have developed more advanced diagnostic techniques (e.g., WMS, Hyperspectral-DA) discussed in the following subsections.

4.2. Hyperspectral direct-absorption spectroscopy

Strictly speaking, scanned-DA is typically used to describe cases where the laser's wavelength/frequency is tuned over a narrow spectral range (≈ 0.1 to 10 cm^{-1}) to resolve one or several absorption transitions. Here, *hyperspectral direct-absorption spectroscopy* (hyperspectral-DA) will be used to refer to all direct-absorption techniques spanning a region of the spectrum greater than 10 cm^{-1} ; further distinction will only be provided when necessary. Such techniques have been referred to as wavelength-agile DA [34,36,132,133], swept-wavelength DA [38], supercontinuum absorption [134], and frequency-comb spectroscopy [135], typically to indicate differences in the type of light source used and these differences are discussed in detail in Section 6. Regardless of these differences, all hyperspectral-DA techniques are used to measure a large portion of an absorption band, frequently at very high rates (10 to 100 kHz). The linewidth of these sources varies greatly, from order of kHz (e.g., frequency combs) to near-GHz (e.g., FDML sources). This unique combination of features has mandated the use of a variety of unique data processing and spectral-fitting techniques to overcome challenges associated with large datasets and the need to accurately model significant portions of an absorption band, at times, convoluted with an estimated instrument function. Despite these complexities, hyperspectral-DA techniques have demonstrated the ability to overcome most of the challenges limiting conventional scanned-DA, and as a result, have emerged as one of the most promising LAS technologies for characterizing harsh combustion environments.

4.3. Wavelength-modulation spectroscopy

Wavelength- and frequency-modulation spectroscopy were first developed in the early 1980s [20] to reduce the influence of laser and detector noise, thereby improving measurement fidelity in gas-

sensing applications. Since then, wavelength-modulation spectroscopy has been used extensively to study a wide range of harsh combustion environments [2,27,39,136] particularly due to several experimental and theoretical advancements enabling robust, calibration-free WMS techniques [40,41,137–140]. Typically, the first- and second-harmonic signals are used to calculate gas properties and will be the focus here. However it should be noted that using higher harmonics ($3f$, $4f$, etc.) has been shown to exhibit some unique advantages, as discussed in Section 5.5 and [141–144]. Several variants of WMS have been used and will be discussed here, namely: fixed-WMS, peak-picking scanned-WMS, and scanned-WMS. A schematic illustrating scanned-WMS- $2f/1f$ is shown in Fig. 9b and Fig. 10 illustrates how the WMS- $2f/1f$ signals associated with each of the aforementioned techniques differ in the Fourier and time domain. A detailed discussion of these differences can be found in [145].

In fixed-WMS the laser's wavelength is sinusoidally modulated (typically via injection current modulation) about a given location on an absorption feature of interest. The modulation shifts absorption information to the harmonics of the modulation frequency, f , and the harmonic signals ($1f$, $2f$, $3f$ etc.) can be extracted from the raw detector signal using digital lock-in filters during post-processing [41] or using analog lock-in amplifiers prior to data acquisition. In this case, the lock-in filter bandwidth defines the theoretical sensor bandwidth. By modulating at high frequencies (f typically from 10 kHz to 1 MHz), the harmonic signals are elevated above lower-frequency noise sources (e.g., electronic, environmental) which can improve their SNR [146]. Cassidy and Reid [137] first showed that when WMS is performed using injection-current tuned lasers (e.g., diode lasers, quantum-cascade lasers), the higher harmonics can be normalized by the $1f$ signal to remove their dependence on the DC light intensity impinging on the detector. This attribute enables $1f$ -normalized WMS to be immune to intensity variations (e.g., from beam steering or window fouling or other non-absorption losses) that vary in time slowly compared to f .

In peak-picking scanned-WMS the wavelength modulation is accompanied by a small-amplitude wavelength scan to resolve the peak of the WMS- $2f/1f$ signal near linecenter, thereby providing a known wavelength reference. This improves measurement robustness (removing concerns of unknown laser-wavelength drift) while minimizing the additional frequency content centered around each harmonic, thereby reducing potential for cross talk and facilitating frequency multiplexing of multiple lasers. In this case, only the value of the WMS- $2f/1f$ signal near the transition linecenter is used to calculate gas properties (see [145]) and the measurement bandwidth is set by the scan frequency.

In scanned-WMS the nominal wavelength of the laser is scanned across an absorption transition to extract WMS spectra, thereby enabling spectral fitting and removing the need for *a priori* knowledge of the transition line broadening [139]. In this case, gas properties can be extracted from measured WMS spectra analogous to scanned-wavelength direct absorption using the spectral-fitting technique developed by Goldenstein et al. [139] (later extended by

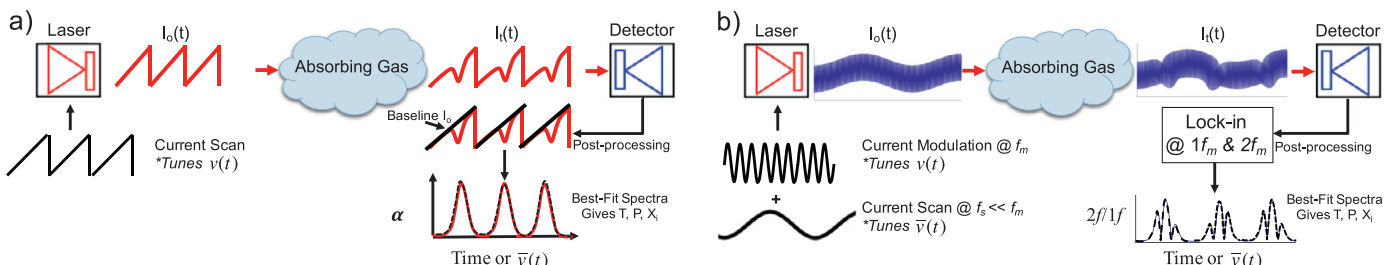


Fig. 9. Schematics for scanned-wavelength direct absorption (a) and scanned-WMS (b).

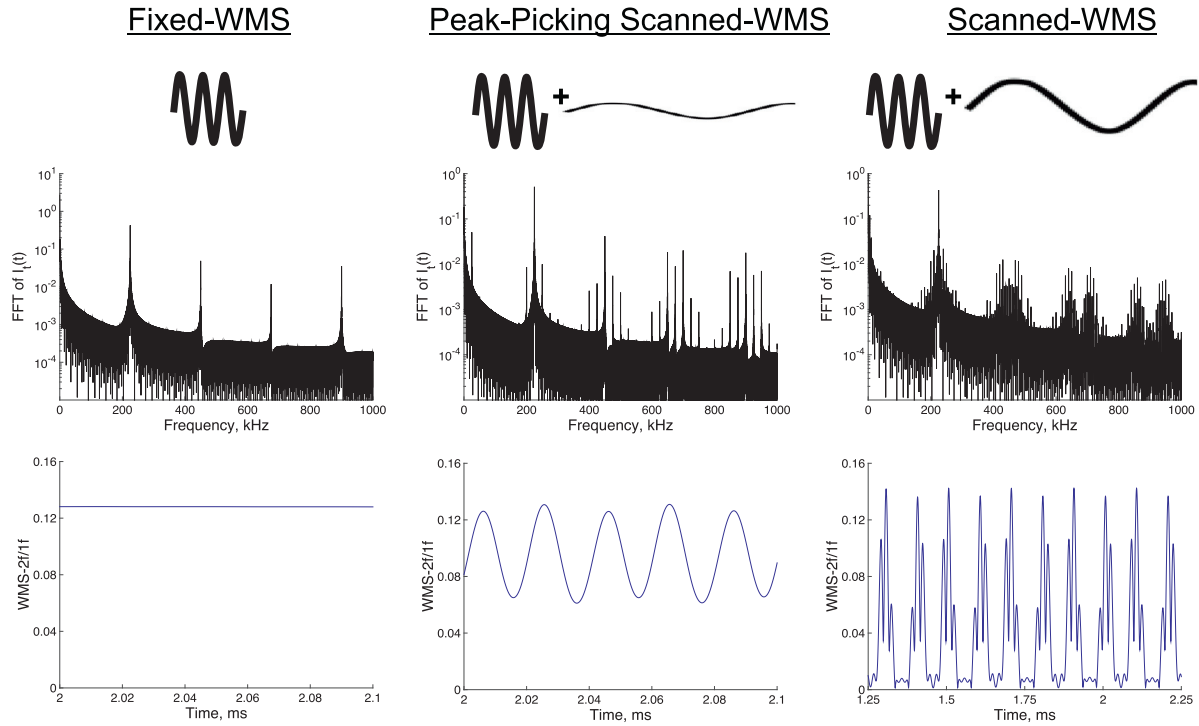


Fig. 10. FFT of transmitted light intensity for a fixed-WMS, peak-picking scanned-WMS, and scanned-WMS experiment interrogating the H₂O absorption transition near 7185.59 cm⁻¹ and corresponding WMS-2f/1f time-histories for a diode laser modulated at 200 kHz. The scan frequency for the peak-picking scanned-WMS figures is 25 kHz and that for the scanned-WMS figures is 5 kHz.

Qu et al. [140] to include more laser parameters). Fig. 11 shows an example of a measured and best-fit WMS-2f/1f spectrum for a single-scan measurement at 1 kHz. In this method, WMS spectra are simulated by passing the simulated laser-intensity time-history ($I_t(t)$, given by Eq. (16)) through digital lock-in filters to extract the WMS spectra of interest (e.g., WMS-1f, -2f, etc.).

$$I_t(t) = I_0(t) \exp \left[- \sum_j S_j(T) P \chi_{\text{Abs}} \phi(\nu(t), T, P, \chi) L \right] \quad (16)$$

Here $I_0(t)$ and $\nu(t)$ are given by a summation of sinusoids describing the laser's intensity- and wavelength-tuning response to the sinewaves applied to its injection current (see [139]). It is important to note that modern calibration-free WMS models are applicable to all optical depths [40,41,138–140], however only the most recent

[138–140] accurately account for the laser intensity varying during injection-current scanning (performed to scan the laser's nominal wavelength across the absorption transition of interest). It should be noted that methods for recovering absorption transition lineshapes have also been developed using WMS-1f signals [147,148]; however, this approach requires use of non-resonant wavelengths (analogous to fixed-wavelength direct absorption) to account for non-absorbing losses.

4.4. Cavity-enhanced techniques

The previous sections discussed absorption techniques primarily aimed at improving sensor accuracy and robustness by rejecting signal noise or increasing the amount of useful information extracted by the sensor. However, in reality the sensitivity of all absorption measurements is fundamentally limited by the strength of the interrogated absorption transition(s) and/or the path length over which light interacts with the absorbers. The former is dictated by the physics of the target species (i.e., Einstein-A coefficient, degeneracy, and Boltzmann statistics), however, the latter can be manipulated by the experimentalist by conducting the measurement in an optical cavity. This section will discuss a few of the most useful cavity-enhanced LAS techniques for increasing the sensitivity of LAS sensors.

There are three primary cavity-enhanced LAS techniques applicable to combustion applications: (1) intracavity-absorption spectroscopy, (2) cavity-ring down spectroscopy, and (3) cavity-enhanced absorption spectroscopy or integrated-cavity output spectroscopy (ICOS). In intracavity-absorption spectroscopy the test gas is located within the laser cavity. Absorption transitions within the gain curve of the laser are sensitively detected by measuring the reduction in gain at these specific wavelengths. There is a long (40+ years) history of intracavity absorption using broadband laser sources (e.g., broadband dye lasers or relatively broadband gas lasers) and the application to combustion diagnostics has long been recognized. As

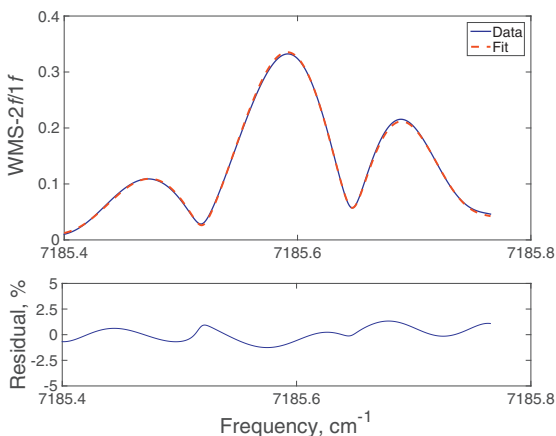


Fig. 11. Measured and best-fit WMS-2f/1f spectrum of the H₂O transition near 7185.59 cm⁻¹. The best-fit spectrum yields the transition linecenter, integrated absorbance, and collisional width analogous to scanned-wavelength direct absorption. Figure adapted from [139].

such, we refer the reader to an excellent article by Harris [149], as well as a few recent papers employing fiber lasers [150,151].

Fig. 12 illustrates the operating principles of CRDS and CEAS. Typically in CRDS, pulsed laser light is injected on-axis into an optical cavity (formed by two dielectric coated mirrors) and the light intensity exiting the cavity is measured to determine the characteristic decay time (τ). In the limit of no scattering losses, the decay time is dictated by the reflectivity of the cavity mirrors and the single-pass absorbance (α_{SP}) given by Eq. (2). With the mirror reflectivity (R_M) known (e.g., from a measurement in the empty cavity), Eq. (17) can be inverted to solve for α_{SP} and, thus, gas properties.

$$\begin{aligned} I_t(t) &= I_0 \exp(-t/\tau) \\ &= I_0 \exp\left(-\left((1-R_M)+\alpha_{SP}(v)\right)ct/L\right) \end{aligned} \quad (17)$$

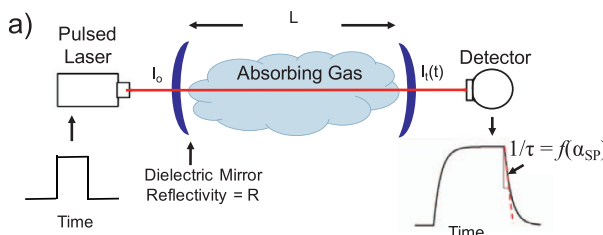
CRDS with high-finesse (i.e., high-reflectivity) cavities can increase the optical path by 10^4 or more, thereby enabling highly sensitive measurements of trace species. However, these cavities suffer from very small transmission (typically requiring mode-locking with the TEM00 cavity-mode) and long residence times of the light which limits their time response. Furthermore, high-finesse cavities are highly susceptible to window fouling (e.g., from dust or soot) and require extreme care to maintain high mirror reflectivity.

In comparison, in CEAS continuous-wave laser light can be injected into an optical cavity and the intensity of light exiting the cavity is measured on a photodetector. Although CEAS can be performed with on-axis injection [152], for scanned-wavelength measurements with a spectrally narrow laser, the use of off-axis injection significantly reduces laser-coupling noise on the light transmitted through the cavity [152,153]. By using off-axis injection the reflections are separated in space as they move around the perimeter of each mirror and many roundtrips are required before the light retraces its initial trajectory and overlaps upon itself. This leads to an effective cavity length on the order of m to km and, therefore, a free-spectral range that is comparable to the laser linewidth and is much smaller than the absorption transition HWHM. As a result, scanned-wavelength techniques can be employed to measure absorption spectra and the non-absorbing baseline. Gas properties are calculated using Eq. (18) (an analogue of Beer's Law) and a spectroscopic model.

$$\alpha_{CEAS}(v) = -\ln\left(\frac{I_t}{I_0}\right) = \ln\left(1 + G\alpha_{SP}(v)\right) \quad (18)$$

Here, α_{CEAS} is the measured, cavity-enhanced absorption and G is the cavity gain set by the mirror reflectivity (determined by CRDS or calibration).

CEAS has been used extensively in high-finesse configurations for trace-gas sensing [154–157] and the use of WMS has also been explored [158], however, like CRDS these methods suffer from long cavity residence times and susceptibility to mirror fouling. Recently, low finesse (gain of $100\times$ in path length) cavities have been integrated into shock tubes to improve the measurement sensitivity of combustion species while maintaining measurement rates (≈ 100 kHz) sufficient to resolve reaction kinetics [159,160] and these studies are highlighted in Section 8.1.



It should be noted that there is a long history of using intracavity laser absorption and CRDS for combustion diagnostics, especially to monitor the concentration of minor reactive species. Much of this work has focused on the distribution of radicals in low-pressure flames using transitions in the visible and ultra-violet to test models of flame chemistry. Since this work is beyond the scope of this paper (being outside the IR domain), we refer the interested reader to excellent reviews by Cheskis [161] and by Mercier and Desgroux [162] who have been pioneers of intracavity laser absorption and CRDS for combustion applications.

5. Measurement challenges and solutions

This section will discuss some of the most common challenges and current solutions pertaining to IR-LAS sensors for combustion gases. Our discussion will focus on challenges with evolving solutions, and we will simply refer the reader to the appendices in [163,164] for more standard solutions to an assortment of conventional problems (e.g., free-space fiber coupling, wavelength jitter).

5.1. Solutions for nonuniform flows

Laser-absorption spectroscopy provides a path-integrated measurement. In cases where the gas conditions vary along the measurement line-of-sight, the measured absorbance is given by Eq. (19).

$$\alpha(v) = \int_0^L \sum_j S_j(T) P \chi_{Abs} \phi_j(v, T, P, \chi) dl \quad (19)$$

The path integral in Eq. (19) complicates the relationship between the measured absorbance and gas properties and a thorough discussion regarding the influence of nonuniform temperature, pressure, and composition can be found in [165]. Briefly, the measured absorbance is influenced by linear and non-linear dependences on pressure and absorbing-species mole fraction and a non-linear dependence on temperature through the transition line-strength and lineshape function. The non-linear dependencies can lead to the path-integrated measurement deviating from path-averaged gas properties unless certain measures are taken [165].

Despite this complication several researchers have developed strategies to provide useful and quantitative measurements of gas properties in non-uniform gases [32,165–176]. This section will focus on discussing solutions applicable to single-LOS measurements, however, a discussion of some of the most widely used and emerging tomographic LAS techniques will conclude this section.

5.1.1. Single line-of-sight solutions

Several researchers have developed strategies to identify temperature non-uniformities [168,170,172] and quantify the measurement uncertainty they induce [176]. Seitzman and Scully [168] developed a broadband sensor for monitoring temperature non-uniformity and H_2O mole fraction in a gas-turbine combustor. By measuring the absorbance in at least three spectral windows with

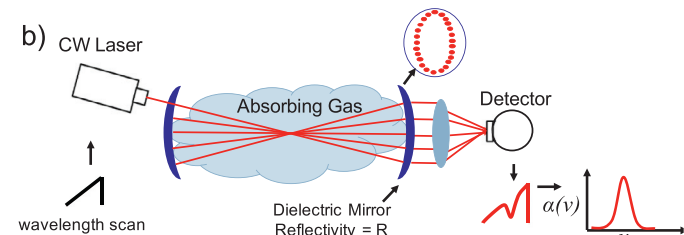


Fig. 12. Schematics for cavity ringdown spectroscopy (a) and off-axis cavity-enhanced absorption spectroscopy (b). Figures adapted from [10].

different temperature dependence, two temperatures can be calculated (one “cold” and one “hot”) with the difference between them quantifying how thermally non-uniform the flow is. A similar strategy was later used by Palaghita and Seitzman [171], Liu et al. [172], and Goldenstein et al. [145] using diode lasers to resolve individual absorption transitions for a simplified interpretation. Rieker et al. [43] built upon this technique by monitoring differences in the frequency content (from an FFT) of the “cold” and “hot” temperatures and showed that the measurements of fluctuations could be used to predict scramjet unstart.

Strategies have also been developed to reduce sensitivity to non-uniform gas conditions [167–169]. For example, Ouyang and Varghese [167] developed a strategy for measuring absolute absorbing-species concentration in the presence of thermal and concentration boundary layers. This strategy relies on the use of transitions with specific values of lower-state energy such that the absorption measurement is insensitive to gases in the boundary layer, and relations are put forth to identify suitable values of E' for a given temperature of interest in the limit of small boundary layers. In their broadband absorption sensor, Seitzman and Scully [168] used a spectral window where the absorbance is nearly independent of temperature to measure H_2O mole fraction with a maximum error of 8% for an unknown temperature (or temperature non-uniformity) from 1000 to 2100 K.

Several LAS techniques have been developed to correct for or tolerate the large non-uniformities encountered in flames [165,166,177]. Schoenung and Hanson [166] acquired thermocouple and line-of-sight absorption measurements at multiple locations spanning the transverse (relative to the flow) axis of the flame to correct the path-integrated absorption measurement of CO assuming axisymmetric temperature and species distributions. Goldenstein et al. [165] developed a two-color LAS strategy for measuring the absorbing-species column density, N_i , and absorbing-species-weighted path-averaged temperature, T_{n_i} , given by Eqs. (20) and (21), respectively, and showed that this technique is more accurate over a broad temperature range than a constant-linestrength approximation (similar to that used in [168]).

$$N_i \equiv \int_0^L n_i dl \quad (20)$$

$$T_{n_i} \equiv \frac{\int_0^L T n_i dl}{\int_0^L n_i dl} \quad (21)$$

This strategy requires use of absorption transitions with a linestrength that varies near linearly with temperature over the domain of the temperature non-uniformity. This can be achieved by using transitions with specific values of lower-state energy and is shown to be accurate over large temperature non-uniformities (500 to 1000 K) at combustion temperatures (> 1000 K). This strategy was later deployed to study flames in a scramjet combustor [178] and low-pressure burner [177].

Single-LOS strategies have also been developed to measure LOS distributions of temperature and composition [170,173]. Sanders et al. [170] developed a strategy for recovering a discretized LOS distribution of temperature by scanning a VCSEL across 10 O₂ A-band transitions with a unique temperature dependence. In this technique the LOS is discretized into bins and a system of linear equations is solved to determine the mole fraction and temperature in each bin. The discretized solution is then least-squares fit to a distribution function to provide a finer solution grid (provided that a representative distribution function is known *a priori*). The authors clarify that this technique works best when a distribution function can be assumed as the discretization technique alone may either be too coarse or ill-conditioned. Liu et al. [173] later built upon this technique by developing (1) a profile-fitting technique to solve for the defining parameters of a postulated temperature distribution profile

and (2) a temperature binning technique to determine the probability density function of prescribed temperature bins along the LOS. These techniques were demonstrated in a two-temperature experiment using 5 fiber-coupled diode lasers targeting H₂O absorption transitions.

5.1.2. Laser-absorption tomography

A wide range of laser-absorption-tomography (LAT) (a subclass of chemical species tomography (CST)) techniques have been developed and used to reconstruct 2D chemical-species, temperature, and pressure fields in combustion gases [129,179–189], and several excellent reviews have been devoted to this subject [190–192]. In particular, the most recent review by Cai and Kaminski [192] provides an excellent overview of LAT and its application to combustion studies. In tomography, multiple lines-of-sight are used to sample a heterogeneous measurement volume from unique viewpoints and the measured projections (i.e., path-integrated absorption) are used to reconstruct the 2D (or even 3D) field. In contrast to medical-imaging techniques employing 1000s of LOS (e.g., MRI, CT scan), LAT typically employs only 10 to 100s of LOS due to the optical-access limitations imposed by combustion applications. This sparse sampling precludes the use of the Fourier-transform-based algorithms (e.g., filtered backprojection) employed in medical imaging, and requires a distinct approach.

In most LAT applications, the 2D field is reconstructed from measured projections by solving a linear systems of equations, $Ax = b$, where the $m \times n$ matrix A specifies the known path length of each ray through each pixel, the m -vector b contains the measured projections for each line-of-sight, and the n -vector x specifies the unknown (i.e., to-be-solved for) absorbance or species-concentration in each pixel. A multitude of algorithms have been developed to solve for x (e.g., in a least-squares sense or though minimization of an objective quantity) and address the ill-posed nature of this problem (i.e., multiple solutions often exist or the solution is unstable and sensitive to input noise) [193,194], including algebraic-reconstruction tomography (ART), simultaneous-ART (SART) [195], statistical image reconstruction (SIR) [196], and total-variation-based compressed sensing (TVCS) [197,198]. Daun et al. [191] points out that it is particularly important to distinguish between two cases in order to identify the most well-suited approach: (1) A is *discrete ill-posed* [199] (e.g., when employing dense sampling of the tomography space) or, more likely in combustion applications, (2) the matrix equation is rank deficient (e.g., when employing sparse sampling) and, therefore, *a priori* information about the flow field is required to identify a unique solution.

Recently, hyperspectral-tomography (HT) techniques have been developed and deployed to reconstruct 2D temperature and H₂O-concentration fields [179,180,183,200]. This method utilizes many absorption transitions, thereby adding increased spectral information to the reconstruction process. In practice, the temperature and species-concentration fields are reconstructed by minimizing the function:

$$D(T^{rec}, X^{rec}) = \sum_{j=1}^J \sum_{i=1}^I \frac{[p_m(L_j, \lambda_i) - p_c(L_j, \lambda_i)]^2}{p_m(L_j, \lambda_i)^2} \quad (22)$$

where $p_m(L_j, \lambda_i)$ is the measured projection at location L_j and a wavelength λ_i , $p_c(L_j, \lambda_i)$ is the corresponding projection calculated using the reconstructed T and X profile (denoted T^{rec} and X^{rec}), and J and I are the total number of wavelengths and projection locations, respectively. For context, 12 unique wavelengths (chosen using the methods presented in [201]) were used for the jet-engine exhaust sensing presented in [183]. The authors state that this method has several advantages, including: (1) reducing the number of projections required for accurate tomographic reconstruction,

(2) improved tolerance to noise, and (3) the ability to image temperature and species concentration simultaneously.

5.2. Beam steering and emission

In harsh combustion environments the effective baseline I_0 may vary in time due to non-absorbing transmission losses (e.g., from window fouling, light scattering or beam steering) or fluctuations in background emission. If these losses or gains in light intensity are not properly accounted for or avoided, the gas properties inferred from the detector signal will be incorrect.

In direct absorption, these challenges are typically mitigated using rapid and/or broad wavelength scanning such that these confounding effects are constant during the measurement time and can be more accurately accounted for. For example, baseline emission levels can be recorded in-between pulses or scans, assumed constant during the measurement, and subtracted from the measured detector signal during the measurement time. In addition, non-absorbing transmission losses in I_0 can be accounted for if constant or near-constant during the measurement by floating the baseline intensity in spectral-fitting routines. Broad wavelength tuning can improve the robustness of the latter by increasing the amount of spectroscopic information relative to the uncertainty in baseline.

In WMS, high-frequency modulation and 1f-normalization are used to reject background emission and non-absorbing variations in light intensity that vary slowly compared to f . As a result, measured 1f-normalized WMS spectra are inherently immune to such transmission variations and no corrections are required during post-processing. However, despite 1f-normalization, variations in I_0 that occur at frequencies comparable to f can introduce noise in the WMS signals. To reduce this noise one must improve the light collection efficiency or modulate at higher frequencies to escape the frequency spectrum of the noise and/or increase the bandwidth over which 1f-normalization applies.

Several researchers have also developed strategies for minimizing beam-steering effects via optical engineering. For example, Petersen [204] (and most recently Spearin et al. [115]) found that using an integrating sphere can dramatically reduce beam-steering effects in high-pressure gases and rigorous design rules for maximizing light-collection efficiency are presented. Kranendonk et al. [205] developed a general design framework for minimizing the influence of beam steering without requiring *a priori* knowledge of the beam steering field. Whitney et al. [206] provides a detailed analysis and discussion describing how to minimize beam-steering effects in sensors employing multi-mode fibers, and presents the design of a

sensor using a fused-fiber lens and fiber-fused detector that minimizes the influence of a spatially non-uniform detector response. Most recently, Strand [207] showed that using an aspheric-lens doublet to collimate and focus light exiting a multi-mode catch fiber onto a detector can also dramatically improve tolerance to beam steering in fiber-coupled assemblies.

5.3. Broad and blended spectra

Broad and blended absorbance spectra complicate the determination of gas properties in three primary ways: (1) the absorption spectra at a given wavelength is governed by multiple transitions which have a unique dependence on gas conditions (T, P, χ), (2) non-absorbing wavelengths may not exist nearby, complicating or precluding *in situ* determination of the non-absorbing baseline, and (3) differential absorbance and WMS-2f signals are smaller.

The first complication has been addressed by several researchers by developing wavelength- and modulation-depth-selection routines that account for the influence of neighboring transitions [203,208–210]. For example, An et al. [208,209] developed a quantity (the frequency-dependent lower-state energy) for quantifying the temperature sensitivity of a given wavelength and showed it could be used to identify the optimal wavelengths for thermometry. Goldenstein et al. [203] showed that by using wavelengths and specific modulation depths in regions of temperature-dependent spectral curvature, two-color WMS-2f/1f thermometry and mole fraction sensing could be performed using a single modulation depth over a range of 1000 to 3500 K and 5 to 50 bar (see Fig. 13b).

The second complication only pertains to direct-absorption techniques, and this challenge has been overcome by using an additional non-resonant light source (e.g., see [108,126,128,211]) or broadly tunable light sources (e.g., see [33,34,202,212,213]). Fig. 13a illustrates the wealth of spectral information that hyperspectral light sources can extract, enabling the baseline intensity to be floated in spectral-fitting routines. Several strategies for hyperspectral-base-line fitting have been developed and demonstrated (at low and high pressures), and indicate that using a baseline that is smooth relative to the absorption spectra is best [214,215]. However, in the former approach it is critical to use non-resonant wavelengths as close to the resonant wavelengths as possible to minimize differences in wavelength-specific transmission losses (e.g., from droplet or particulate scattering) [126].

The last complication pertains to WMS, and this challenge has been overcome by using large modulation depths [42,210,216,217] and, most recently, by combining large modulation depths with

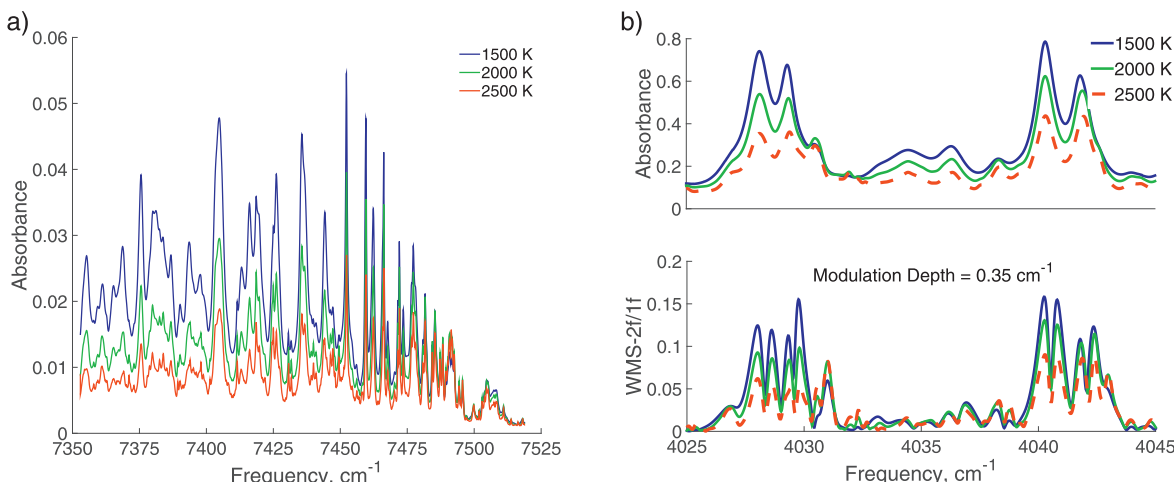


Fig. 13. Simulated transmission spectra of MEMS VCSEL used for hyperspectral-DA in [202] (a) and absorbance and WMS-2f/1f spectra near wavelengths used in [203] to measure H₂O and temperature (b). Simulated spectra are for 10% H₂O, P = 25 bar, L = 5 cm, legend indicates temperature.

strong mid-infrared absorption [46,101,106,203]. WMS-1f sensing has also been demonstrated as an effective technique for sensing molecules with extremely broad spectra (e.g., large hydrocarbons and gasoline [218]). While WMS-1f is not immune to non-absorbing transmission losses, it is immune to background emission, as well as, laser and detector noise that exist outside the bandwidth of the lock-in filter used.

5.4. Breakdown of the impact approximation

As discussed previously in Section 5.4, at high number densities the impact approximation can break down, thereby introducing errors in spectroscopic models that do not account for this. Since the impact approximation primarily affects the absorption transition wings, such errors can be mitigated by using wavelengths near linecenter. However, if multiple absorption transitions are overlapping (as is likely the case at number densities where the impact approximation breaks down), the contribution from neighboring transitions to the region near linecenter may be significant. In this case, Rieker et al. [63,79] showed that WMS-2f signal can be less susceptible to such errors since the contribution to differential absorbance (across the modulation depth) resulting from the far-wings of neighboring transitions can be small.

5.5. Non-zero WMS background

Real semiconductor lasers do not respond perfectly linearly to injection-current tuning (i.e., sinusoidal current modulation results in intensity modulation with frequency components at 1f, 2f, 3f, etc.). As a result, the higher harmonic signals exhibit a non-zero background from higher-order intensity modulation (often referred to as residual amplitude modulation (RAM)). The RAM background decreases with increasing harmonic [141,142,144,219], but increases with increasing modulation frequency and modulation depth [40]. Li et al. [40] showed that for telecommunication-grade TDLs the second-order intensity modulation exhibits a quasi-quadratic dependence on the modulation depth, with a maximum value of $\approx 3\%$ for 100% intensity modulation. However, it should be noted that we have found these results can vary substantially depending on the type of diode laser and manufacturer. To solve this issue, calibration-free WMS models that account for higher-order intensity modulation can be used [40,41,138,139] or a measured intensity time history (in the absence of absorbers) can be used to simulate WMS signals in the recently developed brute-force calibration-free WMS models [138,139]. The latter approach can also be used to account for WMS background signals resulting from etalon effects in the beam path, and as a result, is currently the most accurate method if the etalons are stable. However, several researchers have shown that dithering of optical components [220], intelligent triggering timing [143], intelligent selection of the modulation depth [139], and the use of higher harmonics (e.g., 4f) [141,142,144] can all be used to reduce WMS background signals originating from etalon effects.

5.6. 1f-normalization with large absorbance

1f normalization is optimal for, but not limited to, cases where the absorbance is small such that the 1f signal is dominated by the laser's intensity modulation. As the peak absorbance increases, the 1f signal near linecenter approaches zero. As a result, even small noise levels are magnified, leading to a WMS-2f/1f signal that can vary widely and erroneously near linecenter. This effect typically becomes problematic at absorbances greater than ≈ 0.5 . However, the 1f signal away from linecenter typically remains sufficiently large for 1f normalization. This can be exploited by normalizing the higher harmonic signals by the scan-averaged 1f signal, as opposed

to the local 1f signal which, to the best of our knowledge, was first demonstrated in [138].

6. Sources and hardware

This section will discuss the capabilities and limitations of both established and emerging light sources and hardware that are relevant to IR-LAS. Our discussion will focus on light sources, although detectors, optical fibers and materials will also be discussed. A detailed discussion regarding the selection of optical equipment for laser spectroscopy can also be found in Chapter 13 of Hanson, Spearin, and Goldenstein [10].

6.1. Near-infrared hardware

Historically, the majority of LAS sensors for combustion systems have operated in the near-infrared (≈ 760 to ≈ 2500 nm) in order to leverage the robust and affordable hardware born out of the telecommunication industry in the 1990s. While the detection limit of these sensors is limited by the weaker absorption strength of the overtone and combination bands located in the near-IR, they have achieved widespread success, particularly in the detection of highly anharmonic absorbers (e.g., H₂O, HF, HCl, NH₃) due to their greater absorption strength (only ≈ 10 times less than their fundamental bands) and in flows with large quantities of weaker absorbers or potential for long path-length measurements. This section will discuss some of the most widely used near-IR light sources and hardware to highlight their strengths and weaknesses.

6.1.1. Distributed-feedback (DFB) and distributed-Bragg reflector (DBR) tunable diode lasers

Diode lasers fabricated with a Bragg grating distributed along the gain medium (DFB) or as a cavity end-mirror (DBR) provide single-mode laser output that can be injection current tuned over a moderate wavelength range, which is useful for scanned-wavelength absorption techniques. In general, lasers with DFB architecture have a wider tuning range while the DBR architecture leads to more stable single-mode performance at higher laser powers. Although either DFB or DBR lasers are quite suitable for LAS sensors, the vast majority of the single-mode lasers that are currently commercially available in the telecommunications region are DFB devices and most of the applied TDLAS work described later employed DFB TDLs. As a result, the remainder of this section will focus on the characteristics of DFB TDLs.

DFB TDLs are one of the most widely used lasers due to their ease-of-operation, low cost, wavelength stability, rapid wavelength tunability, and ability to be manufactured over a wide range of custom wavelengths (760 nm to 3 μ m). These DFB TDLs typically produce 5 to 25 mW of power with a laser linewidth < 5 MHz, leading to negligible instrument broadening. In addition, DFB TDLs are frequently available in fiber-pigtail packages further facilitating their integration into LAS sensors suitable for the field. In a DFB TDL, a p-n junction acts as a lasing medium and the bandgap (i.e., the energy gap between the conduction and valence bands) of the semiconductor sets the range of wavelengths emitted. A diffraction grating (located near the p-n junction) is used to effectively filter the emitted light and reflect a single wavelength back into the gain medium for lasing. By changing the temperature of the laser (directly or via current tuning i.e., ohmic heating) the grating resonance is adjusted, and the emitting wavelength is tuned.

In practice, these lasers are typically operated by commercial temperature and current controllers with wavelength tuning achieved via external injection-current modulation. Depending on the manufacturer and type of semiconductor used, the wavelength of DFB TDLs can typically be injection-current tuned from 1 to

10 cm⁻¹ during DC operation. The tuning range typically decreases to around 0.01 to 0.1 cm⁻¹ at modulation frequencies on the order of 100 kHz [40,203]. This tunability enables the measurement of several adjacent absorption lines at modest rates (order of 1 kHz) [221] and portions thereof at high-frequencies (order of 100 kHz) as done in WMS [40,203,216].

6.1.2. Vertical cavity surface emitting lasers (VCSELs)

VCSELs are a type of diode laser where light is emitted perpendicular to the semiconductor wafer (in comparison to edge-emitting lasers that emit radiation parallel to the surface). The resonator is formed by two Bragg mirrors with an active region spanning only a few μm in-between. In comparison to edge-emitting DFB or DBR lasers, VCSELs produce much lower optical power (order of 1 mW). However, they can exhibit superior wavelength tunability (near 10 cm⁻¹ at modulation frequencies near 1 MHz) which has been exploited to acquire increased spectral information, for example, for resolving line-of-sight temperature distributions [170] and collision-broadened lines in high-pressure gases [33,213]. At present, VCSELs are available from 750 to 1000 nm and near 1300, 1550 and 2000 nm and have been used to measure O₂ [33,170], H₂O [213], CO and CO₂ [222], and CO [223], respectively, to name only a few examples. In addition, recently a micro-electro-mechanical (MEMS) VCSEL capable of scanning from 1330 to 1365 nm at 100 kHz became commercially available and has been used for hyperspectral measurements of H₂O and temperature [224] in combustion flows [202].

6.1.3. Fourier-domain mode locked (FDML) lasers

FDML lasers [225,226] are capable of providing broad spectral coverage (up to 100 nm) at high repetition rates (order of 100 kHz) with a moderate linewidth (\approx 3 GHz). A schematic illustrating the operating principles of FDML lasers is shown in Fig. 14 (taken from [227]). These lasers consist of three primary components: a fiber-coupled semiconductor optical amplifier (SOA), a ring-fiber-based resonator, and a Fabry-Perot tunable filter (FP-TF). Upon startup, broadband amplified spontaneous emission (ASE) leaving the SOA travels to the sinusoidally modulated FP-TF which passes a time-varying wavelength, thereby effectively sweeping the wavelength exiting the FP-TF. This filtered light (dispersed in time) then passes back to the SOA for amplification via stimulated emission and the process repeats. By modulating the FP-TF with a drive period corresponding to the round-trip time of light in the cavity, each wavelength passed by the filter is passed on each subsequent roundtrip ensuring amplification and refinement of the wavelength sweep. The sweep rate can be varied by altering the length of the fiber-ring cavity [212].

FDML lasers have been deployed in a variety of combustion flows for hyperspectral (\approx 10 to 100 nm) measurements of H₂O (and gas properties thereof) near 1.3 to 1.4 μm [36–38,183,212]. Their high sweep-rates makes them well suited for studying transient combustion flows but this, combined with their broad spectral coverage, mandates the use of extremely fast detection electronics (order of

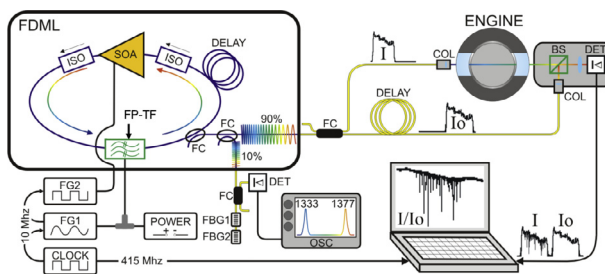


Fig. 14. Schematic for hyperspectral absorption sensing using FDML lasers. Figure adapted from [227].

100 MHz – 1 GHz bandwidth) in order to resolve the fast wavelength scanning (as is the case for all rapid hyperspectral techniques). It is worth noting that the MEMS VCSEL has effectively rendered such FDML sources obsolete due to its narrower linewidth (near 500 MHz at a repetition rate near 50 kHz) and ease of use [224].

6.1.4. Dispersed supercontinuum sources

Like FDML lasers, dispersed supercontinuum sources (DSS) can provide high-repetition rate, broadband measurements of absorption spectra with a moderate linewidth (\approx 1GHz to 1 THz) [132,134,228–234]. To name a few examples, supercontinuum sources have been used to measure acetylene [132,228,229], and H₂O and CO₂ in gas cells [132], CH₄ in atmospheric pressure jets [231] and flames [134,234], and H₂O in an HCCI engine [230].

These sources use a dispersing optical fiber (recent work has shown that using an all-normal-dispersion fiber improves single-shot measurement SNR substantially [235] thereby reducing the need for averaging) or other non-linear optical component to separate the wavelengths contained within a broadband ps- or fs-pulse in time. The net result is that faster-travelling wavelengths reach the detector first, effectively producing a swept wavelength source and enabling the measurement of transmission spectra, and ultimately absorption spectra, in the time-domain. These concepts are illustrated in Fig. 15. Until recently, most previous studies using DSSs were focused on fundamental studies with long and/or multi-pass path lengths (> 10 cm) and lacked use and validation in combustion gases [132,228,229,231–233]. Blume and Wagner [134] recently reported single-pass measurements (spanning 4.1 cm) of CH₄ mole fraction in a well-characterized non-premixed, laminar CH₄-air flame. The DSS enabled measurement across 110 cm⁻¹ of the CH₄ absorption band near 1650 nm with a resolution of 0.152 cm⁻¹ at a repetition rate of 2 MHz. A spectral-fitting routine was employed to calculate absolute mole fractions and measurements were able to

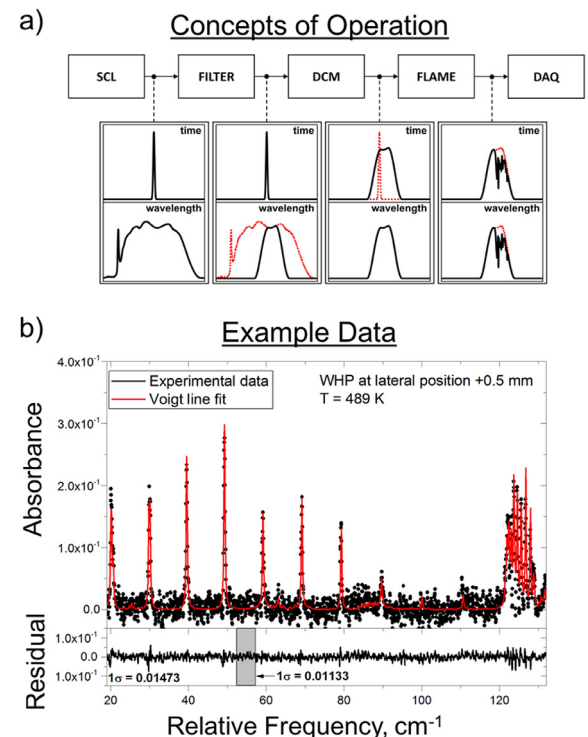


Fig. 15. Schematic illustrating the principles of a supercontinuum source (a) and example of CH₄ spectra measured using a supercontinuum source (b). Figures adapted from [134].

resolve 3% CH₄ by volume (1210 ppm-m) after averaging 9760 pulses for a near 200 Hz measurement rate. The results were also shown to agree well with previous measurements acquired in the burner indicating that DSSs have the potential for accurate measurements of combustion species in flames.

6.1.5. Optical fibers

Silica-based fibers and fiber components have been developed by large investments from the telecommunications industry and, as a result, fiber optics (e.g., couplers, interferometers) are widely available from 1.25 to 2 μm. Now, single-mode and polarization-maintaining fibers with low bend-losses are available well beyond 2 μm (e.g., NuFern). These fiber components enable the lasers, detectors and automatic data processing electronics to be remotely located away from combustion systems, thereby avoiding exposure to elevated temperatures and, potentially, large acoustic and electrical noise.

6.1.6. Detectors

In near-IR-LAS, the most commonly used detectors are made from silicon (Si) and indium gallium arsenide (InGaAs). Silicon detectors are responsive from ≈200 to 1100 nm, and are frequently used in sensors for O₂ that exploit the A-band transitions near 760 nm. InGaAs and extended-InGaAs detectors are sensitive from ≈800 to 1700 nm and 1200 to 2600 nm, respectively. These detectors do not require cooling, and have a rapid time response ranging from 100s of kHz to GHz depending on element size and amplification. Further, they exhibit excellent noise-equivalent power values (order of 1×10^{-12} W/Hz^{1/2}). While other options exist for a portion of this wavelength range (namely, germanium (Ge), indium arsenide antimonide (InAsSb), indium antimonide (InSb), and mercury cadmium telluride (MCT)), the trade-offs associated with using these alternative detectors (e.g., lower bandwidth, thermoelectric or cryo-cooling requirements) are typically not justified in the near-IR. That said, alternate detector materials should be considered when working at wavelengths near the red extrema (≈ 2500 nm) of the InGaAs bandwidth. More information regarding these detectors can be found in Section 6.2.4.

6.2. Mid-infrared hardware

Advances in mid-infrared (≈2.5 to 12 μm) optical equipment over the past 15 years has provided several new capabilities for LAS sensing in combustion environments. Most significantly, the fundamental vibrational frequencies of most combustion species are in this domain, and typically provide several orders of magnitude greater absorption relative to the overtone and combination bands in the near-infrared. This allows for (a) more sensitive detection and/or (b) detection at shorter pathlengths. Increasingly convenient access to the mid-infrared has enabled new applications of LAS in short path-length combustion systems that were simply not feasible in the near-infrared nor were conducive for studying via fixed-wavelength mid-IR gas lasers (e.g., HeNe near 3.39 μm, CO near 5 μm, CO₂ near 10.6 μm). For example, the high-fidelity measurements of CO in scramjet [236] and detonation combustors [237,238] were made possible through the use of quantum-cascade lasers enabling access to 10^4 times greater absorption strength compared to that accessible via telecommunication-grade lasers. More of these new applications are highlighted in the latter part of this paper. Here we offer brief descriptions of key hardware for laser absorption in the mid-IR, with a focus on recent advancements.

6.2.1. Quantum cascade lasers (QCLs)

QCLs are semiconductor lasers that can emit in the mid-infrared to far-infrared (≈3.5 to 100 μm) with similar tuning capability and usability to room-temperature diode lasers. Unlike diode lasers the

emission wavelength is not purely a material property (i.e. band gap), but rather the result of an engineered superlattice, a layered composite of semiconducting materials that introduces a variable electric potential across the length of the system. Electron transitions and photon emission occur and cascade (via tunneling) between the subbands of each layer. The respective energy levels between each layer and emission wavelength depend on the respective layer thicknesses and can be designed to cover a broad spectral region with a given material set. The first demonstration of the quantum cascade laser occurred at Bell Laboratories in 1994 [239]. Rapid improvement in manufacturing and lasing properties (i.e., tuning range, efficiency, power) has followed [240–242]. Similar to diode lasers, wavelength tuning of a QCL can be achieved with a distributed feedback or external cavity architecture, with the latter offering greater range (≈100 cm⁻¹) at the expense of slower tuning and reduced scan-to-scan repeatability. Both tuning architectures can provide narrow linewidth emission (<5 MHz), suitable for the LAS techniques discussed previously. QCLs are now available for a wide range of wavelengths from multiple vendors (e.g., Alpes, Adtech, Daylight Solutions, Hamamatsu, Pranalytica).

6.2.2. Interband cascade lasers (ICLs)

ICLs leverage interband transitions and electron-hole recombination similar to a diode, but also use a layered heterogeneous band-structure to achieve cascading of photon emission similar to a QCL. As such, ICLs may be viewed as a hybrid of conventional diode lasers and quantum cascade lasers. The use of interband transitions (as opposed to intersubband transitions) allows for lower electrical input powers compared to QCLs, but also yields a more narrow range of wavelengths over which lasing can be achieved at room temperature (≈2.9 to 5.7 μm) [243]. Invented around the same time as the QCL was demonstrated [244], the first continuous wave ICL was demonstrated in 2008 [245]. Subsequent advancements in tuning response and efficiency [246,247] have enabled commercially available, compact, narrowband DFB ICL lasers that fill a gap (≈3 to 4 μm) in the mid-wave infrared between conventional room-temperature diodes and quantum-cascade lasers. This region is especially important to combustion due to the very strong C-H stretch vibrational mode common to all hydrocarbons near 3.4 μm.

6.2.3. Optical fibers

Since conventional silica-based fibers do not transmit light beyond ≈ 2.3 μm, alternatives are required for the mid-IR. Fiber materials for the mid-infrared are more expensive, generally less robust mechanically, and have higher attenuation, thus limiting the length that is acceptable for meaningful transmission levels. However, bend and injection losses are often more important than transmission loss for the relatively short fiber length (<100 m) needed to remotely locate combustion sensors. With increasing demand for mid-IR fibers, a number of materials have matured commercially in the last fifteen years or so [248,249]. At present, several types of mid-infrared fibers are available for use in harsh environments. Fig. 16 highlights some of these fiber materials and their respective transmission spectra in the infrared. Two of the more attractive fiber types are fluoride glasses (ZBLAN and InF₃) and hollow-core waveguides. Both fiber types are mechanically more robust than chalcogenide, which is known to be brittle [250] and together offer transmission across a broad wavelength range from ≈2 to 12 μm. The fluoride glass fibers offer lower attenuation than the hollow-core waveguides in the 2 to 5 μm wavelength domain and are available in greater lengths (>5 m). The fluoride glass fibers are also available as single-mode and were successfully utilized for multiple projects highlighted in this paper (for example see Section 13.1). The hollow-core waveguides offer transmission over a broader wavelength range compared to the fluoride glasses and also typically come in larger diameters for ease of coupling which is especially

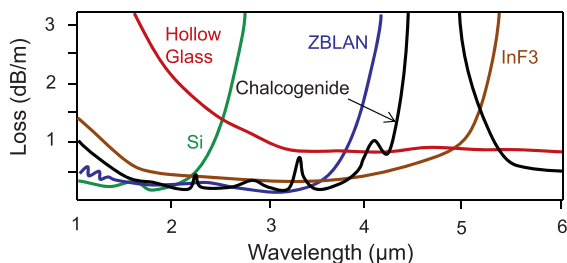


Fig. 16. Transmission loss of various mid-IR optical fibers as a function of wavelength. Figure adapted from [164].

needed for non-Gaussian beams. Additionally, because there is no solid core to the fiber, there is less risk of spurious back reflections that often occur during fiber coupling and lead to wavelength and intensity jitter. The hollow-core fibers do tend to induce substantial light attenuation when bent and may require purging to avoid absorption due to ambient CO₂ and H₂O.

6.2.4. Detectors

Indium-antimonide (InSb) and mercury-cadmium-telluride (HgCdTe or MCT) are the most common semiconductor materials used for mid-infrared detectors. These detectors are available in both photoconductive and photovoltaic operation modes. In the former, the electrical resistance is influenced by the incident photons and, in the latter, current is generated by the photoelectric effect. For these mid-IR materials, photovoltaic operation is typically preferred due to its lower dark current. InSb photovoltaic detectors are sensitive from ≈ 1 to $5.5 \mu\text{m}$ and must operate at cryogenic temperatures ($\approx 80 \text{ K}$); they are typically packaged with a dewar for liquid-nitrogen cooling. MCT detectors (photovoltaic or photoconductive) can be sufficiently cooled thermo-electrically providing for a more portable and less cumbersome package that can be mounted at any orientation, which is useful for engine sensing applications. The amount of cadmium in the MCT alloy can be chosen to tune the sensitive wavelength region within a broad range of ≈ 2 – $15 \mu\text{m}$. However, it is worth noting that the dark current rises when tuning the MCT's responsivity to longer wavelengths. For the mid-wave IR (3– $5 \mu\text{m}$), InSb detectors tend to outperform MCT with regards to signal-to-noise ratio, but advances in multi-stage thermo-electric cooling schemes have reduced this advantage. It should be noted that both IR detector materials are susceptible to spatially non-uniform response in the active region. Selection of an appropriate mid-IR detector involves a tradeoff in size/area, sensitivity, and bandwidth requirements for a given application.

6.2.5. Optical materials

Table 3 lists a number of common optical materials (frequently used as windows) that transmit in the infrared. Quartz, or fused silica (SiO₂), is the most common and inexpensive optical material, but it only transmits up to $\approx 3.5 \mu\text{m}$, thus it is not suitable for sensing in

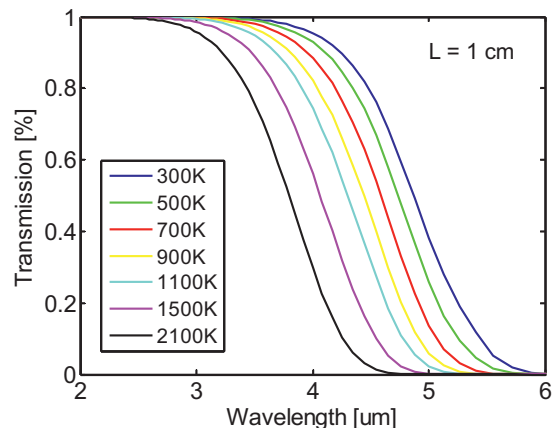


Fig. 17. Transmission through a 1 cm thick sample of sapphire as a function of wavelength for various temperatures. Results were calculated using the model presented in [251]. Figure adapted from [164].

most of the mid-infrared. Sapphire (Al₂O₃) is an excellent material for harsh environments due to its superior strength and high melting point, which makes it suitable for most high-pressure combustion applications. Sapphire also has relatively high thermal conductivity and low thermal expansion, making the material highly resistant to thermal shock. For many cases, sapphire is the ideal material selection for optical ports/windows in high-temperature gas flows. However, sapphire transmission degrades around $5 \mu\text{m}$ and the transmission cutoff has a strong temperature dependence. This should be considered when designing an LAS sensor for CO₂ ($\approx 4.3 \mu\text{m}$), CO ($\approx 4.8 \mu\text{m}$), or NO ($\approx 5.2 \mu\text{m}$) at high temperatures. An empirical model of the temperature-dependent transmission of sapphire was developed by Thomas et al. [251], and results are shown in Fig. 17 for a temperature range of 300 to 2100 K with a window thickness of 1 cm. If probing a wavelength in the ≈ 3.5 to $6 \mu\text{m}$ domain, it is important to understand that time-varying transmission may occur (e.g., during thermal transients) if using the diagnostic in a high-temperature system.

Transmission cutoffs aside, quartz and sapphire are the best infrared materials for spectroscopic windows on harsh combustion systems and should be used when feasible. Other classes of mid-infrared optical materials are less robust than quartz or sapphire but may be needed for transmission beyond $5 \mu\text{m}$. The fluoride crystals including BaF₂, CaF₂, and MgF₂ have broad transmission from the ultra-violet up to $12 \mu\text{m}$ (in the case of BaF₂) and low indices of refraction ($n_{\text{refractive}}$) which helps mitigate back reflections and etalons, but they are somewhat weak and highly susceptible to thermal shock due to their large thermal expansion coefficients. Furthermore, when heated the fluoride crystals become relatively hygroscopic and are not recommended for use in moist environments above 800 K. Zinc Selenide (ZnSe) and Zinc Sulfide (ZnS) offer even broader transmission into the far-infrared (up to $20 \mu\text{m}$). They are a bit stronger than the fluoride crystals, and offer greater resistance to thermal shock, but are relatively brittle. Perhaps most problematic for high-temperature applications, these zinc materials oxidize above 500 K. The surface reaction issues with both the fluoride and zinc optical materials may be resolved with high-temperature coatings. Germanium and Silicon are also good infrared optical materials at room temperature, but these materials rapidly become opaque as temperature is elevated [252]. It should be noted that for shock tube applications, the windows are only exposed to a high temperature gas for a very short time period (order of ms), thus many of these temperature-dependent issues are less important, since minimal heat transfer occurs during that time.

Table 3
Properties of mid-infrared optical materials.

Material	$\lambda_{\text{low}} [\mu\text{m}]$	$\lambda_{\text{high}} [\mu\text{m}]$	$T_{\text{melt}} [\text{K}]$	$n_{\text{refractive}}$	$E_{\text{rupture}} [\text{ksi}]$
SiO ₂	0.16	3.5	1980	1.5	7
Al ₂ O ₃	0.17	5	2300	1.75	65
BaF ₂	0.15	12	1620	1.45	3.9
CaF ₂	0.15	8	1700	1.4	5.3
MgF ₂	0.13	7	1520	1.35	7.2
ZnSe	0.55	20	1800	2.4	8
ZnS	0.38	14	1450	2.5	8.7
Ge	1.8	21	1200	4	7
Si	1.2	10	1690	3.5	18.1

6.3. Emerging sources

This section will discuss several novel light sources and/or techniques that have recently been developed and demonstrated in IR-LAS sensors. These methods have been shown to offer improvements in measurement rate, spectral bandwidth, and measurement fidelity.

6.3.1. Chirped QCLs

While chirped quantum-cascade laser absorption (QCLAS) is not particularly new [253,254], and others have applied it to study combustion gases [255], Chrystie et al. [256] recently demonstrated the first use of a chirped-QCL (near 7.62 μm) for measurements of H_2O and temperature at rates as high as 3.125 and 0.25 MHz, respectively. The authors demonstrated this technique with measurements acquired in a static cell at known conditions and behind reflected shock waves in a reacting gas, thereby demonstrating the utility of this method for studying highly transient combustion processes (e.g., chemical kinetics). The ability to acquire calibration-free species and temperature measurements at MHz (or near) rates that employ wavelength tuning for increased robustness represents a significant advancement. This achievement has the potential for offering improved understanding of a variety of highly-transient combustion processes.

This technique operates by pulsing a QCL's current with a high-frequency, long-duration squarewave which, within the pulse, rapidly increases the temperature of the laser causing its wavelength to vary (i.e., *chirp*). In LAS applications, the pulse duration and amplitude are specified such that the laser's wavelength chirps (i.e., tunes) across an absorption transition analogous to scanned-wavelength direct-absorption experiments. In this method, a primary concern is the chirp-induced broadening of the laser linewidth. The greater the chirp rate, the greater the instantaneous linewidth and the lower the resolution. The work reported in [256] exhibited chirp rates from 20 to 60 MHz/ns yielding spectral resolutions of 0.013 to 0.021 cm^{-1} and was ultimately the limiting factor preventing faster thermometry measurements (since a greater chirp rate is needed to scan across two transitions). These concepts are illustrated in Fig. 18.

6.3.2. Frequency comb spectrometers

Frequency combs are an emerging class of lasers that simultaneously emit a multitude of evenly spaced individual wavelength elements (i.e., comb teeth). Recently, Rieker et al. [135] used a dual-comb spectrometer (DCS) to measure gas temperature, H_2O , HDO, CO_2 , $^{13}\text{CO}_2$, and CH_4 simultaneously across a 2 km open path through the turbulent atmosphere. The DCS spanned 1600 to 1670 nm with 80,000 comb teeth and a tooth spacing of 100 MHz. The authors reported one-sigma variations of <1 ppm for CO_2 and <3 ppb for CH_4 after 5 min of signal averaging, and absorbance noise levels of 5×10^{-4} over longer averages.

The operating principles of DCS are shown in Fig. 19 (taken from [135]). In DCS, two frequency combs with teeth at optical frequencies (i.e., in the THz regime) are locked together with a fixed offset (Δf_i) in their repetition rate (f_r). These combs are combined together to create a rf-comb (via heterodyning) where each tooth (in the MHz regime) exhibits a one-to-one relationship with its corresponding pair of THz teeth that are attenuated according to Beer's Law and the absorbance spectrum of each chemical species in the test gas. The measured detector signal therefore yields an interferogram which can be processed to yield a measured transmission and absorption spectrum.

DCS offers a number of unique capabilities including broad spectral coverage (e.g., 5990 to 6260 cm^{-1} in [135]), ultra-narrow linewidth (order 1 Hz per comb tooth), and precisely known absolute wavelength (frequency of each tooth known to better than 1 kHz). These attributes make DCS an ideal tool for high-fidelity

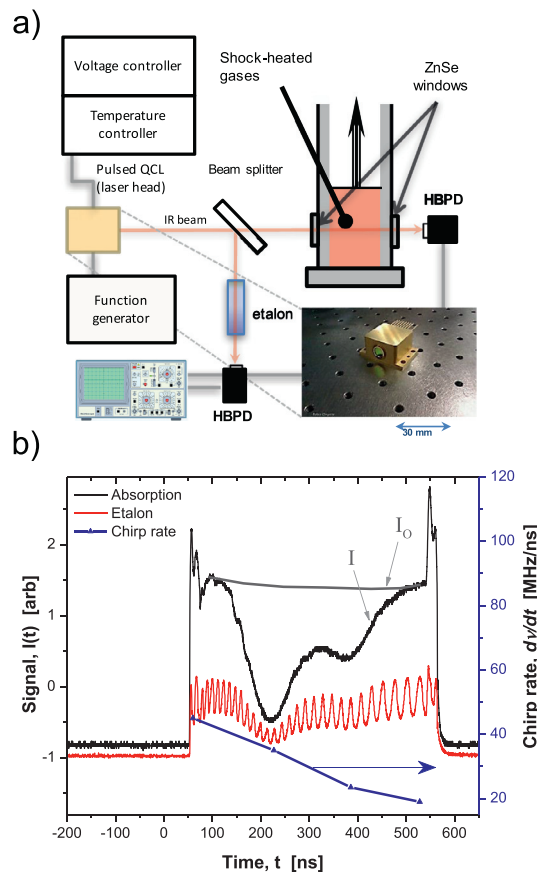


Fig. 18. Schematic of experimental setup for chirped QCLAS (a) and example of raw transmission data for a single pulse chirped across H_2O absorption transitions near 7.6 μm (b). Figures adapted from [256].

measurements of molecular spectra and are in stark contrast to several other hyperspectral sources (e.g., FDML, Supercontinuum) that exhibit comparatively broad linewidths (on the order of 0.1 cm^{-1}) or lack wavelength stability (e.g., external cavity quantum-cascade lasers). These benefits, however, currently come with the requirement to average many pulses which reduces the ultimate measurement rate. Regardless, it is clear that DCS-based sensors offer great potential to expand the measurement capabilities offered by more established IR-LAS technologies.

During the compilation of this manuscript, Schroeder et al. [257] presented the first use of a DCS sensor in an industrial environment. The authors presented measurements of temperature, H_2O , and CO_2 at 0.1 Hz in the exhaust of a 16 MW gas turbine, thereby demonstrating the potential of this technology to be applied to a wide range of practical combustion systems. In addition, it should be noted that other methods for comb spectroscopy exist that rely on traditional grating-based spectrometers or Fourier transform spectrometers. This technique was recently used to measure H_2O in a laboratory flat-flame burner [153].

6.4. Compact sensors

The need to characterize combustion systems with limited optical access has driven the development of numerous compact LAS sensors [42,177,202,206,212,258–266] and the majority of these sensors have leveraged robust telecommunication-grade optical hardware. Specifically, Wehe et al. [258,259] embedded a diode-laser-based sensor into a probe for gas temperature, velocity, and H_2O in hypervelocity flows, Schultz et al. [262] and Strand and Hanson [263] developed fiber-coupled sensor packages for model scramjets housed in vacuum chambers, Ebert et al. [266] and Whitney

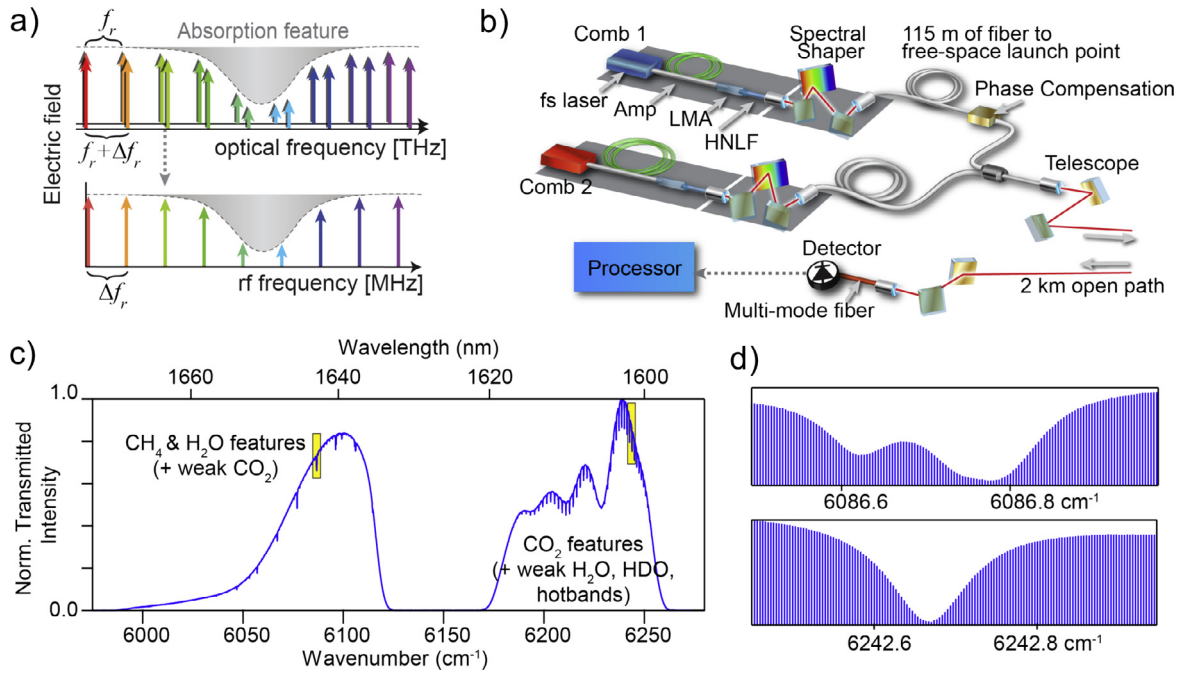


Fig. 19. Frequency spectrum of DCS interrogating an absorption transition (a), schematic of experimental setup (b) and example transmission spectra (c) and (d). Figures adapted from [135].

et al. [206] developed compact arrangements for providing line-of-sight access in IC engines, and Caswell et al. [212] developed a fiber-optic package providing counter-propagating beams for facilitating velocimetry sensing. While the aforementioned examples are certainly compact compared to other laser-diagnostic techniques (e.g., PLIF, CARS), this section will highlight only the most compact sensors, specifically, single-ended LAS sensors.

6.4.1. Probe-based single-ended sensors

Several researchers have developed single-ended probes for studying IC-engines via IR-LAS [42,260,261,267–269]. Hall and Koenig [267] were the first to implement IR fibers into a spark-plug probe (similar to that shown in Fig. 20) for delivering and receiving IR light. The authors used a broadband IR source to monitor the absorption of fuel from 3.3 to 3.5 μm, thereby enabling monitoring of the fuel-air ratio near the spark plug. A similar configuration and diagnostic technique was more recently used by Cundy et al. [269]. Tomita et al. [268] used a similar probe design, but used two sapphire rods cleaved at 45° to direct light in and out of the engine and used a HeNe near 3.39 μm to monitor fuel absorption. More recently, Rieker et al. [42] integrated a fiber-coupled WMS-1f/1f-based TDLAS sensor into a spark plug and demonstrated crank-angle resolved measurements of temperature and H₂O concentration in motored and fired tests. The sensor used a SMF to pitch laser light

near 1.4 μm across a 6 mm gap and a small mirror was used to reflect light back towards a multi-mode catch fiber (see Fig. 20). Jeffries et al. [260] later used a similar probe for crank-angle-resolved mid-IR measurements of gasoline. The authors used a fiber-coupled DFG technique to generate two colors near 2951 and 2970 cm⁻¹ for exploiting the strong C-H stretch absorption band for high-sensitivity measurements of gas temperature and gasoline concentration. The injection current of each pump laser was modulated at a unique frequency to enable frequency-multiplexing and demultiplexing of each color with a sensor bandwidth of 10 kHz. The WMS-1f signal of each laser was then extracted via post-processing using digital lock-in amplifiers and the two-color ratio of WMS-1f signals was used to calculate temperature analogous to as done in fixed-wavelength direct-absorption techniques. Details regarding the development of this sensor can be found in [218] and quantitative measurements of gasoline were enabled via a spectroscopic model developed by Klingbeil et al. [44]. Fig. 21 illustrates time-resolved measurements of gasoline concentration acquired at pressures up to 40 atm during fired operation. Measurements of air-fuel ratio acquired during operation agreed well with the air-fuel ratios inferred from analysis of independently acquired exhaust emissions measurements. In

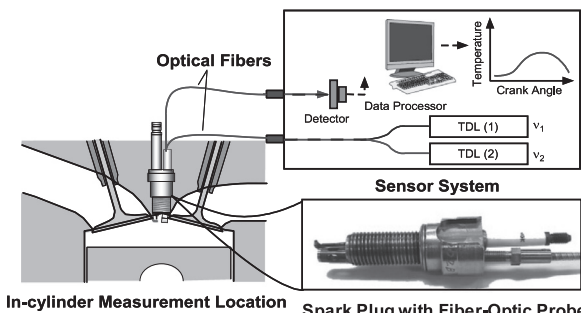


Fig. 20. Schematic of fiber-coupled TDLAS temperature and H₂O sensor embedded into a spark plug. Figure adapted from [42].

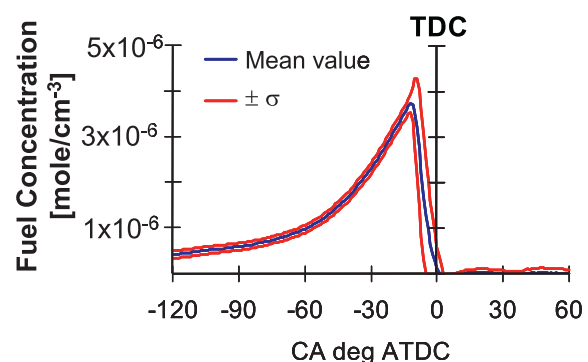


Fig. 21. Time-resolved measurements of gasoline concentration acquired near spark plug using WMS-1f sensor during fired operation. Figure adapted from [260].

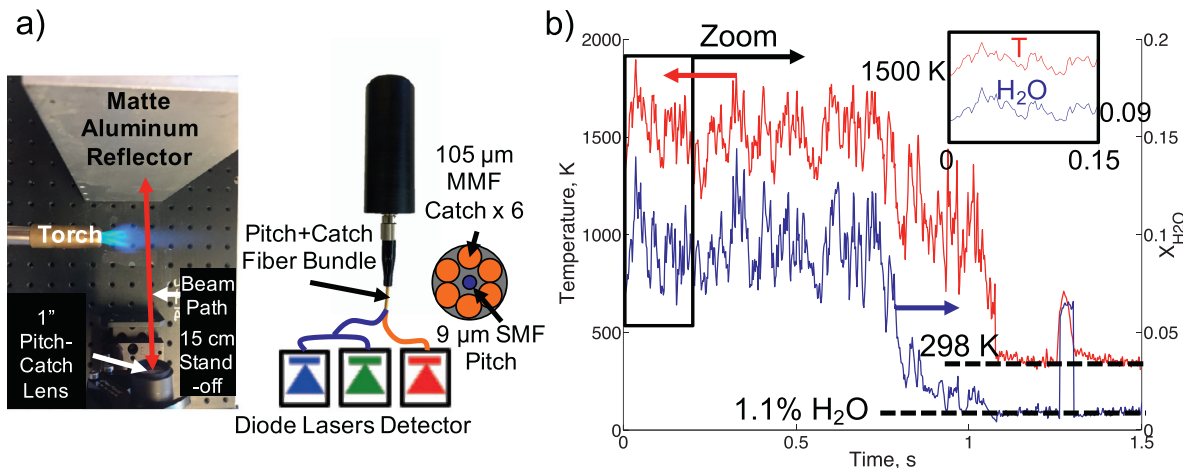


Fig. 22. Schematic of a single-ended LAS sensor using a fiber-bundle (a) for stand-off measurements of gas temperature, pressure, and H_2O near $1.4 \mu\text{m}$ (b). Figures adapted from [265].

addition, Rein and Sanders [261] also used a similar probe in an IC-engine, but used a fiber-coupled FTIR spectrometer to measure H_2O , CO_2 and temperature. While useful, the primary disadvantage of all the aforementioned designs is that probes can perturb the local flow field and heat transfer to the probe surfaces can influence the local gas temperature and perturb the local chemistry.

6.4.2. Single-ended sensors using native surfaces

Due to the intrusive nature of probes, several researchers have recently developed single-ended LAS sensors relying on backscattering off native surfaces (e.g., a combustor wall) [202,264,265]. Wang and Sanders [264] recently demonstrated a single-ended near-IR LAS sensor for monitoring H_2O near $1.4 \mu\text{m}$ with scanned-WMS-2f/1f. They showed that WMS-2f/1f with $f = 100 \text{ kHz}$ was able to reject speckle noise and demonstrated accurate measurements off a rough moving surface indicating a similar sensor package could be deployed in an engine/combustor with moving parts. Goldenstein et al. [265] developed a single-ended, fiber-coupled near-IR diode-laser sensor for stand-off measurements of gas temperature, pressure, and composition using scanned-WMS-2f/1f. This sensor employed a fiber-bundle with 6 multi-mode catch fibers surrounding a single single-mode pitch fiber housed in a 25.4 mm diameter lens tube. This configuration was shown to provide collection efficiencies (fraction of incident photons collected) from 1 to 10^4 parts-per-million at stand-off distances from 10 m to 10 cm, respectively. The sensor was demonstrated with measurements of temperature, pressure, and H_2O in a flame at a stand-off distance of 15 cm and CH_4 at a stand-off distance of 10 m. Diode lasers near $1.4 \mu\text{m}$ and $1.65 \mu\text{m}$ were used to interrogate H_2O and CH_4 transitions, respectively. A schematic showing the sensor package is shown in Fig. 22. Most recently, Rein et al. [202] deployed a single-ended, fiber-coupled MEMS VCSEL sensor operating near $1.4 \mu\text{m}$ for measurements of temperature and H_2O at 100 kHz in a rotating-detonation combustor (RDC). This sensor utilized a single-mode pitch fiber and multi-mode catch fiber housed side-by-side in the fiber bundle developed by Caswell et al. [212] (see Fig. 23) to transmit and receive laser light reflected off the RDC center-body. A single lens was used to collimate the incident light and collect the backscattered light after traversing 1.52 cm (round trip) through the test gas.

During the revision of this manuscript, Peng et al. [270] presented the first demonstration of single-ended mid-IR sensing of combustion gases. The authors utilized a hollow-core fiber bundle to deliver mid-IR laser light near 2.5 , 4.2 , and $4.8 \mu\text{m}$ to a test article, and used a cage-system-based optical package (capable of being mounted

directly to an engine) to collect and demultiplex the backscattered laser light onto two detectors. This sensor was demonstrated with simultaneous time-resolved measurements of temperature, H_2O , CO , and CO_2 in a laboratory flame.

7. Sensor-design process

The design of modern IR-LAS sensors for combustion systems is a complex process with many factors to consider. While much of this complexity results from the need to overcome fundamental measurement challenges (discussed in Section 5) within the constraints of a specific problem, some of it arises from the immense freedom today's researchers have when designing such a sensor. In all cases, the sensor-design process is immediately constrained by the measurement needs for the application/problem of interest, and many excellent papers have been devoted to describing the design process of a given tailor-made sensor (see manuscripts highlighted in the following sections). That said, the goal of this section is merely to put forth a high-level roadmap for guiding the design of an IR-LAS sensor for a general combustion application/problem.

7.1. Identify measurement needs and challenges

The sensor-design process should always begin by identifying the measurement needs and challenges. The former of these is the most obvious, as it is typically set by the sponsor or question driving the research. The measurement needs for a given application typically

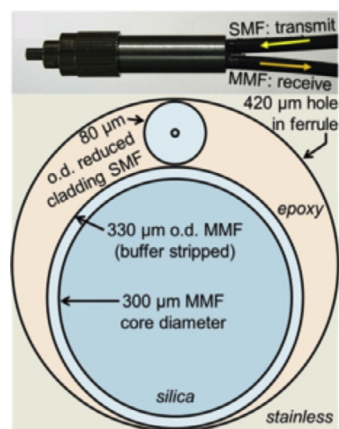


Fig. 23. Schematic of dual fiber-optic used to acquire single-ended measurements of gas temperature and H_2O in a rotating-detonation combustor in [202]. Figure adapted from [212].

define: (1) the range of thermodynamic conditions and species concentrations of interest, (2) the measurement bandwidth needed to resolve the transients of interest, (3) the optical path length, and (4) environmental factors. The measurement challenges can be harder to identify; however, common challenges are: (1) achieving optimal absorbance levels and temperature sensitivity, (2) avoiding interfering absorption and emission, (3) using techniques and spectroscopic models that accurately account for collisional broadening, (4) using methods that are insensitive to or, account for, line-of-sight non-uniformities (if present), and (5) using diagnostic techniques and optical assemblies that are insensitive to beam steering and non-resonant transmission losses. Solutions to these problems are continually evolving; however, [Section 5](#) discusses several state-of-the-art solutions to the aforementioned problems and others. Many of these solutions rely on intelligent selection of wavelengths, hardware, and IR-LAS technique; the general approach to each is discussed next.

7.2. Selection of wavelength, hardware, and LAS technique

With the measurement needs and challenges understood, the next step should be to identify the wavelength(s) that are optimal for the application and measurements of interest. The primary goal should be to identify wavelengths that provide optimal absorbance levels (≈ 0.1 to 3) while maintaining sensitivity to the measurement targets (e.g., temperature) and avoiding interfering absorption. At pressures where individual transitions can be easily resolved, this is a relatively straightforward process (e.g., see [221]) and robust single line-of-sight solutions have even been developed to account for pronounced line-of-sight non-uniformities (see [Section 5.1.1](#)). More complicated wavelength-selection routines are more appropriate when the spectra-of-interest are significantly blended (e.g., at high pressures) and/or hyperspectral sources are used (see [Section 5.3](#)).

During the wavelength-selection process one must simultaneously consider the ramifications associated with working in different spectral regions. Perhaps most importantly, one must realize that the capabilities and limitations of light sources, fibers, and detectors can vary greatly throughout the near-IR, let alone the entire IR. For example, while injection-current tunable DFB TDLs, ICLs, and QCLs are now readily available from ≈ 0.8 to $16\text{ }\mu\text{m}$, their tuning abilities, optical powers, and stability vary significantly. Further, the current capabilities of optical fiber vary greatly with wavelength and, in general, become less robust and more inefficient when going deeper into the IR. These differences alone may render the optimal wavelength region inaccessible for a given application or problem. These issues and others are discussed in detail in [Section 6](#).

Further complicating matters, the light sources and, perhaps, detectors that are suitable for a given wavelength region are likely not compatible with all IR-LAS techniques. For example, hyperspectral sources are currently not readily available in the mid-IR which currently limits these techniques to species with strong near-IR absorption bands and/or in applications with relatively large path lengths. In contrast, lasers suitable for scanned-DA and WMS (e.g., DFB or external cavity TDLs, VCSELs, ICLs, and QCLs) are currently available throughout the majority of the IR, making these techniques widely applicable. That being said, in the vast majority of hostile combustion applications we elect to use WMS- $2f/1f$ techniques due to its noise rejection benefits and insensitivity to non-absorbing transmission losses; however, in cases with large SNR, scanned-DA remains an attractive technique due to its reduced complexity. In the near-IR, WMS- $2f/1f$ and hyperspectral absorption have repeatedly demonstrated the ability to provide high-fidelity measurements in a wide range of harsh combustion systems (e.g., power plants, detonation combustors etc.), many of which are highlighted in the sections that follow. As a result, in this wavelength region choosing between these two methods is largely a question of personal

preference and expertise. However, if sensor cost and longevity are a concern, WMS-based sensors employing telecommunication-grade TDLs are currently a better option in this regard.

In short, the design of virtually all IR-LAS sensors involves a variety of trade-offs and a silver-bullet solution does not currently exist. As light sources and optical components continue to evolve, so will the choice of sensors that are optimal for a given application and problem. The remainder of this manuscript will highlight recent works that advanced the current state of IR-LAS sensing in combustion applications.

8. Sensors for fundamental combustion chemistry studies

Here we begin our review of recent applications of IR-LAS for studying combustion gases with an overview of sensors used for investigating combustion chemistry. These systems include various flame apparatuses as well as shock tubes, where the primary goal is the determination of fundamental rate constants or insights about reaction pathways that describe the kinetic behavior of fuels or fuel byproducts.

8.1. Shock tubes

Studies of chemical kinetics in shock tubes have driven the development of a wide range of IR-LAS sensors. Shock tubes provide exceptionally uniform properties along the line-of-sight and are relatively quiescent (compared to most combustion flows), providing ideal conditions for high-fidelity time-resolved LAS measurements of species and gas properties. In reciprocity, species time histories, especially those with multiple time-scales, place internal constraints on combustion kinetics models that are more rigid than global parameters such as ignition delay times, and have led to significant advances in the modeling of combustion chemistry [271]. As such, the application of infrared LAS in the context of shock tube kinetics has a rich history that has been discussed in other review papers, including the recent paper by Hanson and Davidson [127]. Here we highlight only very recent works in order to identify emerging areas in IR-LAS for combustion. Several of these works were first developed and demonstrated on shock tubes prior to utilization in other environments.

8.1.1. Thermometry

In chemical-kinetics studies, accurate knowledge of temperature is critical for the determination of rate constants due to their exponential temperature dependence described by the Arrhenius equation. In shock tubes, test temperature can be well-defined ($\approx 1\%$ uncertainty) by the measurement of incident shock velocity and utilization of the normal-shock relations. However, in experiments with transient temperature, only the initial value is well known by this method, and there are also cases where temperature measurements better than 1% uncertainty are desired as temperature may still be the largest uncertainty factor when propagated to a measured rate constant. Given the relative importance of temperature, a number of efforts over the past ten years have been dedicated to providing a sensitive LAS-based thermometer for shock-tube studies. Several nascent combustion species (e.g., H_2O , CO, NO and CO_2) that are infrared active have been investigated for two-color thermometry, with reported uncertainties ($\approx 1\%$) that are competitive with the conventional approach while also providing time-resolved data for transients [105,272,273].

H_2O and CO_2 have received perhaps the most attention for shock tube thermometry, being relatively chemically inert and major combustion products that can also be seeded into an initial reactant mixture. The mid-infrared spectra, and recent advances in laser technology in this domain, has enabled notable progress in the development of LAS sensors interrogating these species. Farooq et al.

[102,274] and Ren et al. [275] utilized the CO₂ spectra near 2.7 μm for temperature sensing behind reflected shock waves using two-color wavelength-modulation spectroscopy. Spearrin et al. [103,276] later introduced a cross-band thermometry technique for CO₂ that leverages the inverse temperature dependence of two lines from the 2.7 μm and 4.2 μm vibrational bands, respectively, for enhanced sensitivity and a broader temperature range. Recent efforts for H₂O thermometry include a pulsed-scanning, or intra-pulse chirp method, developed by Chrystie et al. [256] to resolve H₂O lineshapes near 7.6 μm as already discussed in Section 6.3. It is worth noting that Uddi et al. [277] used a QCL near 7.6 μm to measure H₂O and temperature at up to 20 bar in a rapid-compression machine; however, this work employed scanned-wavelength direct absorption with much lower time resolution (200 Hz). Campbell et al. [276] has further shown that scanned-WMS may be used for partially-resolving H₂O lineshapes while still temporally-resolving temperature transients behind reflected shock waves. Though both species (CO₂ and H₂O) are very useful, CO₂ does not readily adsorb to surfaces and has a much higher vapor pressure, making it easier to seed into a gas mixture.

8.1.2. High-pressure studies and sensor development

Species sensing at high pressures is another important capability for shock tube studies (as well as other combustion experiments) as most practical combustion devices operate at tens or hundreds of atmospheres, and there is a need for improving our understanding of kinetic behavior in this domain. LAS is inherently more challenging to implement at elevated pressures due to lineshape broadening and the associated blending of many spectral lines that complicate the interpretation of an absorption measurement, not to mention the practical challenges of increased beam steering and boundary layer effects. It can be quite challenging to validate absorption models (a prerequisite for quantitative LAS) at high-pressure and high-temperature conditions as creating a controlled, well-known environment at these extremes is difficult. Shock tubes serve an important role in this regard since temperature and pressure can be known quite well behind the reflected shockwave (albeit for short time) in a non-reactive experiment. Further, the impulsive nature of the experiment also lends to greater safety than static or steady-flow experiments since the extreme conditions behind the reflected shock typically only lasts a few milliseconds. Shock tubes have played an important role in the development of high-pressure infrared LAS diagnostics in recent years, in addition to facilitating kinetics studies. Here we identify a few notable works that extend measurement capabilities to pressures above 10 atm.

The helium-neon gas laser near 3.39 μm has been used for fixed-wavelength LAS measurements of numerous hydrocarbons for fuel

pyrolysis and oxidation studies in shock tubes [278,279]. Similarly, the carbon dioxide gas laser (\approx 10.6 μm) has been used for ethylene measurements at pressures higher than 50 atm [279–281]. Often, these two gas lasers are used simultaneously to observe larger hydrocarbons decomposing into smaller hydrocarbons (e.g., ethylene). Semiconductor diode and quantum-cascade lasers have enabled the detection of several other combustion species at elevated pressures. Farooq et al. [217] demonstrated WMS of CO₂ near 2.7 μm above 10 atm during heptane oxidation in a shock tube. Most recently, Spearrin et al. [101,106] and Goldenstein et al. [203,210] used these tunable sources for acquiring measurements of CO₂, CO, H₂O, and temperature at pressures up to \approx 50 atm in a shock tube, and later applied these sensors to a pulsed-detonation combustor [237]. For thermometry in high-enthalpy air, Spearrin et al. [115] validated and demonstrated a sensor based on NO detection at pressures up to \approx 150 atm in a shock tube using a quantum-cascade laser near 5.2 μm [115]. This sensor inferred the temperature by comparing the measured concentration of NO to that given by temperature-dependent thermochemical equilibrium calculations; example results are shown in Fig. 24.

8.1.3. Fuel intermediates

At high temperatures, large hydrocarbon fuels breakdown into smaller *intermediate* species. Time-histories of fuel intermediates during combustion typically occur on at least two time-scales: formation and decomposition. Multiple time scales provide more rigid constraints for kinetic modeling which makes these species, similar to other intermediates like OH and CO, high-value targets in shock tube studies. Unfortunately, most hydrocarbons have been historically inaccessible in the infrared due to gaps in wavelength coverage for semiconductor lasers despite the strong fundamental vibrational bands such as C-H stretch (\approx 3 μm) and C-H bend (\approx 10–12 μm) that are shared by many important combustion species. Gas lasers such as the HeNe and CO₂ lasers have enabled some species sensing in this domain, but the lack of continuous tuning capability and usual interference associated with a mixture of hydrocarbons has limited the expansion of these LAS methods beyond a few species. Fortunately, the emergence of interband and quantum cascade lasers over the past fifteen years has removed this constraint, providing near continuous wavelength coverage from the near to far infrared (\approx 1–15 μm) via tunable, room-temperature, coherent light sources. Correspondingly, this has led to many new sensors for fuel intermediates.

As mentioned previously, early work in the detection of fuel intermediates for shock tube kinetics studies focused on ethylene due to its importance and abundance in large alkane decomposition pathways and accessibility with a CO₂ gas laser near 10.6 μm

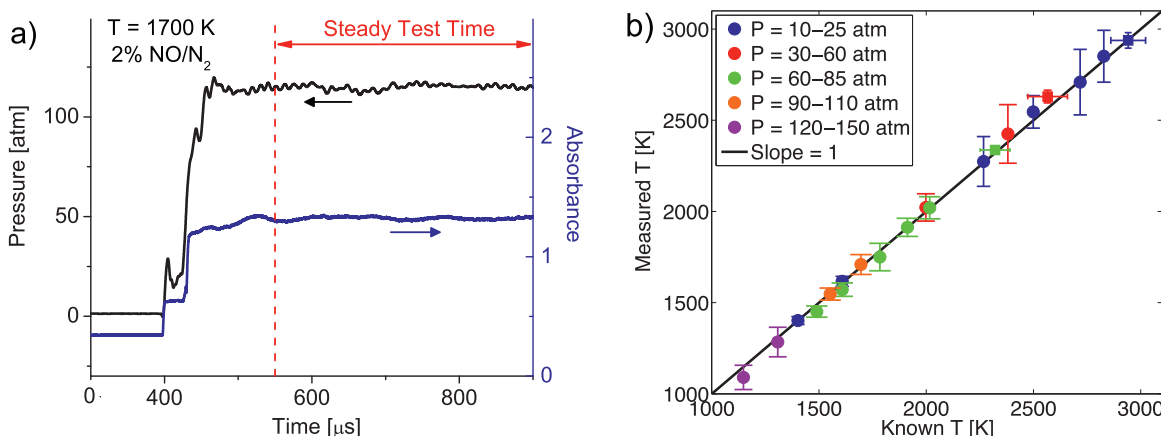


Fig. 24. Measured time history of NO absorption behind a reflected shock wave (a) and summary of thermometry performance (b) for LAS thermometer based on equilibrium of nitric oxide at high pressures (15 to 150 atm) and temperatures. Figures adapted from [115].

[111,281]. This was followed by efforts that utilized difference frequency generation (DFG) lasers to target methane [282] and formaldehyde [283] in the 3.4 to 3.6 μm region. Improved methods for methane detection with regards to interference in combustion gases have more recently been developed by Sur et al. [110] using an interband cascade laser near 3.2 μm and Sajid et al. [109,284] using a quantum-cascade laser near 8 μm . Similarly, interband and quantum cascade lasers have helped expand the list of fuel intermediates measurable in shock tubes to include acetylene [285,286], propene [113], and isobutene [114].

8.1.4. Cavity-enhanced studies

As discussed in Section 4.4, optical cavities can be used to improve the sensitivity of an LAS measurement by increasing the distance over which light interacts with the absorbing species. Increased sensitivity in the detection of a given gas species facilitates improved shock tube experiments in two primary ways. First, experiments may be more highly diluted with an inert bath gas such that the test time involves damped transients of temperature and pressure when reaction occurs. Damped transients, especially temperature, reduce experimental uncertainties. Second, enhanced sensitivity allows for the detection of certain species that may have been considered infeasible over the typical inner diameter of a shock tube ($\approx 10 \text{ cm}$).

Several variations of cavity-enhanced absorption have been deployed in shock tubes. Sun et al. has demonstrated low-finesse, off-axis integrated cavity output spectroscopy for carbon monoxide [159] and acetylene [160] detection in the infrared. Fig. 25 shows the formation of CO from the thermal decomposition of only 10 ppm acetone, thereby highlighting the ability of CEAS to provide high-fidelity species time histories in highly dilute gases. With a cavity-enhanced absorption gain factor of 91, a detection limit of $\approx 100 \text{ ppb}$ of CO was achieved at combustion temperatures using a DFB-QCL near 4.6 μm . Later, Nations et al. [287] used a similar approach to study the formation of excited O-atoms (via low-lying electronic transitions in the IR near 800 nm) behind reflected shock waves at extreme temperatures (5000–8000 K). Additionally, Alquaity et al. [288] utilized a pulsed QCL near 10.6 micron in a cavity-ringdown spectroscopy technique for sensitive measurements of ethylene. Both of these techniques involve replacing the shock tube windows with mirrors that are partially transmissive. Another technique, intra-cavity absorption spectroscopy, does not require high reflectivity mirrors but rather involves gas detection within the cavity of a broadband laser. Fjodorow et al. recently demonstrated this approach to measure acetylene near 1.5 μm in a shock tube using a home-made erbium fiber laser [289].

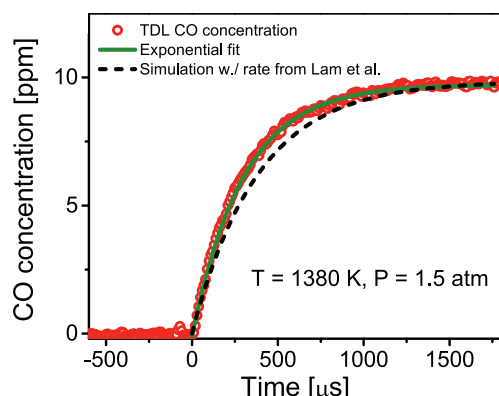


Fig. 25. Formation of CO (red) measured via CEAS during thermal decomposition of acetone behind a reflected shock wave. Figure adapted from [159]. (Please consult the web version of this article to clarify the references to color within the legend.)

All of these cavity-enhanced techniques require more complex alignment than conventional LAS and take advantage of the relatively quiescent environment behind a reflected shock wave. As such, their extension to more harsh combustion conditions has promise, but comes with additional practical challenges.

8.2. Laboratory flames

Laboratory flames, ranging from low-pressure flat-flame burners to high-pressure flow reactors, are used for the study of combustion chemistry primarily by assessing the variation of species and gas properties in space (along the axis of flow), as opposed to time for shock tubes. Historically, species measurements in flames have typically been acquired using gas chromatography (GC) and mass spectrometry (MS) methods coupled with sampling probes. A number of chemistry studies using low-pressure burners have also leveraged ultraviolet laser absorption and fluorescence measurement techniques, but the implementation of IR-LAS has been sparse. A few recent efforts are discussed here.

Similar to shock tube studies, temperature is a critical parameter for interpreting the chemistry governing flames. Li et al. [290] introduced an H₂O two-line thermometry technique near 2.9 μm for low-pressure flames and demonstrated this with measurements of spatially resolved temperature and H₂O concentration in methane-fueled flames. To minimize the influence of line-of-sight non-uniformities, sapphire rods were used to direct the light across a relatively uniform portion of the flame. Smith et al. [177] improved upon this thermometry technique by implementing scanned-WMS spectral fitting and by using two sapphire rods cleaved at 45° to direct light in and out of the flame.

Around the same time, several efforts were conducted to measure C₂H₂ and CO in flames via scanned-wavelength direct absorption. Measurements of C₂H₂ concentration were acquired in both diffusion [291] and laminar flames [292] using a TDL near 1.53 μm , while CO was measured in a counter-flow diffusion flame using a TDL near 2.3 μm . Measurements were acquired at multiple positions to resolve 1D distributions of each species. More recently, Nau et al. [293] used a quantum cascade laser near 4.5 μm to measure CO, CO₂, and temperature in 2D (via tomography) in fuel-rich methane flames. Girard et al. [294] further utilized an interband cascade laser to measure CO₂ and temperature near 4.2 μm in low-pressure methane and ethylene flames over both fuel-lean and fuel-rich conditions. In addition to these studies, which provided insight into 1D-chemistry models, many other IR-LAS sensors have simply been demonstrated in flames. Such demonstrations have been omitted from this section.

9. Sensors for power plants and gasifiers

LAS-based measurements are frequently needed to characterize the behavior of industrial-scale combustion systems since their harsh and often corrosive environment complicates the use of intrusive sensors (e.g., thermocouples, sampling probes). As such, there is a long history of IR-LAS for such systems. To our knowledge, the earliest TDLAS measurements in a large-scale industrial combustor were conducted by Ebert et al. [296] who measured the concentration of O₂ and H₂O in a waste incinerator. This work was followed by TDLS measurements of O₂, CH₄, CO₂, and H₂O in a natural-gas fired power plant [297] and CO and H₂O in a coal-fired power plant [298]. Ebert et al. [299] later used a TDL near 2.3 μm to provide more sensitive measurements of CO in a 3.5 MW waste incinerator and, more recently, Ortwein et al. [300] used a VCSEL near 1.74 μm to measure HCl in a gasification process stream. TDLS sensors for such systems are maturing and Zolo Technology currently provides a commercial sensor for H₂O, CO, O₂, and CO₂ along multiple paths, enabling tomographic reconstruction of the distribution of combustion products

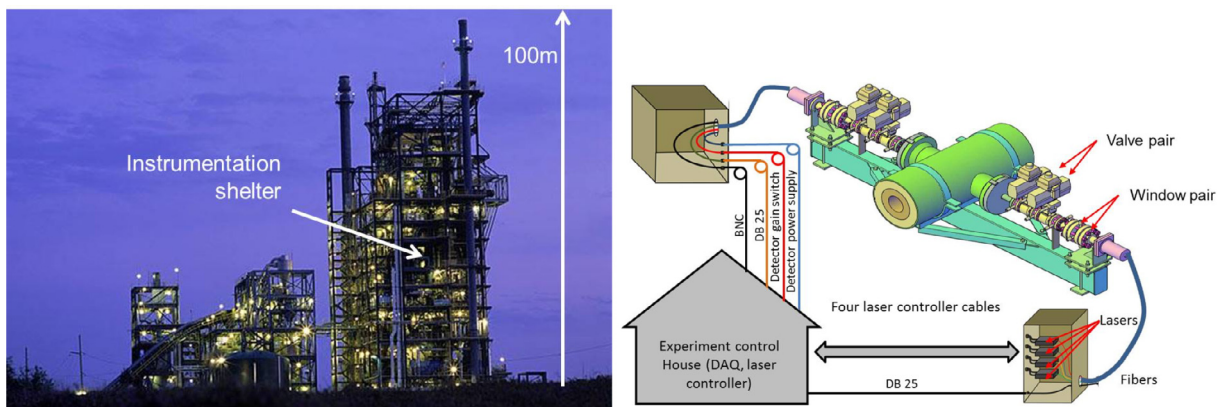


Fig. 26. Photo of the circulating fluidized bed coal gasifier (right structure) and the coal processing and pulverization and preparation plant (left structure) at the National Center for Carbon Capture. The measurement station was located on the 6th floor on piping containing the flow of hot, pressurized gasifier products after fluidized bed particles were removed from the flow. Sketch showing the sensor installation on the process product delivery pipe. Laser light is delivered with a 2 m long fiber bundle, then collimated along a LOS across the gas flow, and focused onto a detector. All ADP was located remotely (≈ 30 m) in an instrument shelter. Figures adapted from [295].

and gas temperature [301]. More recently, measurements of NO and CO were acquired in the exhaust of coal-fired boilers [302,303]. These works discussed and illustrated many of the difficulties of field measurements in industrial-scale combustion applications. For example, combustion-driven power plants and glass furnaces operate continuously for months (or even years) precluding any opportunity to install new window ports or change engineering designs. Again, when the large-scale combustor is heated to operating temperatures, the entire assembly (fire-box, boiler, exhaust ducts) all move significant distances by thermal expansion, and the firewalls were not designed to be mechanically stable requiring at least remotely driven beam alignment and at best an auto-alignment arrangement. Since much of this early work has already been reviewed [2,304], now we will direct our focus to more recent work done in coal-fired power plants and gasifiers.

9.1. Large non-resonant transmission losses

The biggest challenge for LAS sensing in coal-fired systems is to overcome the large non-resonant transmission losses resulting from the heavy loading of particulates (e.g., soot, coal dust, ash). Recently, Sun et al. [305] demonstrated that this challenge could be overcome using WMS-2f/1f which enables calibration-free measurements despite unknown levels of non-resonant extinction (as discussed in Section 4.3 and 5.2). The authors demonstrated measurements of temperature and H_2O in a university-scale coal gasifier despite losing 99.99% of the laser light to particulate scattering.

9.2. Collisional broadening in gases with unknown composition

Another challenge complicating LAS measurements in gasifiers is their high-operating pressures (20 to 50 atm) and the widely variable composition of the product gas. This severely complicates the modeling of absorption spectra and, therefore, quantitative interpretation of WMS-2f/1f signals. Recently this challenge was overcome by Sur et al. [295] by using the scanned-WMS simulation and spectral fitting techniques developed by Sun et al. [138] and Goldenstein et al. [139]. By determining the line broadening *in situ*, these methods enabled quantitative, calibration-free measurements of CO near 2326 nm, CO_2 near 2017 nm, CH_4 near 2290 nm, and H_2O near 1352 nm in the product stream (just downstream of the circulating fluidized bed reactor as marked on the photo on the left side of Fig. 26) of an engineering-scale coal gasifier [295] at the National Carbon Capture Center in Wilsonville, AL. This facility run by the Southern Company for DoE is meant to explore the feasibility of commercial-scale coal gasification for power generation. Fig. 26 illustrates the size of the facility including the coal-pulverization

plant and the gasifier facility. The TDLAS sensor architecture is illustrated on the right side of Fig. 26. The automatic data processing and the laser control electronics were located 30 m away from the measurement location and the lasers were located within 2 m of the window ports due to the lack of quality fiber for the extended NIR wavelengths (2017, 2290, and 2326 nm). Note that higher-quality optical fiber for this wavelength region is now available that would now allow the lasers to be located with their control electronics (30 m from measurement location). Light from the four lasers was combined into a fiber bundle, collimated in free-space and pitched from one side of the process pipe to the other. The four lasers were time-multiplexed to use a single detector and each laser was wavelength scanned and modulated.

The sensor was able to provide time-resolved temperature, CO, CO_2 , CH_4 , and H_2O concentration throughout a 54 day campaign (including a 18-day period of unattended operation) of relatively stable gasification. Typical results are illustrated in Fig. 27. Note the oscillations in time observed for the product gas mole fractions. These unexpected oscillations were correlated with the temperature in the reactor and were synchronous with the batch feeder for pulverized coal injection. The average values of CO, CO_2 and CH_4 measured by the laser absorption sensor were in good agreement with extractive gas chromatography; however, the extractive gas analysis was delayed by ≈ 20 min and had a ≈ 15 min time response due to

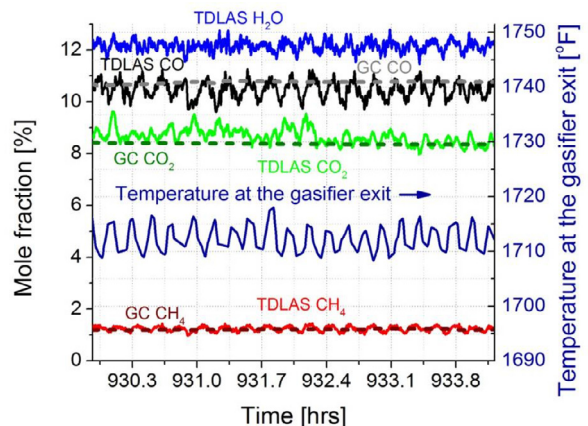


Fig. 27. Scanned-WMS-2f/1f measurements of species mole-fractions (CH_4 , CO_2 , CO, and H_2O) in the exit flow of a coal gasifier. The measurements shown were acquired during the sensor's 39th consecutive day of operation. Also plotted are sampled GC data for CH_4 , CO_2 , and CO, as well as thermocouple measurements of gas temperature acquired at the gasifier exit. The fluctuations in laser-absorption measurements result from actual fluctuations in the composition of the gasifier's product gas. Figure adapted from [295].

the transport of the sampled gas and diffusion in the large conditioning volume (filtering and drying) before the GC. The delay of the sampling system required for GC measurements highlights an advantage of LAS sensing.

Extractive GC measurements are state-of-the-art monitors for combustion-driven power plants and industrial scale gasification. The physical size of these facilities translates into long response times due to the transit time from the extraction point through the sample conditioning (drying and particulate filtering) to the GC. Thus, such sampling systems can provide compliance monitoring for emissions and/or quality measures of the product gas from a gasifier; however, these delays are unsuitable for process control. In the example discussed here, such delays were longer than the fuel-loader cycle time which suppressed the oscillations in gas composition that were more clearly captured by the IR-LAS measurements. The LAS sensors provide the fidelity and time-response needed for process control, and the use of $1f$ -normalized WMS provides a robust defense against transmission losses resulting from time varying particulate scattering, window fouling, and laser aging. The next steps in sensor development involve packaging for commercial use and the development of real time signal analysis software suitable for use by the plant operation staff.

10. Sensors for gas turbines

Several researchers have developed IR-LAS sensors employing a variety of light sources and diagnostic techniques for measuring gas temperature and its non-uniformities, H_2O , CO_2 , and CH_4 in gas-turbine systems. Early work was primarily aimed at characterizing gas-turbine exhaust, some of which pioneered the development of sensors for controlling gas turbines. For example, Seitzman and Scully [168] developed a strategy using a spectrally broad light source near $2.5 \mu\text{m}$ for measuring temperature uniformity and H_2O concentration at the exit of gas turbine combustors, and later this strategy was implemented using diode-laser absorption of three H_2O transitions near $2 \mu\text{m}$ to provide open-loop control of temperature non-uniformities at the exit of a stratified methane-air combustor [171]. Regarding TDLAS sensors, Liu et al. [306] developed a TDLAS sensor for measurements of H_2O and temperature via absorption of two H_2O transitions near $1.4 \mu\text{m}$. This sensor used time-division multiplexing and scanned-wavelength direct absorption, and was demonstrated in the exhaust of an industrial-scale gas turbine coupled to a 20 MW electric generator. Data processing was performed in real-time to provide temperature measurements at 3 Hz. The sensor was validated in controlled static-cell experiments with an accuracy of 2 to 5 K at temperatures from 350 to 1000 K. Around

the same time, Meyer et al. [307] developed a diode laser-based mid-IR source using difference-frequency mixing and demonstrated its use with measurements of CO_2 near $4.5 \mu\text{m}$ in the exhaust of a liquid-fueled model gas-turbine combustor. The use of mid-infrared wavelengths enabled the authors to demonstrate a detection limit of 44 ppm at measurement rates up to 10 kHz.

More recently, gas-turbine sensing has focused on characterizing the fuel loading and combustion processes relevant to lean blowout (LBO), and extending measurements to high-pressure model gas-turbine combustors. These advancements were facilitated through the use of WMS and hyperspectral sources, respectively, and this section will focus on these works. It is also worth noting that hyperspectral laser-absorption tomography was recently used to reconstruct the 2D temperature and H_2O concentration field in the exhaust plane of a General Electric J85 aero-propulsion engine [183]; however, this work has already been thoroughly reviewed by Bolshov et al. [7].

10.1. Lean-blowout control

Several WMS-based sensors have been developed for studying lean-blowout in gas-turbine combustors. Zhou et al. [308] developed diode-laser-based sensors for real-time (onboard post-processing) measurements of gas temperature and H_2O in a swirl-stabilized model gas-turbine combustor. Two single-laser sensors were developed, one near $1.8 \mu\text{m}$ using scanned-DA and one near $1.4 \mu\text{m}$ using WMS- $2f$. The WMS-based sensor provided measurements of gas temperature at 2 kHz and demonstrated higher-SNR (compared to direct absorption) in flowfields with soot or droplet scattering. Later, Li et al. [309,310] extended the WMS- $2f$ sensor near $1.4 \mu\text{m}$ to be the first laser-based sensor for active control of lean-blowout in swirl-stabilized flames within a model gas-turbine combustor. The authors found that by monitoring the fractional power contained in the FFT (of temperature) between 0 and 50 Hz, lean-blowout could be predicted and prevented using an active control system. This enabled continuous flame holding at equivalence ratios only 0.03 higher than the LBO condition. Fig. 28 shows a schematic of the experimental setup used and the power-spectrum of the temperature time-history as a function of differential equivalence ratio (i.e., the difference between the equivalence ratio and the LBO value).

Using similar technology, Li et al. [311] later developed a WMS- $2f$ based TDL sensor for measuring fuel loading using the R(3) line of CH_4 near 1653.7 nm . These measurements enabled determination of the equivalence ratio of the gas entering a model gas-turbine combustion chamber in real time. By measuring the equivalence ratio in a modulated fuel experiment, the authors were able to correlate

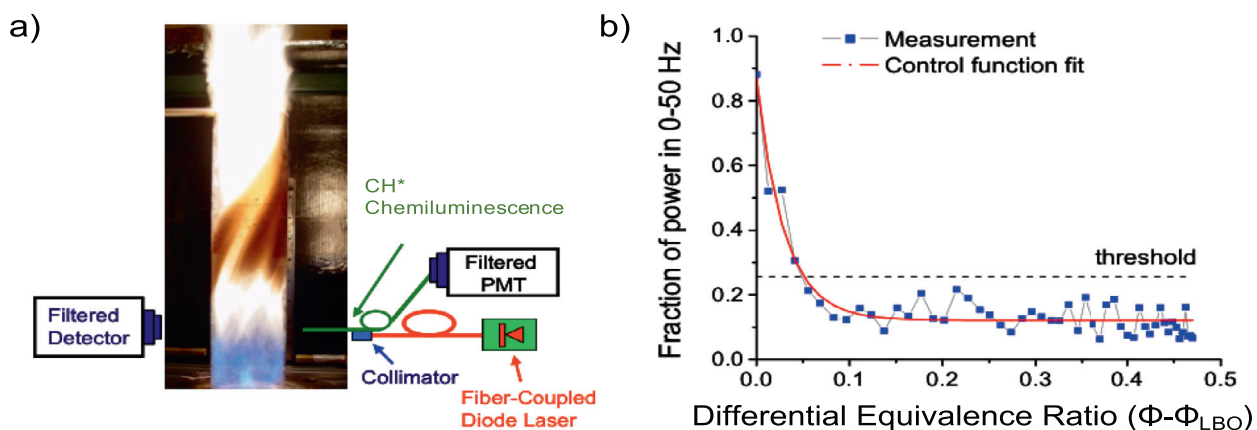


Fig. 28. Experimental setup used to monitor lean-blowout via TDLAS (a) and frequency content in temperature signal as a function of differential equivalence ratio (b). Figures adapted from [2].

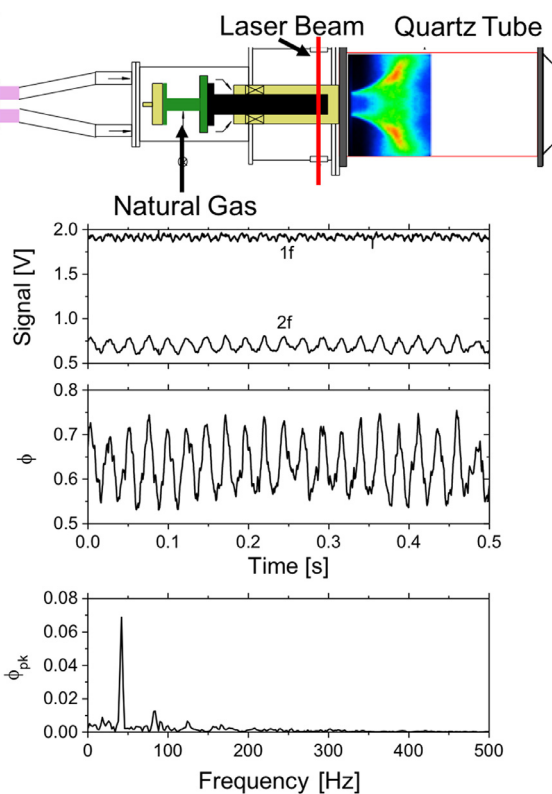


Fig. 29. Schematic of experimental setup used to measure equivalence ratio in a model gas-turbine combustor and example results during a modulated-fuel experiment. Figures adapted from [311].

oscillations in equivalence ratio with that of heat release, and used the results as a direct input into an analytical model for predicting thermoacoustic instability and LBO. Fig. 29 shows a schematic of the experimental setup used and time-resolved measurements of the equivalence ratio calculated from the WMS-2f signal. The results shown highlight the oscillations in equivalence ratio (induced by modulating the fuel flow rate) of the gas entering the combustor, and the FFT reveals that the oscillation occurs at near 50 Hz.

10.2. Gas-turbine combustors at elevated pressure

Kranendonk et al. [38] used an FDML laser spanning 1330 to 1380 nm to measure gas temperature at 200 Hz (after averaging 1000 scans at 200 kHz) via H₂O absorption in a gas-turbine combustor. Measurements were acquired at equivalence ratios and pressures from 0.22 bar to 0.32 bar and 3.4 bar to 6.9 bar, respectively, 6 cm downstream of the brightest region of the JP8-fueled combustor. The sensor revealed steady-state temperatures within 50 to 100 K of the semi-empirical flame temperature (derived from a combination of exhaust gas composition measurements and chemical equilibrium calculations) for each condition studied. The authors note that a significant aspect of this work was demonstrating the sensor's ability to tolerate the bright background emission observed in the gas-turbine combustor compared to previous combustion studies performed using FDML lasers (e.g., [36,37]).

Later, Caswell et al. [312] developed two light sources using fiber Bragg gratings for measuring gas temperature, H₂O, and CH₄ in a high-pressure gas-turbine combustor. In comparison to diode laser- and FDML-based sensors, the authors point out that these light sources can provide absorption information at multiple discrete wavelengths over a wider spectral range (between 1329 and 1667 nm here) at high rates (30 kHz). This sensor employed 4 discrete wavelengths to yield H₂O concentration and optimal thermometry performance from 500 to 2500 K and at pressures from 3 to 30 bar, 4

wavelengths to monitor line broadening near the wavelengths for thermometry, and two non-resonant wavelengths on the extreme ends of the spectral bandwidth to infer I_o . Regarding CH₄ sensing, 4 additional wavelengths near 1665 nm were employed to monitor temperature-sensitive and -insensitive CH₄ absorption, pressure broadening, and inferring I_o . By detecting only discrete wavelengths, a sample rate of only 22 MHz was needed, which is approximately 10 times less than that required by FDML-based sensors of comparable measurement rates. Fiber optics were used to transmit and collect laser light pitched across the combustor inlet and exit and were intelligently designed to rid the need of user alignment. Time-resolved measurements of temperature and CH₄ at the inlet, and temperature and H₂O at the exit are presented at temperatures up to 1700 K and a pressure near 10 bar.

11. Sensors for IC engines

IR-LAS sensors have been used to study and characterize a variety of IC-engine strategies aimed at improving combustion efficiency and reducing emissions. These works have primarily focused on acquiring measurements in circumstances where a path-integrated measurement is easily understood. For example, measurements have been acquired across short, controlled paths (e.g., in spark-plug probes) [42,260,267–269] to provide localized measurements of gas conditions, as well as to monitor combustion progress in homogeneous-charge compression-ignition (HCCI) engines [37,128,227]. However, some 2D measurements of species have been acquired via laser-absorption tomography [313,314]. While IR-LAS sensing has been done in optical engines [128,315], this section will focus on several works which have enabled improved *in situ* measurements of temperature and species concentrations in more practical IC-engine systems. The primary challenge common to all of these works is the need to obtain robust optical access either in-cylinder and/or near hot (≈ 850 K) engine components. This challenge has recently been overcome via the use of several novel optical assemblies which, in several cases, were used in combination with modern light sources and diagnostic techniques to improve measurement fidelity.

11.1. In-cylinder

Several WMS-based sensors have been used to study production-grade IC-engines via spark-plug-based probes, and these works have already been discussed in Sect. 6.4.1 and [42,260]. In comparison to the works discussed in the remainder of this section, these sensors were forced to overcome short optical path lengths (5 to 12 mm) in order to provide time-resolved measurements of gas temperature and H₂O or gasoline mole fraction.

Around the same time, Kranendonk et al. [37] used an FDML laser with a linewidth of ≈ 0.1 nm for measurements of gas temperature in an HCCI engine at 100 kHz and temperatures and pressures ranging from 300 to 800 K and 2 to 18 bar. The laser interrogated the H₂O absorption spectrum from 1335 to 1373 nm and the methods presented in [214] were used to calculate gas properties from the measured spectra. Optical access was provided through two sapphire windows located in pressure-transducer ports machined into the pent-roof combustion chamber. Later, Caswell [227] extended the use of this FDML laser to simultaneous measurements of temperature and H₂O at up to 2000 K and 30 bar in a fired HCCI engine. Fig. 30 shows sample results indicating an impressive RMS temperature error of only 5 K which, to the best of our knowledge, still represents the best precision achieved in IC-engine thermometry. Gas properties were calculated using the methods described in [133] and the BT2 line list [90]. To overcome the fact that BT2 does not contain collisional-broadening parameters, an algorithm was developed to determine best-fit broadening coefficients for several spectral windows, since collisional broadening, for H₂O, is highly dependent on the

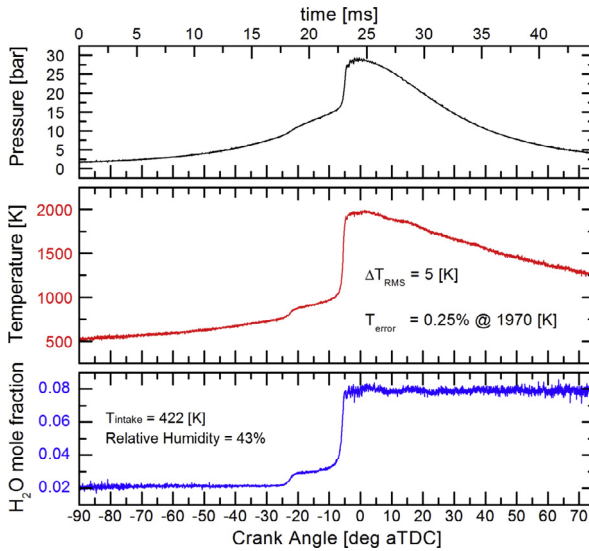


Fig. 30. Example results of temperature and H_2O measured in an HCCI optical engine using a FDML laser. Figure adapted from [227].

transition. While this technique does not attempt to resolve the broadening-coefficients of each individual transition (recognizing that this would be impractical), it was found to improve results significantly compared to previous algorithms that assumed equal line broadening for all transitions. The same research group later developed a spacer ring (to be inserted between the engine block and cylinder head) housing fused fiber-lenses for robust transmission and collection of near-IR laser light despite beam steering [206].

More recently, Witzel et al. [315] developed a scanned-wavelength DA sensor using a tunable diode laser near 1370 nm for measuring H_2O concentration at 4 kHz during the compression stroke of an optically accessible IC-engine. Measurements were acquired at temperatures and pressures from 300 to 500 K and 0.7 to 5.2 bar. The laser light was transmitted through the quartz cylinder off-axis to minimize etalon fringes. Later, this sensor was improved upon by using a VCSEL near 1370 nm to provide greater scan amplitude and

time resolution (10 kHz) [213]. By using a VCSEL the entire H_2O absorption line could be resolved which improved measurement precision by nearly a factor of 2 compared to previous work done with the TDL. Most recently, Ebert et al. [266] integrated the aforementioned diode-laser-based sensor into a production 4-cylinder engine with minimal engine modifications to provide measurements of H_2O concentration at 4 kHz. This sensor used a SMF transmitter mounted to the engine to pitch light across the cylinder. A probe with a 45° mirror was used to collect the light and direct the transmitted light 90° (i.e., upwards) into a 600 μm MMF. The authors used a TDL since the required optical arrangement reduced transmission levels to only 1%, thereby prohibiting the use of the much lower power VCSEL-based sensor described in [213]. Using this sensor the authors were able to achieve a detection limit as low as 7400 ppm of H_2O by volume.

Several researchers have also developed tomography based LAS sensors for time-resolved, in-cylinder imaging of hydrocarbon fuels in single- [314] and multi-cylinder engines [313]. In the latter, trenches for fiber-optics were machined into the engine block to enable fiber-optic light delivery and collection along 27 LOS. Two diode lasers at 1700 and 1651 nm were frequency-multiplexed at 300 and 500 kHz to enable simultaneous monitoring of hydrocarbon absorption and non-resonant extinction. The authors presented qualitative images of fuel concentration at 3 to 4k frames per second, and note that the system provided signal on all beams for > 2 hours of fired operation.

11.2. Engine intake and exhaust

Recently, Jatana et al. [130,316] developed a TDL sensor for simultaneous temperature, H_2O , and pressure in the intake manifold, EGR cooler exit, and turbo-charger inlet of a diesel engine. The sensor used a single DFB TDL near 1388 nm and custom fabricated mounts for mounting the photodetectors and SMF transmitters to the engine. The mounts utilized a ceramic spacer to insulate the optical equipment from the high-temperature (up to 850 K) components without needing water cooling, and the windows were mechanically sealed using mica gaskets. By using telecommunication-grade fibers and splitters this sensor was able to acquire measurements at 4 locations

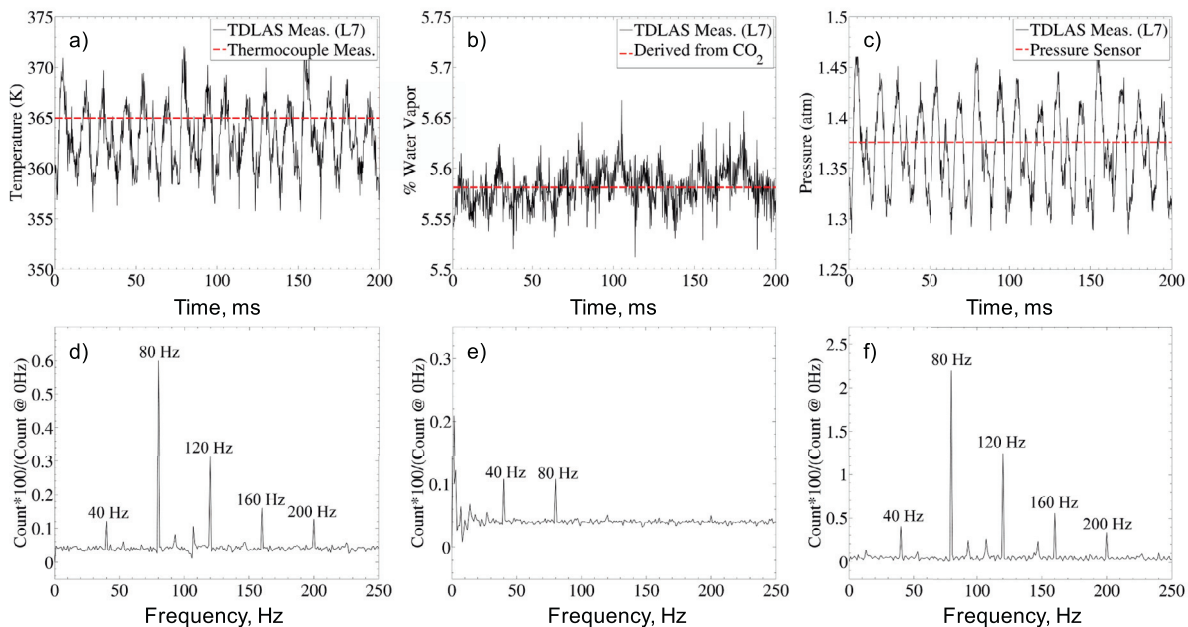


Fig. 31. Measured time history (a–c) and corresponding FFT (d–f) of gas temperature, H_2O mole fraction, and pressure acquired at the exit of an exhaust-gas recirculation (EGR) cooler using LAS. Figures adapted from [130].

simultaneously. During operation, the laser was scanned across 6 H₂O transitions (4 dominant), with E' ranging from 70 to 1742 cm⁻¹, at up to 5 kHz. Gas properties were inferred from a spectral-fitting routine. Fig. 31 shows example temperature, H₂O, and pressure results. The sensor was able to achieve an uncertainty in temperature, pressure, and H₂O mole fraction from 1.4 to 4%, 5.5 to 6.5%, and 6.2 to 8.2%, respectively, for temperatures from 300 to 850 K with measurement precisions ranging from 0.9 to 4%.

12. Sensors for scramjets

Many researchers have developed LAS sensors for a variety of high-speed combustion flows [41,172,175,178,236,258,259,262, 263,317–320]. Among the most frequently studied applications in this category are hypervelocity shock tunnels [258,259,321], ramjets, and scramjets [28,41,129,172,175,182,262,263,317–320]. Early work was conducted in shock tunnels to characterize their hypersonic flow fields [258,259] and similar efforts continue [321]. Of late, most LAS sensing in high-speed flows has been done to characterize scramjet flow fields. The scramjet represents one promising propulsion technology capable of providing airbreathing hypersonic flight with no moving engine parts. The scramjet consists of four primary components: inlet, isolator, combustor, and nozzle. The inlet slows the incoming hypersonic air through an oblique shock-train, raising the temperature and pressure of the gas and the isolator is used to homogenize the flow field entering the combustor. Fuel is directly injected into the high-temperature air stream to initiate combustion and the combustion gases are expanded in the nozzle to produce thrust. During operation, the goal is to combust enough fuel to produce sufficient thrust while avoiding unstart (i.e., a failure mode where the shock train is expelled from the isolator yielding subsonic flow throughout the scramjet flow path). As a result, the performance of a scramjet requires a delicate balance between a variety of complex physical process, namely, fuel-air mixing, chemical kinetics, and shock-boundary-layer interaction. The need to understand these processes *in situ* has driven the development and application of LAS sensors for characterizing scramjets.

Historically, most IR-LAS sensing in scramjets has employed near-IR telecommunication-grade TDLs for measuring temperature, H₂O, and velocity in continuous-flow facilities [43,129,172, 182,317,319,322,323], with only one prior example of measuring CO₂ in [318] (later discussed in [41]). Recently, several efforts have extended sensing capabilities to: 1) the mid-infrared for improved measurements of H₂O [178,320], CO₂ [236,320], and the first measurements of CO [236,320] in a hydrocarbon-fueled model scramjet combustor, 2) 2D via tomography [129,131,184], 3) greater bandwidth for improved sensing in impulse facilities [207,263], and 4) the first in-flight TDLAS measurements for characterizing scramjet flow fields [26–28,324].

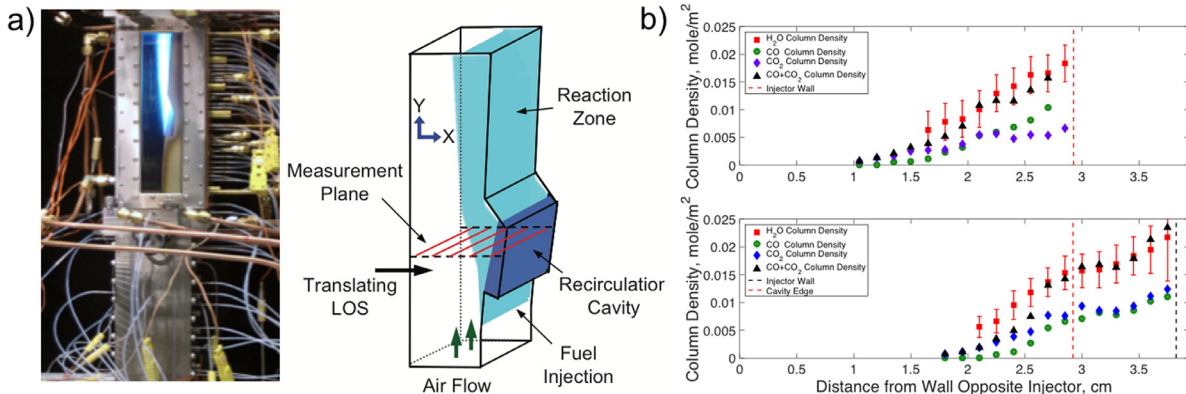


Fig. 32. Schematic of ethylene-fueled, model-scramjet combustor studied using mid-IR LAS (a) and time-averaged species concentrations as a function of space (b). Figures adapted from [236] and [320].

12.1. Continuous-flow facilities

The recent combined effort presented by Goldenstein et al. [178], Spearrin et al. [236], and Schultz et al. [320] represents the first demonstration of mid-infrared LAS sensing of H₂O, CO₂, and CO in scramjets, made possible by the advent of thermoelectrically cooled quantum-cascade lasers and mid-infrared fibers. Furthermore, this work represents one of the first applications of calibration-free scanned-WMS spectral fitting [139] and the use of the two-color strategy for acquiring path-averaged gas properties in highly non-uniform flows (discussed in Section 5.1 and [165]). The combination of these strategies was critical to the acquisition of accurate measurements due to the large temperature and composition gradients within the scramjet combustor studied.

Fig. 32a illustrates a schematic of the model scramjet studied (the University of Virginia's Supersonic Combustion Facility (UVaSCF)) and the orientation of the translating lines-of-sight used by all sensors. Each laser was fiber-coupled in free-space into a mid-IR fiber (multi-mode ZBLAN for H₂O, bifurcated hollow core for CO and CO₂) and an X-Y translation stage was used to translate the measurement line-of-sight throughout the combustor. DFB TDLs near 2482 and 2551 nm were used to measure H₂O and temperature via scanned-WMS-2f/1f, a DFB QCL near 4855 nm was used to measure CO and temperature via scanned-DA and scanned-WMS-2f/1f, and an external-cavity QCL near 4176 nm was used to measure CO₂ via scanned-DA. The use of stronger fundamental-band absorption enabled access to transitions that are 20 to 10⁴ times stronger than in the near-IR (depending on species) which improves measurement sensitivity and enables use of inherently weaker transitions with greater lower-state energy for improved temperature sensitivity and tolerance to thermal non-uniformities [76]. However, these benefits do not come without challenges, namely that use of wavelengths beyond 4 μm in a high-temperature, continuous-flow facility complicates the use of sapphire windows (leading to significant thermally induced temporal fluctuations) and other less robust materials (e.g., ZnSe) that oxidize in high-temperature combustion gases. More information regarding these complications can be found in Section 6.2.5.

Fig. 32b shows time-averaged species measurements as a function of the x-direction (transverse to flow) for two measurement planes. By comparing the results in the top panel (downstream plane) to the bottom panel (upstream plane) it is clear that the combustion products expand into the freestream. Furthermore, at locations near the flame-holding cavity the column-density of CO+CO₂ agrees remarkably well with that of H₂O indicating that most of the carbon and hydrogen atoms originally contained in the fuel (C₂H₄)

have moved to CO, CO₂, and H₂O respectively. Conversely, at locations near the high-speed free-stream (i.e., far from the cavity), the column density of CO+CO₂ is significantly less compared to H₂O indicating the presence of unburned fuel/hydrocarbons at this location in the flow. These results enable a variety of interesting conclusions regarding the spatio-temporal evolution of combustion progress that would not be possible without acquiring multi-species measurements.

Brown et al. [129] demonstrated the use of a tunable diode-laser absorption tomography (TDLAT) sensor for coarse reconstruction of temperature and H₂O at the exit of a ground-test scramjet designed to replicate the HiFiRE 2 scramjet. This sensor employed three time-multiplexed diode lasers near 1.4 μm along 14 lines-of-sight (8 vertical, 6 horizontal). Algebraic reconstruction tomography (ART) was used to reconstruct the 2D distribution of absorbance for each color since it is more suitable than filtered back projection techniques in cases with a limited number of LOS measurements. After the 2D integrated absorption of each color was reconstructed, the gas temperature and water mole fraction were calculated in a 9 × 19 pixel image using standard LAS techniques. During steady-state operation, the 2D distributions of H₂O and temperature indicate burning in the core of the flow with local hotspots and the distributions were found to vary substantially in time, indicating the role of turbulent combustion.

Busa et al. [182] documented the design and initial implementation of a TDLAT system for 2D temperature and H₂O concentration at NASA Langley's direct-connect supersonic combustion test facility (DCSCTF) employing a fan-beam geometry and retroreflector to return the transmitted light to the pitch/catch optics. A rotational stage was used to rotate 5 separate transmitter/reciever boxes 72 degrees for an effective rotation of 360 degrees. Most recently, Busa et al. [131] reported the use of TDLAT and stereoscopic PIV for determination of combustion efficiency via spatially resolved measurements of temperature and H₂O number density (via TDLAT) and velocity (via stereo-PIV) at the exit of the UVA-SCF. The authors used a similar experimental setup to acquire absorption measurements along 1400 lines-of-sight and provide high-resolution (2 mm × 2 mm pixels) measurements of H₂O. By combining these

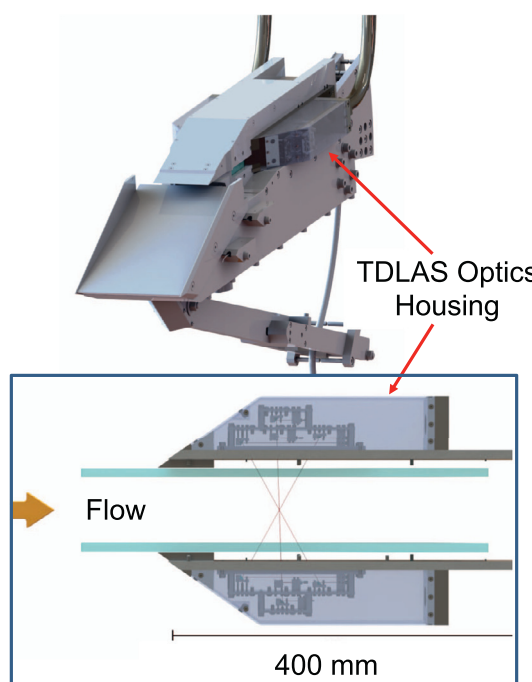


Fig. 34. Model of HyShot II scramjet with TDLAS sensor and example of time-resolved temperature and H₂O acquired via scanned-WMS-2f/1f during an engine-fired test. Figures adapted from [207].

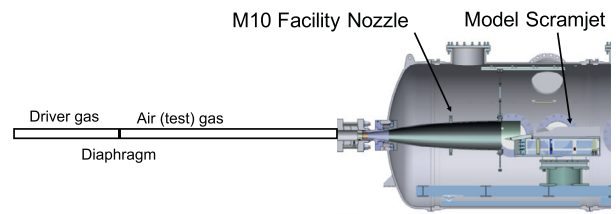


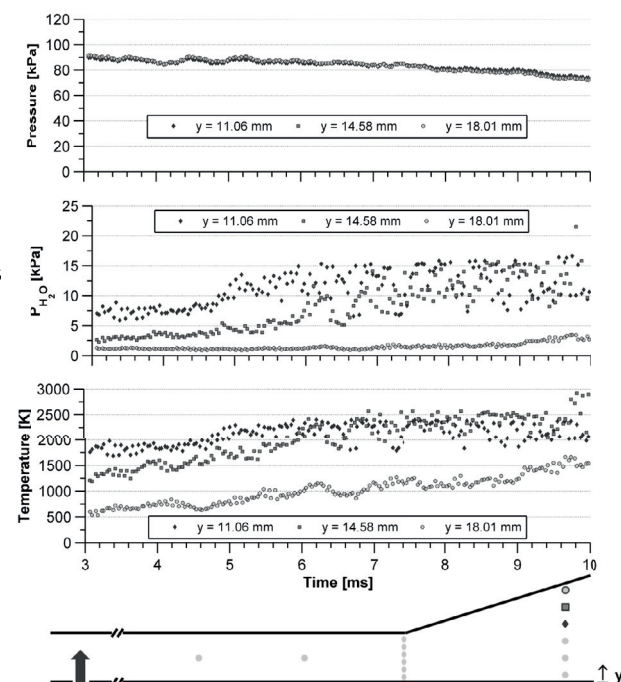
Fig. 33. Schematic of the NASA hypersonic pulse (HyPulse) reflected shock-tunnel facility (operated by ATK General Applied Science Laboratory (GASL)) used for scramjet testing with TDLAS sensors. For more details see [262].

measurements with the measured velocity field (obtained via stereoscopic PIV) and comparing the H₂O flux with that of the H₂-fuel flux, the authors were able to calculate the combustion efficiency of the heterogeneous flow for various operating conditions.

12.2. Impulse facilities

Shock tunnels have been used to generate short-duration hypersonic flows with flight-enthalpies (typically > Mach 5) that are too extreme to sustain in continuous-flow ground-test facilities. In practice, such facilities shock-heat gases to high-enthalpy conditions and then expand them, for example, through a nozzle to generate hypersonic flow (see Fig. 33). As a result, these facilities offer a unique opportunity to study scramjets in the laboratory at more extreme flight conditions. Shock tunnels pose a number of unique challenges including short test times (order of 1 ms), transient flow conditions, and limited optical access. Despite these challenges, several researchers have developed TDLAS sensors for characterizing such tunnels [258,259] and test articles housed within them [262,263,325].

Two TDLAS measurement campaigns were recently conducted in model-scramjet combustors located within shock tunnels at ATK GASL [262] and the German Aerospace Center (DLR) [207]. Fig. 34 shows a schematic of the experimental setup used and example results for a single test. Both sensors utilized DFB TDLs near 1.4 μm with scanned-WMS-2f/1f to measure gas temperature and H₂O



concentration along three lines-of-sight (at various locations depending on test) to quantify the evolution of combustion progress in space. In addition, the work conducted by Strand [207] employed angled beams for velocimetry. The two campaigns used similar optical hardware for light delivery and optical alignment. The fibers were housed in a protective pipe and the pitch and catch optics were located behind a protective shield to protect all components from the high-speed flow. The results shown in Fig. 34 highlight the utility of high-speed (25 kHz), multi-line-of-sight measurements for characterizing the combustion process. The measurements indicate relatively stable combustion, but with some strong-, and rapid-(time-scale of 1 ms) fluctuations in temperature and H₂O despite a temporally stable wall-pressure. The TDLAS measurements also reveal a strong bias of combustion products towards the fuel-injector wall.

12.3. In-flight tests

Brown et al. [28] presented the use of two independently developed TDLAS sensors for onboard measurements of O₂ in a hypersonic vehicle as part of the HiFiRE I test campaign. The sensor developed by Zolo Technologies used scanned-wavelength direct absorption [26] while the sensor developed by Southwest Sciences used scanned-WMS [27]. Both sensors employed angled lines-of-sight across mock-inlet flow paths to infer the flow velocity from the Doppler-shifted absorption, with the ultimate goal of measuring O₂ mass flux entering the combustor. The scanned-DA sensor employed a scan rate of 5 kHz and multiple scans were averaged to yield a measurement rate of 10 Hz. The scanned-WMS sensor used a scan rate of 1 kHz and averaged the output to a measurement rate of 1 Hz. Both sensors used lasers near 760 nm and the WMS sensor also included an onboard reference cell for active laser frequency stabilization and a reference signal for velocimetry. As expected, the measured WMS lineshapes exhibited a greater signal-to-noise ratio than those of DA. During the flight, both sensors maintained alignment and operated as planned for 17 s, after which the telemetry system for the WMS sensor began to operate unreliably. While no quantitative results are reported, it is clear that this work represents an impressive and encouraging demonstration of stand-alone TDLAS sensors for characterizing hostile systems.

More recently, in-flight TDLAS measurements of H₂O and temperature were acquired along 8 lines-of-sight traversing the exit plane of the HiFiRE 2 scramjet combustor [324] (see Fig. 35). Two independent systems were used, each employing a single DFB TDL scanned across multiple H₂O transitions near 1.4 μm at 50 kHz. The authors note that both systems operated successfully in flight, and

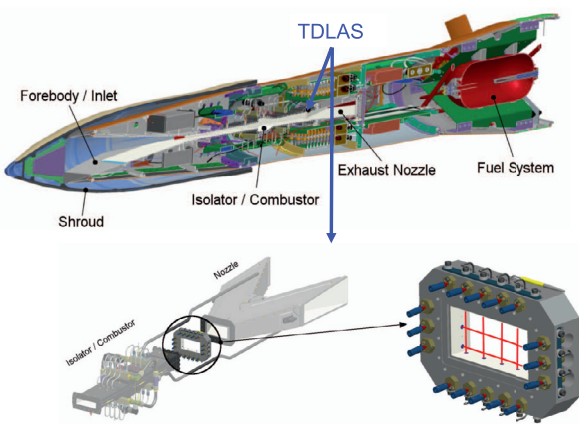


Fig. 35. Schematic of the HiFiRE 2 scramjet and optical assembly used for TDLAS measurements of H₂O and temperature in the scramjet's exhaust. Figure adapted from [324].

point the reader to papers discussing analogous ground-test experiments [129] for greater detail and example results.

13. Sensors for detonation combustors

The thermodynamic advantages of high-temperature and -pressure combustion and the desire to minimize moving parts in combustion systems has driven the development of a variety of detonation-based combustors and engines. To date, pulse-detonation engines/combustors (PDEs, PDCs) have received the most attention due to their relatively simple architecture. In a PDE, fuel is intermittently injected into an open-ended combustor and, upon mixing with air, is ignited to form a deflagration wave which propagates down the combustor until it undergoes deflagration-to-detonation (DDT) transition. After which, the detonation wave propagates through the remainder of the combustor, thereby elevating the temperature and pressure of the unburnt air-fuel mixture (through shock-compression) and initiating combustion. The combustion gases are then expanded to produce thrust or mechanical work. Like PDEs, rotating-detonation engines and combustors (RDEs, RDCs) represent a promising strategy for achieving the benefits of high-pressure combustion without moving parts. However, in contrast to a PDE, in an RDE fuel and air are continuously supplied to an annular combustor and a detonation wave continuously travels around the annulus consuming the air-fuel charge located ahead of the wave. Fig. 36 illustrates this concept via a CFD temperature map reported by Schwer and Kailasanath [326]. This continuous operation has several benefits, including (1) removing the need for a high-frequency repeatable ignition system and (2) enabling much higher operation frequencies (order of kHz compared to 100 Hz for PDE) which leads to higher thrust/power and a comparatively steady output that is more favorable for integration with gas turbines. Due to these benefits, research and development efforts have recently shifted focus to RDEs, however, prior IR-LAS work in PDEs has served as an important stepping stone to current RDE-sensing efforts.

While mechanically simple, the need to understand the complex physics (e.g., DDT, kinetics) governing these systems has driven the application and, in many cases, the development of IR-LAS sensors for high-bandwidth measurements of chemical species and thermodynamic conditions at extreme temperatures and pressures. These devices are capable of producing temperatures and pressures in excess of 4000 K and 100 bar, respectively, with changes in temperature and pressure of comparable magnitude occurring on μs to ms timescales. Further these systems are extremely hostile, producing strong and high-frequency vibrations which can compromise the fidelity of IR-LAS measurements. RDEs pose even greater challenges, most notably, the absence of line-of-sight optical access through the combustor and the demand to resolve detonation events with microsecond resolution. As a result, detonation engines present one of the most challenging environments for LAS sensors.

The first generation of LAS sensors deployed in detonation engines used fixed-wavelength telecommunication-grade diode

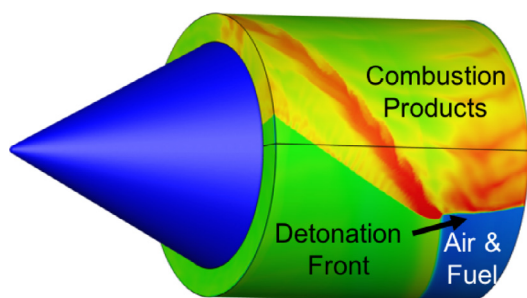


Fig. 36. Simulated temperature distribution in an RDC. Figure adapted from [326].

lasers for monitoring temperature, H₂O, fuel, and particulate volume fraction [126]. Later, the use of cesium-absorption-based sensors for measurements of temperature and pressure at 2000–4000 K and 0.5 to 30 atm [34] and time-of-flight velocimetry [35] were explored using a rapidly scanned VCSEL laser. Mattison et al. [327] developed a scanned-wavelength TDLAS sensor for temperature and H₂O in a PDE and Klingbeil et al. [108] developed one of the first fiber-coupled mid-IR sensors for monitoring JP8 at 3.4 μm in a PDE. While these early works are impressive, this section will focus on several recent manuscripts which have significantly advanced the state of IR-LAS sensors for detonation environments by avoiding the need to (1) correct for non-resonant transmission losses and (2) seed atomic absorbers for high-SNR measurements, while also enabling the measurement of new performance parameters (e.g., enthalpy, mole fraction of carbon oxides). These advancements have come through the use of: (1) hyperspectral direct absorption and (2) WMS at mid-infrared wavelengths. Further, advancements in optical engineering have enabled, to the best of our knowledge, the first single-ended measurements in a combustor.

13.1. Pulse-detonation combustors

Caswell et al. [212,328] used three time-division multiplexed (TDM) FDML lasers to provide simultaneous measurements of gas temperature, H₂O, pressure, and velocity at 50 kHz in an H₂-fueled PDC at two measurement locations upstream and one downstream of a gas turbine. This sensor used three FDML lasers to perform piecewise continuous-swept-wavelength measurements of the H₂O absorption spectrum near 1350.5, 1355.85, and 1362.31 nm to infer gas properties. Interrogating H₂O in these spectral windows (identified via the wavelength-selection algorithm developed by An et al. [209]) enabled near optimal temperature sensitivity. Fig. 37 shows a schematic of the experimental setup used. This sensor also employed novel fiber-optic fixtures that deploy counter-propagating laser beams both angled at 45° relative to the flow direction to provide velocity measurements in a compact manner.

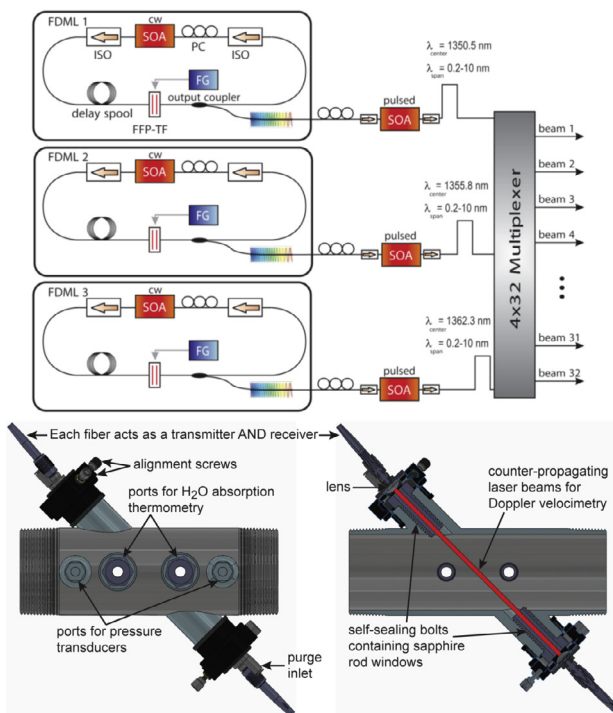
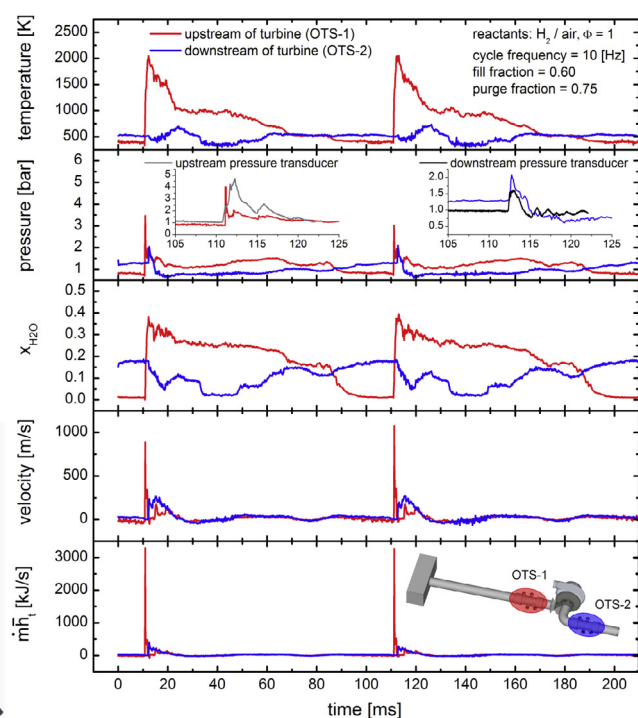


Fig. 37. Experimental setup of FDML-based sensor and example of time-resolved temperature, pressure, H₂O, and velocity measurements used to calculate time-resolved enthalpy in an H₂-fueled PDC. Figures adapted from [212].

Fig. 37 shows time-resolved measurements of temperature, pressure, H₂O, velocity and enthalpy for two consecutive PDC cycles. Gas properties were calculated in a manner similar to that of Kranendonk et al. [214] using the HITEMP database [47]. A linear baseline correction was applied to measured and simulated spectra for consistency and instrument broadening was estimated from measurements of H₂O spectra at 15 torr and 300 K, and was then accounted for in the least-squares fitting routine used to calculate gas properties. Measurements are presented for temperatures and pressures up to 2500 K and 8 bar without the turbine present, and near 2000 K and 4 bar with the turbine present. The authors point out that measurements could not be acquired until 60 μs after the detonation wave passed due to extreme beam steering and pressure broadening. The authors clarify that additional collisional-broadening data is required to improve upon these proof-of-concept pressure measurements. Regardless, this novel use of multi-parameter measurements enabled the calculation of the time-resolved mass flux and enthalpy which provides valuable information for understanding the unsteady performance of the turbine.

Around the same time, Goldenstein et al. [237,329] and Spearin et al. [330] developed and applied WMS-2f/1f-based sensors for temperature, H₂O, CO₂, and CO in an ethylene-fueled PDC. Measurements were acquired in the combustion chamber and in a choked throat of a converging-diverging nozzle to enable determination of the flow speed, mass flow rate, and enthalpy flow rate from measurements of gas temperature, H₂O, CO₂, CO and pressure. Acquiring measurements in a choked throat offers a number of design opportunities, namely, a velocity measurement with sensitivity and accuracy that is nearly independent of pressure (provided that the temperature and species measurements are accurate). This is particularly advantageous when high pressures (up to 50 atm) and pronounced collisional broadening could significantly compromise the precision of a Doppler-shift-based velocity measurement.

The WMS sensors were demonstrated and validated with measurements behind reflected shock waves in shock tubes at known temperatures and pressures up to 2700 K and 50 atm. The details



regarding the sensor design and validation are documented in [101,106,139,203]. DFB diode lasers near 1392 and 1469 nm were used to measure temperature and H₂O in the throat with a bandwidth of 10 kHz, and DFB TDLs near 2474 and 2482 nm were used to measure temperature and H₂O in the combustion chamber with a bandwidth of 9 kHz. A DFB TDL near 2678 nm and a DFB QCL near 4854 nm were used to measure CO₂ and CO with bandwidths of 2 kHz and 20 kHz, respectively. The lasers were modulated at frequencies from 35 to 200 kHz. The near-IR temperature and H₂O sensor used polarization maintaining SMF, while the mid-IR H₂O and CO₂ sensors used ZBLAN fibers, and the CO sensor used an InF₃ SMF. All photodetectors were mounted directly to the PDC to facilitate alignment and improve light collection. The wavelengths and modulation depths of all H₂O lasers were chosen according to the procedure developed by Goldenstein et al. [203] to provide sensitive thermometry and mole fraction sensing from 5 to 50 atm and 1000 to 3000 K. Free-space fiber coupling and delivery systems were designed for the mid-infrared wavelengths as described by Spearrin et al. [101,106]. This involved utilization of newly developed single-mode fluoride glass fibers (≈ 5 m) which significantly mitigated bending losses and multimodal dispersion noise [331] while allowing the more sensitive mid-infrared lasers to be located remotely from the combustor test cell.

Fig. 38 shows time-resolved measurements of temperature, H₂O, CO, CO₂, and pressure for a single cycle. The pressure was measured

at each measurement location using a Kulite pressure transducer. The detection limits of the MIR-H₂O, -CO, -CO₂, and NIR-H₂O sensors varied from 0.083–0.5%, 0.05–0.6%, 0.1–2.2%, and 1–4% by mole, respectively, across the PDC cycle. Despite having to use significantly lower modulation frequencies, the detection limit of the mid-IR sensor was 5 to 10x smaller than that of the near-IR temperature and H₂O sensor, again highlighting the benefits of using strong mid-infrared absorption. Fig. 39 shows the time-resolved enthalpy calculated from the measured temperature, pressure, and gas composition and using a choked-flow assumption. The results indicate peak enthalpy flow rates consistently near 25 MW. The authors present a thorough uncertainty analysis of the enthalpy calculation, recognizing that choked flow is not established until approximately 125 μ s after the detonation wave passes and that the sonic plane is, in reality, located slightly downstream of the throat/measurement plane yielding a Mach number closer to 0.98 at the measurement location. For the uncertainties in temperature, pressure, composition, and Mach number, the authors quote a root-sum-squared uncertainty in the enthalpy flow rate of 15% for the first 125 μ s and 6% for longer times.

13.2. Rotating-detonation combustors

RDEs were first conceptualized in the 1950s, however the complex physics behind their operation delayed the development of

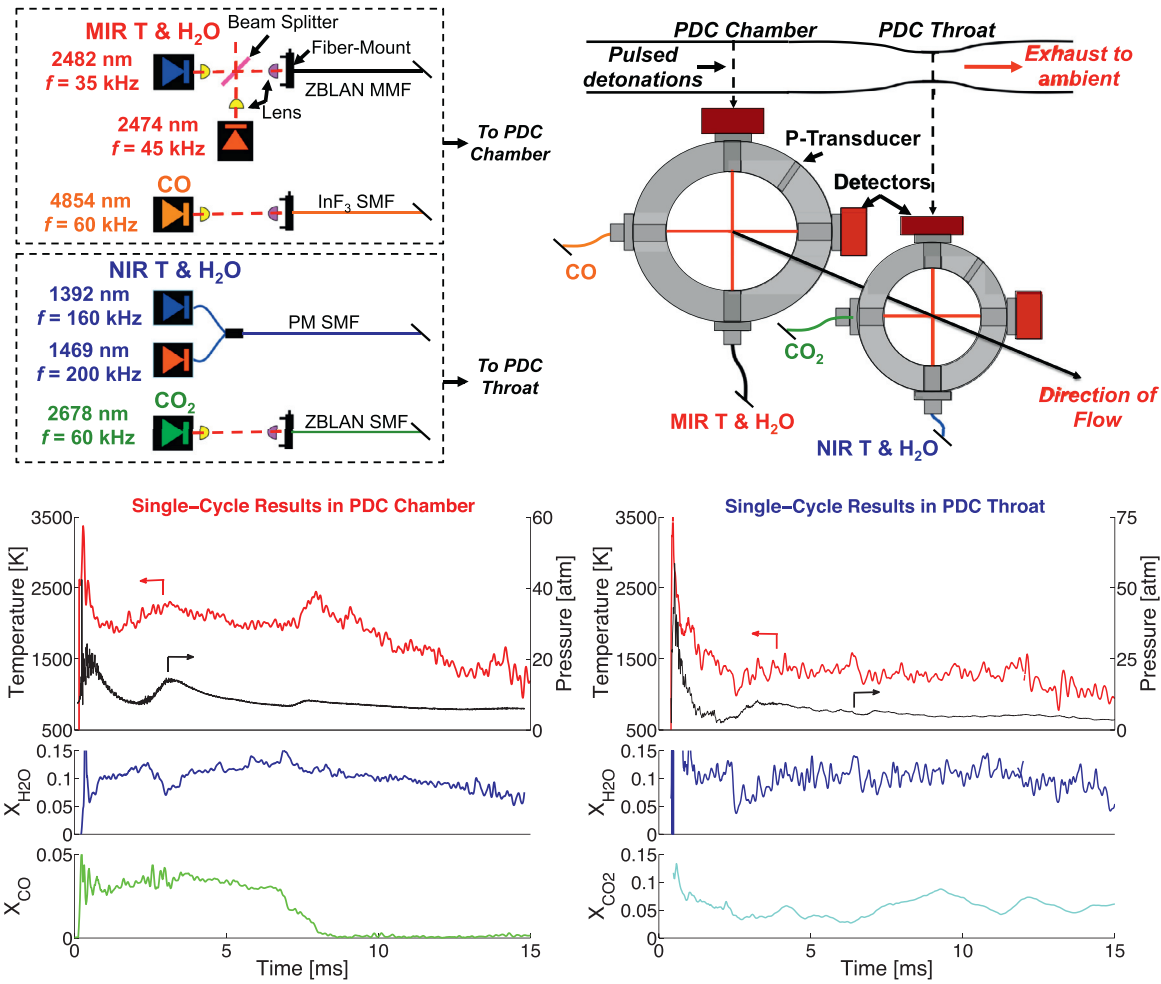


Fig. 38. Experimental setup of DFB TDL- and QCL-based WMS-2f/1f sensors and example of time-resolved temperature, pressure, H₂O, CO₂, and CO measurements used to calculate time-resolved enthalpy in an ethylene-fueled PDC. Figures adapted from [46].

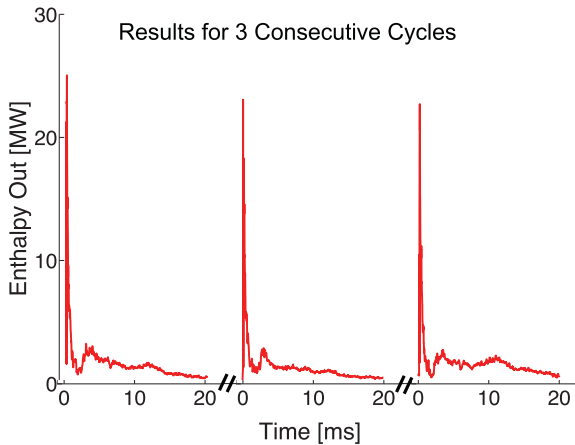


Fig. 39. Time-resolved enthalpy flow rate exiting PDC combustor calculated using the LAS measurements shown in Fig. 38 and a choked-flow assumption. Figure adapted from [46].

functional RDEs until relatively recently. Due to their recent development, only three archival papers have reported the use of LAS sensors for RDEs and all three reported measurements of temperature and H₂O [145,202,332]. These sensors have enabled some insightful observations and conclusions regarding the current state of RDEs and have overcome significant hurdles that complicate the implementation of laser-absorption sensors into RDEs. The remainder of this section will discuss these recent works.

The first LAS sensors for RDEs were deployed to characterize the exhaust of H₂-fueled RDCs [145,332] and only recently have authors begun developing and deploying sensors for RDC combustors [202]. Regarding sensors for RDC exhaust, McGahan et al. [332] used two VCSELs to measure the absorption spectra of H₂O from 7435 to 7442 cm⁻¹ and 7465 to 7471 cm⁻¹, thereby enabling calculation of the gas temperature, H₂O concentration, and velocity using scanned-wavelength direct-absorption. The sensor details provided are relatively sparse, but several conclusions were provided. The TDLAS measurements indicate that the RDE exhaust reaches nominally steady conditions approximately 9 ms after ignition with a velocity of 364 ± 110 m/s and standard deviations in temperature and H₂O concentration of 50 K and 0.08 moles/m³, respectively. The

authors also report how the exhaust gas temperature, velocity and H₂O concentration varied with equivalence ratio and mass flow rate.

Goldenstein et al. [145] developed and deployed dual two-color LAS sensors using WMS-2f/1f for measurements of temperature and H₂O at 10 and 50 kHz in the throat of a converging-diverging nozzle attached to an H₂-fueled RDC. One pair of diode lasers was used to interrogate H₂O transitions near 2551 and 2482 nm with E'' of 704 and 2660 cm⁻¹, respectively, and another pair of diode lasers was used to interrogate H₂O transitions near 1392 and 1469 nm with E'' of 1045 and 3291 cm⁻¹, respectively. This was done to quantify the thermal uniformity of the exhaust using a method similar to that of Seitzman and Scully [168]. Measurements were acquired at global equivalence ratios from near 0.7 to 1 (achieved by varying the mass flow rate of air with fuel flow rate fixed). In all cases, the temperature measurements acquired at 50 kHz clearly revealed oscillations in temperature and H₂O at the characteristic frequency of the detonation wave (≈ 3.25 kHz). The difference between the "hot" and "cold" temperatures measured by the near-IR and mid-IR lasers, respectively, was found to increase from 2 to 8% as the air flow rate increased from 1.2 to 1.5 kg/s indicating a pronounced correlation between the air mass flow rate and thermal stratification of the exhaust. In addition, the H₂O production was found to decrease only slightly with increasing air flow rate (i.e., decreasing equivalence ratio) suggesting that air-fuel mixing was the primary factor leading to the low combustion efficiencies observed (only 40–60%).

Most recently, Rein et al. [202] presented the first measurements of temperature and H₂O in the annular combustor using a single-ended fiber-coupled sensor. The authors used a MEMS VCSEL to measure the absorption spectra of H₂O from 1330 to 1365 nm at 100 kHz and yield temperature and H₂O concentration. A fiber-bundle housing a single-mode pitch fiber and a multi-mode catch fiber (see Fig. 23) was used to pitch laser light into the combustor and collect the light backscattered off the RDE centerbody. The annular gap in the H₂-fueled RDE was 0.76 cm yielding an effective path length of 1.52 cm and measurements were acquired 25.4 and 50.8 mm downstream of the fuel plenum. The authors found a strong correlation between the gas temperature and air-mass flow rate which they primarily attributed to the location of the measurement with respect to that of the detonation wave (it was previously shown that the axial-depth of the detonation wave exhibits a strong correlation with the air mass flow rate [333]). Fig. 40 shows that the nominal gas temperature varied from near 500 K up to 1200 K as the air mass

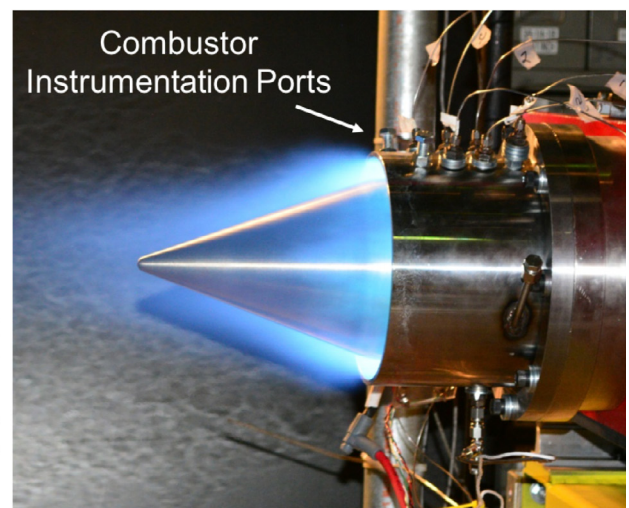
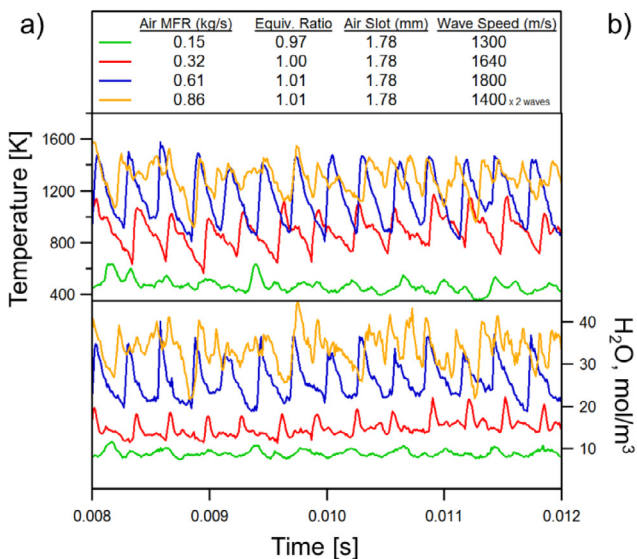


Fig. 40. Example of time-resolved gas temperature and H₂O measurements acquired via a single-ended LAS sensor (see Fig. 23) in an RDC combustor (a) and corresponding experimental setup (b). Figures adapted from [202].

flow rate increased from 0.15 to 0.61 kg/s with a fixed equivalence ratio near 1. In addition, the authors found that the gas temperature measured at the downstream location was significantly colder than that of the upstream location located within the detonation wave.

14. Conclusions

Over the last 15 years, great progress has been made in the development of a wide range of IR-LAS techniques and sensors. Perhaps most importantly, the application of IR-LAS sensors to practical combustion systems has dramatically expanded. To name only a few examples, sensors have been developed for power plants, gasifiers, gas turbines, hypersonic-flow facilities, IC-engines, detonation combustors, and even in-flight experiments onboard a scramjet. In doing so, these sensors have been extended to new limits and capabilities via the development of improved diagnostic techniques and spectroscopic models, novel optical assemblies, and new light sources. This section will highlight the key takeaways of these works and discuss some of the remaining needs and challenges researchers are facing today.

14.1. Key takeaways

14.1.1. Techniques

Improvements in modeling scanned-WMS signals [138,139] have enabled the development of a calibration-free scanned-WMS spectral-fitting technique [139] that requires no more spectroscopic information than conventional scanned-wavelength direct absorption. As a result, this technique extends the advantages of WMS to gases with unknown collisional broadening and/or line-of-sight non-uniformities, and was first deployed in the field to study a scramjet combustor [178] and a coal gasifier [295]. Further, 1f-normalized WMS has enabled high-fidelity measurements of gas properties in particulate-laden flows and in single-ended (i.e., stand-off) configurations despite optical-transmission-loss factors of 10^3 to 10^5 . These advancements offer great potential for extending WMS-based sensors to increasingly harsh environments and more complex conditions, and further improve the prospects for real-time monitoring and control of combustion systems via WMS-based sensors.

A variety of hyperspectral sources and techniques have also emerged. Such techniques have demonstrated the ability to provide multi-parameter measurements of gas properties at rates up to 100 kHz in harsh environments [202,212]. In addition, these sources have enabled the development of hyperspectral tomographic techniques which leverage additional spectral information to reduce the number of projections needed to reconstruct the measurement field [183]. As hyperspectral sources continue to evolve and emerge in new spectral regions, the potential for them to provide improved multi-parameter measurements will continue to grow.

Cavity-enhanced absorption spectroscopy in low-finesse optical cavities has demonstrated the ability to provide improved ($\sim 50\text{--}100\times$ better detection limits) measurements of trace gases formed behind reflected shock waves [159,160,287]. The use of a low-finesse cavity retains the ability to provide rapid ($\sim 50\text{--}100$ kHz) scanned-wavelength measurements of absorption spectra while also being less sensitive (compared to high-finesse cavities) to mirror fouling. The combination of these benefits offers many unique opportunities for time-resolved monitoring of trace gases in relatively harsh environments.

14.1.2. Mid-IR sensing

Mid-infrared semiconductor lasers and fibers have enabled measurements of key-combustion species in environments with concentrations and path lengths that would have precluded high-fidelity monitoring via near-IR sources. Perhaps most notably, these

sources greatly improve our ability to measure CO and CO₂ at conditions and scales relevant to combustion systems. This is illustrated by the CO and CO₂ measurements recently acquired in scramjet and pulse-detonation combustors [236,237]. At present, mid-IR lasers, fibers, and detectors are sufficiently robust, compact, and affordable to enable monitoring of harsh combustors, and we expect their role in combustion research within academia and industry to grow rapidly as this technology improves.

14.1.3. Measurements of high-pressure gases

Advancements in WMS techniques and mid-IR semiconductor lasers have enabled the development and application of improved sensors for monitoring temperature, H₂O, CO, CO₂, and NO in high-pressure gases [101,106,115,203,210]. These sensors have demonstrated the ability to measure temperature and species concentrations at 10s of kHz in the laboratory and the field, at conditions ranging from 10 to 150 atm. Measurements at known conditions behind reflected shock waves were used to validate the accuracy of these sensors and, in some cases, to refine the spectroscopic models at extreme thermodynamic conditions. We expect the development of these techniques to facilitate the study of a wide range of real-world combustors; however, this remains an active area of research.

14.1.4. Optical engineering

Numerous researchers have developed clever optical assemblies for integrating IR-LAS sensors into combustion systems with limited optical access. Internal-combustion engines and, more recently, rotating detonation engines have driven the development of many of these assemblies. For example, cleaved sapphire rods and compact optics have been used to provide optical access into burners [177] and IC-engines [206,266], respectively. Further, fiber-bundles have been used to integrate IR-LAS sensors into spark-plugs [42,260,267–269], detonation combustors [202,212], and to provide single-ended measurements via the collection of backscattered laser light [202,265,270]. Single-ended sensing represents a particularly promising emerging frontier as it offers the potential to study many new applications and problems that were deemed inaccessible before.

14.2. Remaining needs and challenges

Despite the progress in the development of IR-LAS sensors for combustion, extensive research remains needed. Spectroscopic databases for molecular spectra at high-temperatures and -pressures continue to suffer from unsatisfactory accuracy, primarily due to errors and complexities associated with calculating collisional-broadening coefficients and lineshapes. Furthermore, these databases are applicable to a relatively small number of species of interest to combustion (namely, CO, CO₂, H₂O, NO, OH). As a result, research to improve the accuracy and breadth of spectroscopic databases relevant to combustion is needed, particularly to improve sensor accuracy and assist the design of sensors for high pressures.

Improvements in mid-infrared hardware and optical materials are also needed. While useful, the power, stability, tuning ability, and life-time of mid-infrared lasers is frequently inferior to their near-IR analogues. This currently limits the accuracy and precision of mid-infrared sensors below what is theoretically obtainable (e.g., due to their increased absorption strength) and complicates the integration of mid-infrared sensors into practical combustion systems outside the laboratory. Improvements in mid-infrared fiber and optical materials are also needed. Mid-IR fibers suffer from significantly larger bend losses and transmission losses which complicates or precludes remote placement of lasers. Materials that can tolerate high temperatures, pressures, and combustion gases with high transmission levels beyond 5 μm are also needed. This currently represents a major obstacle to improved detection of several species important

to combustion systems (e.g., NO, NH₃, hydrocarbons). Extending recently developed single-ended LAS packages to the mid-infrared is also needed.

Lastly, sensors for multi-species measurements and measurements at high pressures remain research fronts. While some promising work has been conducted, the potential of IR-LAS to expand sensing capabilities in these areas has yet to be realized. Prospects for improvement include the use of hyperspectral light-sources which can access multiple absorption bands and WMS techniques incorporating novel modulation techniques and frequency-multiplexing of multiple narrowband light sources.

We expect that the role of IR-LAS in combustion will continue to grow as researchers continue to improve and expand the capabilities of IR-LAS and improved light sources and hardware are developed. While some techniques are only in their infancy, others have matured into robust sensors capable of characterizing a wide range of practical combustion systems. As a result, we now embark on a time where the potential to not only improve our understanding of, but also control combustion devices has never been greater.

Acknowledgments

The authors thank their many colleagues worldwide for allowing their work to be discussed and shown here. Further, the authors thank Scott Sanders and Gregory Rieker for their valuable feedback regarding the status of hyperspectral sources and techniques, as well as the many present and past students of the Hanson Group at Stanford University who have helped support many of the LAS-sensing efforts discussed here. Lastly, Ronald Hanson expresses his deepest gratitude to the AFOSR, ARO, ONR, DoE and NSF for supporting the research and application of LAS sensors over the last 40 years.

References

- [1] Wolfrum J. Lasers in combustion: from basic theory to practical devices. *Proc Combust Inst* 1998; 1–41.
- [2] Hanson RK. Applications of quantitative laser sensors to kinetics, propulsion and practical energy systems. *Proc Combust Inst* 2011;33:1–40. doi: 10.1016/j.proci.2010.09.007. <http://linkinghub.elsevier.com/retrieve/pii/S1540748910003913>.
- [3] Allen MG. Diode laser absorption sensors for gas-dynamic and combustion flows. *Meas. Sci. Technol.* 1998;9(4):545–62. <http://www.ncbi.nlm.nih.gov/pubmed/11543363>.
- [4] Werle P. A review of recent advances in semiconductor laser based gas monitors. *Spectrochim Acta, Part A* 1998;54(2):197–236. doi: 10.1016/S1386-1425(97)00227-8.
- [5] Lackner M. Tunable diode laser absorption spectroscopy (TDLAS) in the process industries—a review. 23.
- [6] Schulz C, Dreizler A, Ebert V, Wolfrum J. 20. Combustion diagnostics. Springer handbook of experimental fluid mechanics; 20071241–315. doi: 10.1007/978-3-540-30299-5. <http://www.springerlink.com/index/10.1007/978-3-540-30299-5>.
- [7] Bolshov M, Kuritsyn Y, Romanovskii Y. Tunable diode laser spectroscopy as a technique for combustion diagnostics. *Spectrochim Acta, Part B* 2015;106:45–66. doi: 10.1016/j.sab.2015.01.010. <http://www.sciencedirect.com/science/article/pii/S058485471500021X>.
- [8] Eckbreth AC. Laser diagnostics for combustion temperatures and species. 2nd London: Taylor and Francis; 1996.
- [9] Kohse-Hoinghaus K, Jeffries JB. Applied combustion diagnostics. New York: Taylor and Francis; 2002.
- [10] Hanson RK, Spearin RM, Goldenstein CS. Spectroscopy and optical diagnostics for gases. Switzerland: Springer International Publishing; 2016.
- [11] Rothman LS, Gordon I, Babikov Y, Barbe A, Chris Benner D, Bernath P, et al. The HITRAN2012 molecular spectroscopic database. *J Quant Spectrosc Radiat Transf* 2013;130:4–50. doi: 10.1016/j.jqsrt.2013.07.002. <http://linkinghub.elsevier.com/retrieve/pii/S0022407313002859>.
- [12] Sulzmann KGP, Lowder JEL, Penner SS. Estimates of possible detection limits for combustion intermediates and products with line-center absorption and derivative spectroscopy using tunable lasers. *Combust Flame* 1973;20(2):177–91. doi: 10.1016/S0010-2180(73)80172-5.
- [13] Hanson RK, Kuntz PA, Kruger CH. High-resolution spectroscopy of combustion gases using a tunable diode laser. *Appl Opt* 1977;16(8):2045–8.
- [14] Hanson RK. Shock tube spectroscopy: advanced instrumentation with a tunable diode laser. *Appl Opt* 1977;16(6):1479–81.
- [15] Hanson RK, Falcone PK. Temperature measurement technique for high-temperature gases using a tunable diode laser. *Appl Opt* 1978;17(16):2477–80. doi: 10.1364/AO.17.002477. <http://www.ncbi.nlm.nih.gov/pubmed/20203804>.
- [16] Reid J, Shewchun J, Garside BK, Ballik EA. High sensitivity pollution detection employing tunable diode lasers. *Appl Opt* 1978;17(2):300–7. doi: 10.1364/AO.17.000300. <http://www.opticsinfobase.org/viewmedia.cfm?uri=ao-17-2-300&seq=0&html=true>.
- [17] Reid J, Garside BK, Shewchun J, El-Sherbiny M, Ballik EA. High sensitivity point monitoring of atmospheric gases employing tunable diode lasers. *Appl Opt* 1978;17(11):1806–10. doi: 10.1364/AO.17.001806. <http://www.ncbi.nlm.nih.gov/pubmed/20198072>.
- [18] Reid J, El-Sherbiny M, Garside BK, Ballik EA. Sensitivity limits of a tunable diode laser spectrometer, with application to the detection of NO₂ at the 100-ppt level. *Appl Opt* 1980;19(2):3349–54. doi: 10.1364/AO.19.003349.
- [19] Reid J, Labrie D. Second-Harmonic detection with tunable diode lasers – Comparison of experiment and theory*. *Appl Phys B* 1981;26:203–10.
- [20] Bjorklund GC. Frequency-modulation spectroscopy: a new method for measuring weak absorptions and dispersions. *Opt Lett* 1980;5(1):15–7. doi: 10.1364/OL.5.000015.
- [21] Cassidy DT, Reid J. Harmonic detection with tunable diode lasers-two-tone modulation*. *Appl Phys B* 1982;22:279–85.
- [22] Bjorklund GC, Levenson MD, Lenth W, Ortiz C. Frequency modulation (FM) spectroscopy. *Appl Phys B* 1983;32(3):145–52. doi: 10.1007/BF00688820.
- [23] Lenth W. High frequency heterodyne spectroscopy with current-modulated diode lasers. *IEEE J Quantum Electron* 1984;20(9):1045–50. doi: 10.1109/JQE.1984.1072505.
- [24] Cassidy DT. Trace gas detection using 1.3 μm ingaasp diode laser transmitter modules. *Appl Opt* 1988;27:610–4.
- [25] Philippe LC, Hanson RK. Laser-absorption mass flux sensor for high-speed air-flows. *Opt Lett* 1991;16(24):2002–4. doi: 10.1364/OL.16.002002. <http://www.ncbi.nlm.nih.gov/pubmed/19784209>.
- [26] Saprey A, McCormick P, Masterson P, Zhao Q, Sutherland L, Smith I, et al. Development of flight-worthy TDLAS-based oxygen sensor for HIFIRe-1. In: Proceedings of the 45th AIAA/ASME/SAE/ASEE joint propulsion conference & exhibit; 2009AIAA2009–4971.
- [27] Chen S-J, Paige M, Silver J, Williams S, Barhorst T. Laser-based mass flow rate sensor onboard HIFIRe Flight 1. In: Proceedings of the 45th AIAA/ASME/SAE/ASEE joint propulsion conference & exhibit; 2009AIAA2009–5065. August 2009.
- [28] Brown M, Barhorst T. Post-flight analysis of the diode-laser-based mass capture experiment onboard HIFIRe flight 1. In: Proceedings of the 17th AIAA international space planes and hypersonic systems and technologies conference; 2011AIAA2011–2359.
- [29] Arroyo MP, Hanson RK. Absorption measurements of water-vapor concentration, temperature, and line-shape parameters using a tunable ingaasp diode laser. *Appl Opt* 1993;32(30):6104–16. doi: 10.1364/AO.32.006104.
- [30] Baer DS, Hanson RK, Newfield ME, Gopaul NK. Multiplexed diode-laser sensor system for simultaneous h₂O, O₂, and temperature measurements. *Opt Lett* 1994;19(22):1900–2. doi: 10.1364/OL.19.001900.
- [31] Baer DS, Nagali V, Furlong ER, Hanson RK, Newfield ME. Scanned- and fixed-wavelength absorption diagnostics for combustion measurements using multiplexed diode lasers. *AIAA J* 1996;34(3):489–93. doi: 10.2514/3.13094. <http://arc.aiaa.org/doi/abs/10.2514/3.13094>.
- [32] Furlong ER, Mihalcea RM, Webber ME, Baer DS, Hanson RK. Diode-laser sensors for real-time control of pulsed combustion systems. *AIAA J* 1999;37(6):732–7.
- [33] Wang J, Sanders ST, Jeffries JB, Hanson RK. Oxygen measurements at high pressures with vertical cavity surface-emitting lasers. *Appl Phys B* 2001;72(7):865–72. doi: 10.1007/s003400100539. <http://www.springerlink.com/index/10.1007/s003400100539>.
- [34] Sanders ST, Mattison DW, Ma L, Jeffries JB, Hanson RK. Wavelength-agile diode-laser sensing strategies for monitoring gas properties in optically harsh flows: application in cesium-seeded pulse detonation. *Opt Express* 2002;10(12):14–505. <http://www.ncbi.nlm.nih.gov/pubmed/19436388>.
- [35] Sanders ST, Mattison DW, Jeffries JB, Hanson RK. Time-of-flight diode-laser velocimeter using a locally seeded atomic absorber: application in a pulse detonation engine. *Shock Waves* 2003;12(6):435–41. doi: 10.1007/s00193-003-0182-5. http://www.springerlink.com/openurl.asp?genre=&article_id=doi:10.1007/s00193-003-0182-5.
- [36] Kranendonk LA, Walewski JW, Kim T, Sanders ST. Wavelength-agile sensor applied for HCCI engine measurements. *Proc Combust Inst* 2005;30(1):1619–27. doi: 10.1016/j.proci.2004.08.211. <http://linkinghub.elsevier.com/retrieve/pii/S0082078404002632>.
- [37] Kranendonk LA, An X, Caswell AW, Herold RE, Sanders ST, Huber R, et al. High speed engine gas thermometry by fourier-domain mode-locked laser absorption spectroscopy. *Opt Express* 2007;15(23):28–15115. <http://www.ncbi.nlm.nih.gov/pubmed/19550795>.
- [38] Kranendonk LA, Caswell AW, Hagen CL, Neuroth CT, Shouse DT, Gord JR, et al. Temperature measurements in a gas-turbine-combustor sector rig using swept-wavelength absorption spectroscopy. *J Propul Power* 2009;25(4):859–63. doi: 10.2514/1.41587. <http://arc.aiaa.org/doi/abs/10.2514/1.41587>.
- [39] Fernholz T, Teichert H, Ebert V. Digital, phase-sensitive detection for *in situ* diode-laser spectroscopy under rapidly changing transmission conditions. *Appl Phys B* 2002;75(2–3):229–36. doi: 10.1007/s00340-002-0962-0. <http://link.springer.com/10.1007/s00340-002-0962-0>.

- [40] Li H, Rieker GB, Liu X, Jeffries JB, Hanson RK. Extension of wavelength-modulation spectroscopy to large modulation depth for diode laser absorption measurements in high-pressure gases. *Appl Opt* 2006;45(5):1052–61.
- [41] Rieker GB, Jeffries JB, Hanson RK. Calibration-free wavelength-modulation spectroscopy for measurements of gas temperature and concentration in harsh environments.. *Appl Opt* 2009;48(29):60–5546. <http://www.ncbi.nlm.nih.gov/pubmed/19823239>.
- [42] Rieker GB, Li H, Liu X, Liu JTC, Jeffries JB, Hanson RK, et al. Rapid measurements of temperature and H_2O concentration in IC engines with a spark plug-mounted diode laser sensor. *Proc Combust Inst* 2007;31(2):3041–9. doi: 10.1016/j.proci.2006.07.158. <http://linkinghub.elsevier.com/retrieve/pii/S1540748906001660>.
- [43] Rieker G, Jeffries J, Hanson R, Mathur T, Gruber M, Carter C. Diode laser-based detection of combustor instabilities with application to a scramjet engine. *Proc Combust Inst* 2009;32(1):831–8. doi: 10.1016/j.proci.2008.06.114. <http://www.sciencedirect.com/science/article/pii/S1540748908001399>.
- [44] Klingbeil AE, Jeffries JB, Hanson RK. Temperature- and composition-dependent mid-infrared absorption spectrum of gas-phase gasoline: model and measurements. *Fuel* 2008;87(17–18):3600–9. doi: 10.1016/j.fuel.2008.06.020. <http://linkinghub.elsevier.com/retrieve/pii/S0016236108002585>.
- [45] Varghese PL. Tunable infrared diode laser measurements of spectral parameters of carbon monoxide and hydrogen cyanide. Stanford University Ph.D. thesis; 1983.
- [46] Goldenstein CS, Hanson RK. Diode-laser measurements of linestrength and temperature-dependent lineshape parameters for H_2O transitions near 1.4 μm using voigt, rautian, galatry, and speed-dependent voigt profiles. *J Quant Spectrosc Radiat Transf* 2015;152:127–39. doi: 10.1016/j.jqsrt.2014.11.008. <http://linkinghub.elsevier.com/retrieve/pii/S002240731400449X>.
- [47] Rothman LS, Gordon I, Barber R, Dothe H, Gamache RR, Goldman A, et al. HITRAN: The high-temperature molecular spectroscopic database. *J Quant Spectrosc Radiat Transf* 2010;111(15):2139–50. doi: 10.1016/j.jqsrt.2010.05.001. <http://linkinghub.elsevier.com/retrieve/pii/S002240731000169X>.
- [48] Humlicek J. Optimized computation of the voigt and complex probability functions. *J Quant Spectrosc Radiat Transf* 1982;27(4):437–44. <http://www.sciencedirect.com/science/article/pii/0022407382900784>.
- [49] Kuntz M. A new implementation of the humlicek algorithm for the calculation of the voigt profile function. *J Quant Spectrosc Radiat Transf* 1997;51(6):819–24. <http://www.sciencedirect.com/science/article/pii/S0022407396001628>.
- [50] Ruyten W. Comment on a new implementation of the humlicek algorithm for the calculation of the voigt profile function by m. kuntz [JQSRT 57(6) (1997) 819824]. *J Quant Spectrosc Radiat Transf* 2004;86(2):231–3. doi: 10.1016/j.jqsrt.2003.12.027. <http://linkinghub.elsevier.com/retrieve/pii/S002240730300390X>.
- [51] McLean A, Mitchell C, Swanson D. Implementation of an efficient analytical approximation to the voigt function for photoemission lineshape analysis. *J Electron Spectros Relat Phenomena* 1994;69(2):125–32. doi: 10.1016/0368-2048(94)02189-7. <http://linkinghub.elsevier.com/retrieve/pii/0368204894021897>.
- [52] Dicke R. The effect of collisions upon the doppler width of spectral lines. *Phys Rev* 1953;89(2):472–3.
- [53] Rautian S, Sobelman I. The effect of collisions on the doppler broadening of spectral lines. *Sov Phys Uspekhi* 1967;9:701–16.
- [54] Galatry L. Simultaneous effect of doppler and foreign gas broadening on spectral lines. *Phys Rev* 1961;122(1961):1218–23. <http://onlinelibrary.wiley.com/doi/10.1002/cbdr.200490137/abstract>.
- [55] Ngo N, Lisak D, Tran H, Hartmann J-M. An isolated line-shape model to go beyond the voigt profile in spectroscopic databases and radiative transfer codes. *J Quant Spectrosc Radiat Transf* 2013;129:89–100. doi: 10.1016/j.jqsrt.2013.05.034. <http://dx.doi.org/10.1016/j.jqsrt.2013.05.034>.
- [56] Ward J, Cooper J, Smith EW. Correlation effects in the theory of combined doppler and pressure broadening-I. classical theory*. *J Quant Spectrosc Radiat Transf* 1974;14:555–90.
- [57] Rohart F, MaPéder H, Nicolaisen H-W. Speed dependence of rotational relaxation induced by foreign gas collisions: studies on CH_3F by millimeter wave coherent transients. *J Chem Phys* 1994;101(8):6475. doi: 10.1063/1.468342. <http://scitation.aip.org/content/aip/journal/jcp/101/8/10.1063/1.468342>.
- [58] Boone CD, Walker KA, Bernath PF. Speed-dependent voigt profile for water vapor in infrared remote sensing applications. *J Quant Spectrosc Radiat Transf* 2007;105(3):525–32. doi: 10.1016/j.jqsrt.2006.11.015. <http://linkinghub.elsevier.com/retrieve/pii/S00224073106003141>.
- [59] Tennyson J, Bernath PF, Campargue A, Császár AG, Daumont L, Gamache RR, et al. Recommended isolated-line profile for representing high-resolution spectroscopic transitions (IUPAC technical report). *Tech. Rep.* 12; 2014. doi: 10.1515/pac-2014-0208 1409.7782v2.
- [60] De Vizca MD, Castrillo a, Fasoli E, Amadio P, Moretti L, Gianfrani L. Experimental test of the quadratic approximation in the partially correlated speed-dependent hard-collision profile. *Phys Rev A* 2014;90(2):022503. doi: 10.1103/PhysRevA.90.022503. <http://link.aps.org/doi/10.1103/PhysRevA.90.022503>.
- [61] Hartmann J-M, Perrin MY, Ma Q, Tipping RH. The infrared continuum of pure water vapor: calculations and high-temperature measurements. *J Quant Spectrosc Radiat Transf* 1993;49(6):675–91.
- [62] Clough SA, Kneizys FX, Davies RW. Line shape and the water vapor continuum. *Atmos Res* 1989;23(3–4):229–41. doi: 10.1016/0169-8095(89)90020-3.
- [63] Rieker GB, Liu X, Li H, Jeffries JB, Hanson RK. Measurements of near-IR water vapor absorption at high pressure and temperature. *Appl Phys B* 2006;87(1):169–78. doi: 10.1007/s00340-006-2523-4. <http://link.springer.com/10.1007/s00340-006-2523-4>.
- [64] Hartmann J-M, Boulet C, Robert D. Collisional effects on molecular spectra. Elsevier Inc.; 2008.
- [65] Farooq A, Jeffries JB, Hanson RK. High-pressure measurements of CO_2 absorption near 2.7 μm : line mixing and finite duration collision effects. *J Quant Spectrosc Radiat Transf* 2010;111(7–8):949–60. doi: 10.1016/j.jqsrt.2010.01.001. <http://dx.doi.org/10.1016/j.jqsrt.2010.01.001>.
- [66] Nagali V. Diode laser study of high-pressure water-vapor spectroscopy. Stanford University Ph.D. thesis; 1998.
- [67] Christiansen C, Stolberg-Rohr T, Fateev A, Clausen S. High temperature and high pressure gas cell for quantitative spectroscopic measurements. *J Quant Spectrosc Radiat Transf* 2016;169:96–103. doi: 10.1016/j.jqsrt.2015.10.006. <http://linkinghub.elsevier.com/retrieve/pii/S0022407315003180>.
- [68] Eng RS, Calawa AR, Harman TC, Kelley PL, Javan A. Collisional narrowing of infrared water-vapor transitions. *Appl Phys Lett* 1972;21(7):303–5. doi: 10.1063/1.1654387.
- [69] Pine A. Collisional narrowing of HF fundamental band spectral lines by neon and argon. *J Mol Spectrosc* 1980;82:435–48.
- [70] Varghese PL, Hanson RK. Collisional narrowing effects on spectral line shapes measured at high resolution.. *Appl Opt* 1984;23(14):2376–85. <http://www.ncbi.nlm.nih.gov/pubmed/18213005>.
- [71] Rao DR, Oka T. Dicke narrowing and pressure broadening in the infrared fundamental band of HCl perturbed by ar. *J Mol Spectrosc* 1987;122:16–27.
- [72] D'Eu JF, Lemoine B, Rohart F. Infrared HCN lineshapes as a test of galatry and speed-dependent voigt profiles. *J Mol Spectrosc* 2002;212:96–110. doi: 10.1006/jmsp.2002.8520. <http://linkinghub.elsevier.com/retrieve/pii/S002285202985206>.
- [73] Hodges J, Lisak D, Lavrentieva N, Bykov A, Sinitis L, Tennyson J, et al. Comparison between theoretical calculations and high-resolution measurements of pressure broadening for near-infrared water spectra. *J Mol Spectrosc* 2008;249(2):86–94. doi: 10.1016/j.jms.2008.02.022. <http://linkinghub.elsevier.com/retrieve/pii/S0022285208000957>.
- [74] Li H, Farooq A, Jeffries JB, Hanson RK. Diode laser measurements of temperature-dependent collisional-narrowing and broadening parameters of ar-perturbed H_2O transitions at 1391.7 and 1397.8 nm. *J Quant Spectrosc Radiat Transf* 2008;109(1):132–43. doi: 10.1016/j.jqsrt.2007.05.008.
- [75] Ngo N, Ibrahim N, Landsheere X, Tran H, Chepin P, Schwell M, et al. Intensities and shapes of H_2O lines in the near-infrared by tunable diode laser spectroscopy. *J Quant Spectrosc Radiat Transf* 2012;113(11):870–7. doi: 10.1016/j.jqsrt.2011.12.007. <http://linkinghub.elsevier.com/retrieve/pii/S0022407311004213>.
- [76] Goldenstein CS, Jeffries JB, Hanson RK. Diode laser measurements of line-strength and temperature-dependent lineshape parameters of H_2O , CO_2 , and N_2 -perturbed H_2O transitions near 2474 and 2482 nm. *J Quant Spectrosc Radiat Transf* 2013;130:100–11. doi: 10.1016/j.jqsrt.2013.06.008. <http://linkinghub.elsevier.com/retrieve/pii/S0022407313002525>.
- [77] Nagali V, Hanson RK. Design of a diode-laser sensor to monitor water vapor in high-pressure combustion gases. *Appl Opt* 1997;36(36):9518–27. <http://www.ncbi.nlm.nih.gov/pubmed/18264514>.
- [78] Perrin M, Hartmann J. Temperature-dependent measurements and modeling of absorption by $\text{CO}_2\text{-N}_2$ mixtures in the far line-wings of the 4.3 μm CO_2 band. *J Quant Spectrosc Radiat Transf* 1989;42(4):311–7. doi: 10.1016/0022-4073(89)90077-0. <http://www.sciencedirect.com/science/article/pii/002240738900770>.
- [79] Rieker GB, Jeffries JB, Hanson RK. Measurements of high-pressure CO_2 absorption near 2.0 μm and its implications on tunable diode laser sensor design. *Appl Phys B* 2008;94(1):51–63. doi: 10.1007/s00340-008-3280-3. <http://www.springerlink.com/index/10.1007/s00340-008-3280-3>.
- [80] Stefaní S, Piccioni G, Snels M, Grassi D, Adriani A. Experimental CO_2 absorption coefficients at high pressure and high temperature. *J Quant Spectrosc Radiat Transf* 2013;117:21–8. doi: 10.1016/j.jqsrt.2012.11.019. <http://www.sciencedirect.com/science/article/pii/S0022407312005250>.
- [81] Niro F, Jucks K, Hartmann J-M. Spectra calculations in central and wing regions of IR bands. IV: software and database for the computation of atmospheric spectra. *J Quant Spectrosc Radiat Transf* 2005;95(4):469–81. doi: 10.1016/j.jqsrt.2004.11.011. <http://www.sciencedirect.com/science/article/pii/S0022407304004820>.
- [82] Filipov NN, Aspin RE, Sinyakova TN, Grigoriev IM, Petrova TM, Solodov AM, et al. Experimental and theoretical studies of CO_2 spectra for planetary atmosphere modelling: region 600–9650 cm^{-1} and pressures up to 60 atm.. *PCCP* 2013;15(33):13826–34. doi: 10.1039/c3cp50279a. <http://pubs.rsc.org/en/content/articlehtml/2013/cp/c3cp50279a>.
- [83] Tran H, Boulet C, Stefaní S, Snels M, Piccioni G. Measurements and modelling of high pressure pure CO_2 spectra from 750 to 8500 cm^{-1} . icentral and wing regions of the allowed vibrational bands. *J Quant Spectrosc Radiat Transf* 2011;112(6):925–36. doi: 10.1016/j.jqsrt.2010.11.021. <http://www.sciencedirect.com/science/article/pii/S0022407310004449>.
- [84] Alberti M, Weber R, Mancini M. Re-creating Hottel's emissivity charts for carbon dioxide and extending them to 40 bar pressure using HITRAN-2010 data base. *Combust Flame* 2015;162(3):597–612. doi: 10.1016/j.combust-flame.2014.09.005. <http://www.sciencedirect.com/science/article/pii/S001218014002739>.
- [85] Lamouroux J, Régalia L, Thomas X, Vander Auwera J, Gamache R, Hartmann J-M. CO_2 Line-mixing database and software update and its tests in the 2.1 μm and

- 4.3 μm regions. *J Quant Spectrosc Radiat Transf* 2015;151:88–96. doi: [10.1016/j.jqsrt.2014.09.017](https://doi.org/10.1016/j.jqsrt.2014.09.017). <http://www.sciencedirect.com/science/article/pii/S0022407314003896>.
- [86] Sur R, Spearin RM, Peng WY, Strand CL, Jeffries JB, Enns GM, et al. Line intensities and temperature-dependent line broadening coefficients of Q-branch transitions in the ν_2 band of ammonia near 10.4 μm . *J Quant Spectrosc Radiat Transf* 2016;175:90–9. doi: [10.1016/j.jqsrt.2016.02.002](https://doi.org/10.1016/j.jqsrt.2016.02.002). <http://www.sciencedirect.com/science/article/pii/S0022407315302727>.
- [87] Jacquinet-Husson N, Scott N, Chédin A, Crépeau L, Armante R, Capelle V, et al. The GEISA spectroscopic database: current and future archive for earth and planetary atmosphere studies. *J Quant Spectrosc Radiat Transf* 2008;109(6):1043–59. doi: [10.1016/j.jqsrt.2007.12.015](https://doi.org/10.1016/j.jqsrt.2007.12.015). <http://www.sciencedirect.com/science/article/pii/S0022407307003536>.
- [88] Tashkun S, Perevalov V, Teffo J-L, Bykov A, Lavrentieva N. CDSD-1000, The high-temperature carbon dioxide spectroscopic databank. *J Quant Spectrosc Radiat Transf* 2003;82(1–4):165–96. doi: [10.1016/S0022-4073\(03\)00152-3](https://doi.org/10.1016/S0022-4073(03)00152-3). <http://www.sciencedirect.com/science/article/pii/S0022407303001523>.
- [89] Tashkun S, Perevalov V. CDSD-4000: High-resolution, high-temperature carbon dioxide spectroscopic databank. *J Quant Spectrosc Radiat Transf* 2011;112(9):1403–10. doi: [10.1016/j.jqsrt.2011.03.005](https://doi.org/10.1016/j.jqsrt.2011.03.005). <http://www.sciencedirect.com/science/article/pii/S0022407311001154>.
- [90] Barber RJ, Tennyson J, Harris GJ, Tolchenov RN. A high-accuracy computed water line list. *Mon Not R Astron Soc* 2006;368(3):1087–94. doi: [10.1111/j.1365-2966.2006.10184.x](https://doi.org/10.1111/j.1365-2966.2006.10184.x). <http://mnras.oxfordjournals.org/content/368/3/1087.full>.
- [91] Sharp SW, Johnson T, Sams R, Chu P, Rhoderick G, Johnson P. Gas-phase databases for quantitative infrared spectroscopy. *Appl Spectrosc* 2004;58(12):1452–61. doi: [10.1017/CBO9781107415324.004](https://doi.org/10.1017/CBO9781107415324.004) [10.1111/j.1365-2966.2006.10184.x](https://doi.org/10.1111/j.1365-2966.2006.10184.x).
- [92] Chu P, Guenther F, Rhoderick G, Lafferty W. The NIST quantitative infrared database. *J Res Natl Inst Stand Technol* 1999;104(59). <http://search.proquest.com.ezproxy.lib.psu.edu/docview/214782265/pq-origsite=gscholar>.
- [93] Toth RA. Measurements of positions, strengths and self-broadened widths of H_2O from 2900 to 8000 cm^{-1} : line strength analysis of the 2nd triad bands. *J Quant Spectrosc Radiat Transf* 2005;94(1):51–107. doi: [10.1016/j.jqsrt.2004.08.042](https://doi.org/10.1016/j.jqsrt.2004.08.042). <http://linkinghub.elsevier.com/retrieve/pii/S0022407304003528>.
- [94] Toth RA, Brown L, Smith M, Malathy Devi V, Chris Benner D, Dulick M. Air-broadening of H_2O as a function of temperature: 696–2163 cm^{-1} . *J Quant Spectrosc Radiat Transf* 2006;101(2):339–66. doi: [10.1016/j.jqsrt.2005.11.022](https://doi.org/10.1016/j.jqsrt.2005.11.022). <http://linkinghub.elsevier.com/retrieve/pii/S0022407305003626>.
- [95] Liu X, Jeffries JB, Hanson RK. Measurements of spectral parameters of water-vapour transitions near 1388 and 1345 nm for accurate simulation of high-pressure absorption spectra. *Meas Sci Technol* 2007;18:1185–94. doi: [10.1088/0957-0233/18/5/004](https://doi.org/10.1088/0957-0233/18/5/004).
- [96] Liu X, Zhou X, Jeffries JB, Hanson RK. Experimental study of H_2O spectroscopic parameters in the near-IR (6940–7440 cm^{-1}) for gas sensing applications at elevated temperature. *J Quant Spectrosc Radiat Transf* 2007;103(3):565–77. doi: [10.1016/j.jqsrt.2006.07.008](https://doi.org/10.1016/j.jqsrt.2006.07.008).
- [97] Pogány A, Klein A, Ebert V. Measurement of water vapor line strengths in the 1.4–2.7 μm range by tunable diode laser absorption spectroscopy. *J Quant Spectrosc Radiat Transf* 2015;165:108–22. doi: [10.1016/j.jqsrt.2015.06.023](https://doi.org/10.1016/j.jqsrt.2015.06.023). <http://linkinghub.elsevier.com/retrieve/pii/S0022407315002290>.
- [98] Melin ST, Sanders ST. Gas cell based on optical contacting for fundamental spectroscopy studies with initial reference absorption spectrum of H_2O vapor at 1723 K and 0.0235 bar. *J Quant Spectrosc Radiat Transf* 2016;180:184–91. doi: [10.1016/j.jqsrt.2016.04.009](https://doi.org/10.1016/j.jqsrt.2016.04.009). <http://dx.doi.org/10.1016/j.jqsrt.2016.04.009>.
- [99] Li G, Serdyukov A, Gisi M, Werhahn O, Ebert V. FTIR-Based measurements of self-broadening and self-shift coefficients as well as line strength in the first overtone band of HCl at 1.76 μm . *J Quant Spectrosc Radiat Transf* 2015;165:76–87. doi: [10.1016/j.jqsrt.2015.06.021](https://doi.org/10.1016/j.jqsrt.2015.06.021). <http://dx.doi.org/10.1016/j.jqsrt.2015.06.021>.
- [100] Ortwein P, Woiwode W, Wagner S, Gisi M, Ebert V. Laser-based measurements of line strength, selfand pressure-broadening coefficients of the $\text{h}^3\text{c}\text{l}$ r(3) absorption line in the first overtone region for pressures up to 1 MPa. *Appl Phys B: Lasers Opt* 2010;100(2):341–7. doi: [10.1007/s00340-009-3862-8](https://doi.org/10.1007/s00340-009-3862-8).
- [101] Spearin RM, Goldenstein CS, Jeffries JB, Hanson RK. Fiber-coupled 2.7 μm laser absorption sensor for CO_2 in harsh combustion environments. *Meas Sci Technol* 2013;24:055107. doi: [10.1088/0957-0233/24/5/055107](https://doi.org/10.1088/0957-0233/24/5/055107).
- [102] Farooq A, Jeffries J, Hanson R. CO_2 Concentration and temperature sensor for combustion gases using diode-laser absorption near 2.7 μm . *Appl Phys B* 2008;90(3–4):619–28. doi: [10.1007/s00340-007-2925-y](https://doi.org/10.1007/s00340-007-2925-y). <http://link.springer.com/10.1007/s00340-007-2925-y>.
- [103] Spearin RM, Ren W, Jeffries JB, Hanson RK. Multi-band infrared CO_2 absorption sensor for sensitive temperature and species measurements in high-temperature gases. *Appl Phys B* 2014;116(4):855–65. doi: [10.1007/s00340-014-5772-7](https://doi.org/10.1007/s00340-014-5772-7). <http://link.springer.com/10.1007/s00340-014-5772-7>.
- [104] Medvecz PJ, Nichols KM. Experimental determination of line strengths for selected carbon monoxide and carbon dioxide absorption lines at temperatures between 295 and 1250 K. *Appl Spectrosc* 1994;48(11):1442–50. <http://www.osapublishing.org/abstract.cfm?uri=as-48-11-1442>.
- [105] Vanderover J, Wang W, Oehlschlaeger MA. A carbon monoxide and thermometry sensor based on mid-IR quantum-cascade laser wavelength-modulation absorption spectroscopy. *Appl Phys B* 2011;103(4):959–66. doi: [10.1007/s00340-011-4570-8](https://doi.org/10.1007/s00340-011-4570-8). <http://link.springer.com/10.1007/s00340-011-4570-8>.
- [106] Spearin RM, Goldenstein CS, Jeffries JB, Hanson RK. Quantum cascade laser absorption sensor for carbon monoxide in high-pressure gases using wavelength modulation spectroscopy. *Appl Opt* 2014;53(9):1938–46. <http://www.ncbi.nlm.nih.gov/pubmed/24663473>.
- [107] Sur R, Sun K, Jeffries JB, Hanson RK. Multi-species laser absorption sensors for *in situ* monitoring of syngas composition. *Appl Phys B* 2013;115(1):9–24. doi: [10.1007/s00340-013-5567-2](https://doi.org/10.1007/s00340-013-5567-2). <http://link.springer.com/10.1007/s00340-013-5567-2>.
- [108] Klingbeil AE, Jeffries JB, Hanson RK. Design of a fiber-coupled mid-infrared fuel sensor for pulse detonation engines. *AIAA J* 2007;45(4):772–8. doi: [10.2514/1.26504](https://doi.org/10.2514/1.26504).
- [109] Sajid M, Javed T, Farooq A. High-temperature measurements of methane and acetylene using quantum cascade laser absorption near 8 μm . *J Quant Spectrosc Radiat Transf* 2015;165:66–74. doi: [10.1016/j.jqsrt.2015.01.009](https://doi.org/10.1016/j.jqsrt.2015.01.009). <http://www.sciencedirect.com/science/article/pii/S002240731500028X>.
- [110] Sur R, Wang S, Sun K, Davidson DF, Jeffries JB, Hanson RK. High-sensitivity interference-free diagnostic for measurement of methane in shock tubes. *J Quant Spectrosc Radiat Transf* 2015;156:80–7. doi: [10.1016/j.jqsrt.2015.01.023](https://doi.org/10.1016/j.jqsrt.2015.01.023). <http://www.sciencedirect.com/science/article/pii/S0022407315000424>.
- [111] Ren W, Davidson DF, Hanson RK. IR Laser absorption diagnostic for C_2H_4 in shock tube kinetics studies. *Int J Chem Kinet* 2012;44(6):423–32. doi: [10.1002/kin.20599](https://doi.org/10.1002/kin.20599). <http://doi.wiley.com/10.1002/kin.20599>.
- [112] Es-sebbar E-t, Alrefae M, Farooq A. Infrared cross-sections and integrated band intensities of propylene: temperature-dependent studies. *J Quant Spectrosc Radiat Transfer* 2014;133:559–69. doi: [10.1016/j.jqsrt.2013.09.019](https://doi.org/10.1016/j.jqsrt.2013.09.019). <http://dx.doi.org/10.1016/j.jqsrt.2013.09.019>.
- [113] Chrystie RM, Nasir EF, Farooq A. Propene concentration sensing for combustion gases using quantum-cascade laser absorption near 11 μm . *Appl Phys B* 2015;120(2):317–27. doi: [10.1007/s00340-015-6139-4](https://doi.org/10.1007/s00340-015-6139-4). <http://link.springer.com/10.1007/s00340-015-6139-4>.
- [114] Spearin R, Li S, Davidson D, Jeffries J, Hanson R. High-temperature isobutene absorption diagnostic for shock tube kinetics using a pulsed quantum cascade laser near 11.3 μm . *Proc Combust Inst* 2015;35(3):3645–51. doi: [10.1016/j.proci.2014.04.002](https://doi.org/10.1016/j.proci.2014.04.002). <http://www.sciencedirect.com/science/article/pii/S1540748914000030>.
- [115] Spearin RM, Schultz IA, Jeffries JB, Hanson RK. Laser absorption of nitric oxide for thermometry in high-enthalpy air. *Meas Sci Technol* 2014;25(12):125103. doi: [10.1088/0957-0233/25/12/125103](https://doi.org/10.1088/0957-0233/25/12/125103). <http://iopscience.iop.org/0957-0233/25/12/125103/article>.
- [116] Sur R, Peng WY, Strand CL, Spearin RM, Jeffries JB, Hanson RK. Mid-infrared laser absorption spectroscopy of NO_2 at elevated temperatures. *J Quant Spectrosc Radiat Transf* 2016 (In press).
- [117] Werwein V, Brunzendorf J, Serdyukov A, Werhahn O, Ebert V. First measurements of nitrous oxide self-broadening and self-shift coefficients in the 0002–0000 band at 2.26 μm using high resolution fourier transform spectroscopy. *J Mol Spectrosc* 2016;323:28–42. doi: [10.1016/j.jms.2016.01.010](https://doi.org/10.1016/j.jms.2016.01.010). <http://dx.doi.org/10.1016/j.jms.2016.01.010>.
- [118] Schilt S. Impact of water vapor on 1.51 μm ammonia absorption features used in trace gas sensing applications. *Appl Phys B* 2010;100(2):349–59. doi: [10.1007/s00340-010-3954-5](https://doi.org/10.1007/s00340-010-3954-5). <http://link.springer.com/10.1007/s00340-010-3954-5>.
- [119] Owen K, Es-sebbar E-t, Farooq A. Measurements of NH_3 linestrengths and collisional broadening coefficients in N_2 , O_2 , CO_2 , and H_2O near 1103.46 cm^{-1} . *J Quant Spectrosc Radiat Transf* 2013;121:56–68. doi: [10.1016/j.jqsrt.2013.02.001](https://doi.org/10.1016/j.jqsrt.2013.02.001). <http://www.sciencedirect.com/science/article/pii/S0022407313000460>.
- [120] Dhib M, Bouanich J-P, Aroui H, Picard-Bersellini A. Analysis of N_2 , O_2 , CO_2 , and air broadening of infrared spectral lines in the ν_4 band of NH_3 . *J Quant Spectrosc Radiat Transf* 2001;68(2):163–78. doi: [10.1016/S0022-4073\(00\)00020-0](https://doi.org/10.1016/S0022-4073(00)00020-0). <http://www.sciencedirect.com/science/article/pii/S002240730000200>.
- [121] Klingbeil AE, Jeffries JB, Hanson RK. Temperature-dependent mid-IR absorption spectra of gaseous hydrocarbons. *J Quant Spectrosc Radiat Transf* 2007;107(3):407–20. doi: [10.1016/j.jqsrt.2007.03.004](https://doi.org/10.1016/j.jqsrt.2007.03.004). <http://www.sciencedirect.com/science/article/pii/S0022407307007129>.
- [122] Es-Sebbar ET, Benilan Y, Farooq A. Temperature-dependent absorption cross-section measurements of 1-butene ($1-\text{C}_4\text{H}_8$) in VUV and IR. *J Quant Spectrosc Radiat Transf* 2013;115:1–12. doi: [10.1016/j.jqsrt.2012.09.014](https://doi.org/10.1016/j.jqsrt.2012.09.014). <http://dx.doi.org/10.1016/j.jqsrt.2012.09.014>.
- [123] Es-sebbar E, Jolly A, Benilan Y, Farooq A. Quantitative mid-infrared spectra of allene and propyne from room to high temperatures. *J Mol Spectrosc* 2014;305:10–6. doi: [10.1016/j.jms.2014.09.004](https://doi.org/10.1016/j.jms.2014.09.004). <http://link.springer.com/10.1016/j.jms.2014.09.004>.
- [124] Alrefae M, Farooq A. Absorption cross-section measurements of methane, ethane, ethylene and methanol at high temperatures. *J Mol Spectrosc* 2014;303:8–14. doi: [10.1016/j.jms.2014.06.007](https://doi.org/10.1016/j.jms.2014.06.007). <http://dx.doi.org/10.1016/j.jms.2014.06.007>.
- [125] Goldenstein, C.S., Miller V.A., Spearin R.M., Strand C.L. SpectraPlot.com: Spectroscopic Models for Atomic and Molecular Gases. 2016.
- [126] Sanders ST, Baldwin JA, Jenkins TP, Baer DS, Hanson RK. Diode-laser sensor for monitoring multiple combustion parameters in pulse detonation engines. *Proc Combust Inst* 2000;28(1):587–94. doi: [10.1016/S0080-0784\(00\)80258-1](https://doi.org/10.1016/S0080-0784(00)80258-1). [http://link.springer.com/10.1016/S0080-0784\(00\)80258-1](http://link.springer.com/10.1016/S0080-0784(00)80258-1).
- [127] Hanson RK, Davidson DF. Recent advances in laser absorption and shock tube methods for studies of combustion chemistry. *Prog Energy Combust Sci* 2014;44:103–14. doi: [10.1016/j.pecs.2014.05.001](https://doi.org/10.1016/j.pecs.2014.05.001). <http://dx.doi.org/10.1016/j.pecs.2014.05.001>.

- [128] Mattison DW, Jeffries JB, Hanson RK, Steeper R, De Zilwa S, Dec J, et al. In-cylinder gas temperature and water concentration measurements in HCCI engines using a multiplexed-wavelength diode-laser system: sensor development and initial demonstration. *Proc Combust Inst* 2007;31(1):791–8. doi: [10.1016/j.proci.2006.07.048](https://doi.org/10.1016/j.proci.2006.07.048). <http://linkinghub.elsevier.com/retrieve/pii/S1540748906000605>.
- [129] Brown M, Herring G, Cabell K, Hass N, Barhorst T, Gruber M. Optical measurements at the combustor exit of the HiFIRE 2 ground test engine. In: Proceedings of the 50th AIAA aerospace sciences meeting including the new horizons forum and aerospace exposition; 2012. p. 2012AIAA2012-0857, ISBN: 978-1-60086-936-5.
- [130] Jatana GS, Magee M, Fain D, Naik SV, Shaver GM, Lucht RP. Simultaneous high-speed gas property measurements at the exhaust gas recirculation cooler exit and at the turbocharger inlet of a multicylinder diesel engine using diode-laser-absorption spectroscopy. *Appl Opt* 2015;54(5):1220–31. doi: [10.1364/AO.54.001220](https://doi.org/10.1364/AO.54.001220). <http://www.osapublishing.org/viewmedia.cfm?uri=ao-54-5-1220&seq=0&html=true>.
- [131] Busa KM, Rice B, McDaniel JC, Goyne CP, Rockwell RD, Fulton JA, et al. Direct measurement of combustion efficiency of a dual-mode scramjet via TDLAT and SPIV. In: Proceedings of the 53rd AIAA aerospace sciences meeting; 2015. p. 2015AIAA2015-0357, ISBN: 978-1-62410-343-8. doi: [10.2514/6.2015-0357](https://doi.org/10.2514/6.2015-0357). <http://arc.aiaa.org/doi/10.2514/6.2015-0357>.
- [132] Sanders ST. Wavelength-agile fiber laser using group-velocity dispersion of pulsed super-continua and application to broadband absorption spectroscopy. *Appl Phys B* 2002;75(6–7):799–802. doi: [10.1007/s00340-002-1044-z](https://doi.org/10.1007/s00340-002-1044-z).
- [133] Kranendonk LA, Huber R, Fujimoto JG, Sanders ST. Wavelength-agile H_2O absorption spectrometer for thermometry of general combustion gases. *Proc Combust Inst* 2007;31(1):783–90. doi: [10.1016/j.proci.2006.08.003](https://doi.org/10.1016/j.proci.2006.08.003). <http://linkinghub.elsevier.com/retrieve/pii/S1540748906002665>.
- [134] Blume NG, Wagner S. Broadband supercontinuum laser absorption spectrometer for multiparameter gas phase combustion diagnostics. *Opt Lett* 2015;40(13):3141–4.
- [135] Rieker GB, Giorgetta FR, Swann WC, Kofler J, Zolot AM, Sinclair LC, et al. Frequency-comb-based remote sensing of greenhouse gases over kilometer air paths. *Optica* 2014;1(5):290–8. doi: [10.1364/OPTICA.1.000290](https://doi.org/10.1364/OPTICA.1.000290). <http://www.osapublishing.org/optica/abstract.cfm?URI=optica-1-5-290>.
- [136] Silver JA, Kane DJ. Diode laser measurements of concentration and temperature in microgravity combustion. *Meas Sci Technol* 1999;10(10):845–52. doi: [10.1088/0957-0233/10/10/a=303?key=crossref.b065b18e60010ee90787875a1566c376](https://doi.org/10.1088/0957-0233/10/10/303).
- [137] Cassidy DT, Reid J. Atmospheric pressure monitoring of trace gases using tunable diode lasers. *Appl Opt* 1982;21(7):1185–90. <http://www.ncbi.nlm.nih.gov/pubmed/20389829>.
- [138] Sun K, Chao X, Sur R, Goldenstein CS, Jeffries JB, Hanson RK. Analysis of calibration-free wavelength-scanned wavelength modulation spectroscopy for practical gas sensing using tunable diode lasers. *Meas Sci Technol* 2013;24:125203. doi: [10.1088/0957-0233/24/12/125203](https://doi.org/10.1088/0957-0233/24/12/125203).
- [139] Goldenstein CS, Strand CL, Schultz IA, Sun K, Jeffries JB, Hanson RK. Fitting of calibration-free scanned-wavelength-modulation spectroscopy spectra for determination of gas properties and absorption lineshapes. *Appl Opt* 2014;53(3):356–67.
- [140] Qu Z, Ghorbani R, Valiev D, Schmidt FM. Calibration-free scanned wavelength modulation spectroscopy application to H_2O and temperature sensing in flames. *Opt Express* 2015;23(12):16492–9. doi: [10.1364/OE.23.016492](https://doi.org/10.1364/OE.23.016492). <https://www.osapublishing.org/oe/abstract.cfm?uri=oe-23-12-16492>.
- [141] Kluczynski P, Axner O. Theoretical description based on fourier analysis of wavelength-modulation spectrometry in terms of analytical and background signals. *Appl Opt* 1999;38(27):5803–15.
- [142] Kluczynski P, Lindberg AM, Axner O. Characterization of background signals in wavelength-modulation spectrometry in terms of a fourier based theoretical formalism. *Appl Opt* 2001;40(6):770–82. doi: [10.1364/AO.40.000770](https://doi.org/10.1364/AO.40.000770). <http://www.osapublishing.org/viewmedia.cfm?uri=ao-40-6-770&seq=0&html=true>.
- [143] Gustafsson J, Axner O. 'Intelligent' Triggering methodology for improved detectability of wavelength modulation diode laser absorption spectrometry applied to window-equipped graphite furnaces. *Spectrochim Acta, Part B* 2003;58(1):143–52. doi: [10.1016/S0584-8547\(02\)00218-5](https://doi.org/10.1016/S0584-8547(02)00218-5). <http://linkinghub.elsevier.com/retrieve/pii/S0584854702002185>.
- [144] Sun K, Chao X, Sur R, Jeffries JB, Hanson RK. Wavelength modulation diode laser absorption spectroscopy for high-pressure gas sensing. *Appl Phys B* 2013;110:497–508. doi: [10.1007/s00340-012-5286-0](https://doi.org/10.1007/s00340-012-5286-0). <http://www.springerlink.com/index/10.1007/s00340-012-5286-0>.
- [145] Goldenstein CS, Almodovar CA, Jeffries JB, Hanson RK. High-bandwidth scanned-wavelength-modulation spectroscopy sensors for temperature and H_2O in a rotating detonation engine. *Meas Sci Technol* 2014;25:105104.
- [146] Silver JA. Frequency-modulation spectroscopy for trace species detection: theory and comparison among experimental methods. *Appl Opt* 1992;31(6):707–17. <http://www.ncbi.nlm.nih.gov/pubmed/20733651>.
- [147] McGettrick AJ, Duffin K, Johnstone W, Stewart G, Moodie DG. Tunable diode laser spectroscopy with wavelength modulation: a phasor decomposition method for calibration-free measurements of gas concentration and pressure. *J Lightwave Technol* 2008;26(4):432–40. doi: [10.1109/JLT.2007.912519](https://doi.org/10.1109/JLT.2007.912519). <http://ieeexplore.ieee.org/lpdocs/epic03/wrapper.htm?arnumber=4451270>.
- [148] Bain JRP, Johnstone W, Ruxton K, Stewart G, Lengden M, Duffin K. Recovery of absolute gas absorption line shapes using tunable diode laser spectroscopy with wavelength modulation-Part 2: experimental investigation. *J Lightwave Technol* 2011;29(7):987–96.
- [149] Harris SJ. Intracavity laser spectroscopy: an old field with new prospects for combustion diagnostics. *Appl Opt* 1984;23(9):1311–8. doi: [10.1364/AO.23.001311](https://doi.org/10.1364/AO.23.001311).
- [150] Goldman A, Rahinov I, Cheskis S, Lohden B, Wexler S, Sengstock K, et al. Fiber laser intracavity absorption spectroscopy of ammonia and hydrogen cyanide in low pressure hydrocarbon flames. *Chem Phys Lett* 2006;423(1–3):147–51. doi: [10.1016/j.cplett.2006.03.052](https://doi.org/10.1016/j.cplett.2006.03.052).
- [151] Lohden B, Kuznetsova S, Sengstock K, Baev VM, Goldman A, Cheskis S, et al. Fiber laser intracavity absorption spectroscopy for *in situ* multicomponent gas analysis in the atmosphere and combustion environments. *Appl Phys B* 2011;102(2):331–44. doi: [10.1007/s00340-010-3995-9](https://doi.org/10.1007/s00340-010-3995-9).
- [152] Watt RS, Laurila T, Kaminski CF, Hult J. Cavity enhanced spectroscopy of high-temperature H_2O in the near-infrared using a supercontinuum light source. *Appl Spectrosc* 2009;63(12):1389–13–95. doi: [10.1366/000370209790108987](https://doi.org/10.1366/000370209790108987). <http://www.ncbi.nlm.nih.gov/pubmed/20030985>.
- [153] Alrahman CA, Khodabakhsh A, Schmidt FM, Qu Z, Foltynowicz A. Cavity-enhanced optical frequency comb spectroscopy of high-temperature H_2O in a flame. *Opt Express* 2014;22(11):13889. doi: [10.1364/OE.22.013889](https://doi.org/10.1364/OE.22.013889). <http://www.opticsexpress.org/abstract.cfm?URI=oe-22-11-13889>.
- [154] O'Keefe A, Scherer JJ, Paul JB. CW integrated cavity output spectroscopy. *Chem Phys Lett* 1999;307(17):343–9.
- [155] Paul JB, Lapson L, Anderson JG. Ultrasensitive absorption spectroscopy with a high-finesse optical cavity and off-axis alignment. *Appl Opt* 2001;40(27):4904–10. doi: [10.1364/AO.40.004904](https://doi.org/10.1364/AO.40.004904). <http://www.opticsinfobase.org/abstract.cfm?URI=AO.40-27-4904>.
- [156] Paul JB, Scherer JJ, O'Keefe A, Lapson L, Anderson JG, Gmachl CF, et al. Infrared cavity ringdown and integrated cavity output spectroscopy for trace species monitoring. *Proc SPIE* 2002;4577:1–11.
- [157] Moyer E, Sayres D, Engel G, St. Clair J, Keutsch F, Allen N, et al. Design considerations in high-sensitivity off-axis integrated cavity output spectroscopy. *Appl Phys B* 2008;92(3):467–74. doi: [10.1007/s00340-008-3137-9](https://doi.org/10.1007/s00340-008-3137-9). <http://link.springer.com/10.1007/s00340-008-3137-9>.
- [158] Malarla P, Witinski MF, Capasso F, Anderson JG, De Natale P. Sensitivity enhancement of off-axis ICOS using wavelength modulation. *Appl Phys B* 2012;108(2):353–9. doi: [10.1007/s00340-012-4975-z](https://doi.org/10.1007/s00340-012-4975-z). <http://link.springer.com/10.1007/s00340-012-4975-z>.
- [159] Sun K, Wang S, Sur R, Chao X, Jeffries JB, Hanson RK. Time-resolved *in situ* detection of CO in a shock tube using cavity-enhanced absorption spectroscopy with a quantum-cascade laser near 4.6 μm . *Opt Express* 2014;22(20):24559–65. doi: [10.1117/12.455722](https://doi.org/10.1117/12.455722).
- [160] Sun K, Wang S, Sur R, Chao X, Jeffries JB, Hanson RK. Sensitive and rapid laser diagnostic for shock tube kinetics studies using cavity-enhanced absorption spectroscopy. *Opt Express* 2014;22(8):1–11. doi: [10.1117/12.455722](https://doi.org/10.1117/12.455722). <http://proceedings.spiedigitallibrary.org/proceeding.aspx?articleid=901633>.
- [161] Cheskis S, Goldman A. Laser diagnostics of trace species in low-pressure flat flame. *Prog Energy Combust Sci* 2009;35(4):365–82. doi: [10.1016/j.pecs.2009.02.001](https://doi.org/10.1016/j.pecs.2009.02.001). <http://www.sciencedirect.com/science/article/pii/S0360128509000100>.
- [162] Mercier X, Desgroux P. Cavity ring-down spectroscopy for combustion studies. In: Berden G, Engeln R, editors. *Cavity ring-down spectroscopy: Techniques and applications*; chap. 10. John Wiley and Sons; 2010. p. 273–311.
- [163] Goldenstein CS. Wavelength-modulation spectroscopy for determination of gas properties in hostile environments. Stanford University Ph.D. thesis; 2014.
- [164] Spearin RM. Mid-infrared laser absorption spectroscopy for carbon oxides in harsh environments. Stanford University Ph.D. thesis; 2014.
- [165] Goldenstein CS, Schultz IA, Jeffries JB, Hanson RK. Two-color absorption spectroscopy strategy for measuring the column density and path average temperature of the absorbing species in nonuniform gases. *Appl Opt* 2013;52(33):7950–62. doi: [10.1364/AO.52.007950](https://doi.org/10.1364/AO.52.007950). <http://www.opticsinfobase.org/abstract.cfm?URI=ao-52-33-7950>.
- [166] Schoenung M, Hanson RK. CO And temperature measurements in a flat flame by laser absorption spectroscopy and probe techniques. *Combust Sci Technol* 1980;24(5–6):227–37.
- [167] Ouyang X, Varghese PL. Line-of-sight absorption measurements of high temperature gases with thermal and concentration boundary layers. *Appl Opt* 1989;28(18):3979–84.
- [168] Seitzman JM, Scully BT. Broadband infrared absorption sensor for high-pressure combustor control. *J Propul Power* 2000;16(6):994–1001.
- [169] Wang J, Maiorov M, Jeffries JB, Garbuзов DZ, Connolly JC, Hanson RK. A potential remote sensor of CO in vehicle exhausts using 2.3 μm diode lasers. *Meas Sci Technol* 2000;11:1576–84. doi: [10.1088/0957-0233/11/11/306](https://doi.org/10.1088/0957-0233/11/11/306). <http://stacks.iop.org/0957-0233/11/i=11/a=306?key=crossref.b42df6f3125656eb7273bd4a8dc169e>.
- [170] Sanders ST, Wang J, Jeffries JB, Hanson RK. Diode-laser absorption sensor for line-of-sight temperature distributions. *Appl Opt* 2001;40(24):4404–15.
- [171] Palaghita TI, Seitzman JM. Control of temperature nonuniformity based on line-of-sight absorption. In: *Proceedings of the 40th AIAA/ASME/SAE/ASEE joint propulsion conference*. Ft. Lauderdale, FL; 2004. p. AIAA2004-4163.
- [172] Liu JTC, Rieker GB, Jeffries JB, Gruber MR, Carter CD, Mathur T, et al. Near-infrared diode laser absorption diagnostic for temperature and water vapor in a scramjet combustor.. *Appl Opt* 2005;44(31):6701–11. <http://www.ncbi.nlm.nih.gov/pubmed/16270559>.
- [173] Liu X, Jeffries JB, Hanson RK. Measurement of non-uniform temperature distributions using line-of-sight absorption spectroscopy. *AIAA Journal*

- 2007;45(2):411–9. doi: [10.2514/1.26708](https://doi.org/10.2514/1.26708). <http://arc.aiaa.org/doi/abs/10.2514/1.26708>.
- [174] Gruber MR, Carter CD, Ryan M, Rieker GB, Jeffries JB, Hanson RK, et al. Laser-based measurements of OH, temperature, and water vapor concentration in a hydrocarbon-fueled scramjet. In: Proceedings of 44th AIAA/ASME/SAE/ASEE joint propulsion conference and exhibit; 2008/AIAA2008–5070.
- [175] Chang LS, Strand CL, Jeffries JB, Hanson RK, Diskin GS, Gaffney RL, et al. Supersonic mass flux measurements via tunable diode laser absorption and non-uniform flow modeling. In: Proceedings of 49th AIAA aerospace sciences meeting, Orlando, FL; 2011. p. AIAA2011–1093.
- [176] Li F, Yu X, Cai W, Ma L. Uncertainty in velocity measurement based on diode-laser absorption in nonuniform flows.. Appl Opt 2012;51(20):4788–97. <http://www.ncbi.nlm.nih.gov/pubmed/22781256>.
- [177] Smith CH, Goldenstein CS, Hanson RK. A scanned-wavelength-modulation absorption-spectroscopy sensor for temperature and h_2o in low-pressure flames. Meas Sci Technol 2014;25:115501. doi: [10.1088/0957-0233/25/11/115501](https://doi.org/10.1088/0957-0233/25/11/115501).
- [178] Goldenstein CS, Schultz IA, Spearin RM, Jeffries JB, Hanson RK. Scanned-wavelength-modulation spectroscopy near 2.5 μm for h_2o and temperature in a hydrocarbon-fueled scramjet combustor. Appl Phys B 2014;116:717–27. doi: [10.1007/s00340-013-5755-0](https://doi.org/10.1007/s00340-013-5755-0).
- [179] Ma L, Cai W, Caswell AW, Kraetschmer T, Sanders ST, Roy S, et al. Tomographic imaging of temperature and chemical species based on hyperspectral absorption spectroscopy. Opt Express 2009;17(10):8602–13. doi: [10.1364/OE.17.008602](https://doi.org/10.1364/OE.17.008602). <http://www.osapublishing.org/viewmedia.cfm?uri=oe-17-10-8602&seq=0&html=true>.
- [180] An X, Kraetschmer T, Takami K, Sanders ST, Ma L, Cai W, et al. Validation of temperature imaging by h_2o absorption spectroscopy using hyperspectral tomography in controlled experiments.. Appl Opt 2011;50(4):A29–37. <http://www.ncbi.nlm.nih.gov/pubmed/21283218>.
- [181] Busa K, Bryner E, McDaniel J, Goyne C, Smith C, Diskin G. Demonstration of capability of water flux measurement in a scramjet combustor using tunable diode laser absorption tomography and stereoscopic PIV. In: Proceedings of the 49th AIAA aerospace sciences meeting including the new horizons forum and aerospace exposition; 2011/AIAA2011–1294. doi: [10.2514/6.2011-1294](https://doi.org/10.2514/6.2011-1294). <http://arc.aiaa.org/doi/abs/10.2514/6.2011-1294>.
- [182] Busa K, Ellison E, McGovern B, McDaniel J, Diskin G, DePiro M, et al. Measurements on NASA langley durable combustor rig by TDLAT: preliminary results. In: Proceedings of the 51st AIAA aerospace sciences meeting including the new horizons forum and aerospace exposition; 2013/AIAA2013–0696. doi: [10.2514/6.2013-696](https://doi.org/10.2514/6.2013-696). <http://dx.doi.org/10.2514/6.2013-696> <http://arc.aiaa.org/doi/abs/10.2514/6.2013-696>.
- [183] Ma L, Li X, Sanders ST, Caswell AW, Roy S, Plemons DH, et al. 50-Khz-rate 2D imaging of temperature and h_2o concentration at the exhaust plane of a J85 engine using hyperspectral tomography.. Opt Express 2013;21(1):1152–62. <http://www.ncbi.nlm.nih.gov/pubmed/23389008>.
- [184] Busa KM, McDaniel JC, Brown MS, Diskin GS. Implementation of maximum-likelihood expectation-maximization algorithm for tomographic reconstruction of TDLAT measurements. In: Proceedings of the 52nd aerospace sciences meeting AIAA SciTech; 2014. doi: [10.2514/6.2014-0985](https://doi.org/10.2514/6.2014-0985) <http://arc.aiaa.org/doi/abs/10.2514/6.2014-0985> 2014–0985
- [185] Cai W, Kaminski CF. Multiplexed absorption tomography with calibration-free wavelength modulation spectroscopy. Appl Phys Lett 2014;104:154106. doi: [10.1063/1.4871976](https://doi.org/10.1063/1.4871976).
- [186] An X, Brittelle MS, Lauzier PT, Gord JR, Roy S, Chen G-H, et al. Demonstration of temperature imaging by h_2o absorption spectroscopy using compressed sensing tomography. Appl Opt 2015;54(31):9190. doi: [10.1364/AO.54.009190](https://doi.org/10.1364/AO.54.009190). <https://www.osapublishing.org/abstract.cfm?URI=ao-54-31-9190>.
- [187] Liu C, Xu L, Chen J, Cao Z, Liu Y. Development of a fan-beam TDLAS-based tomographic sensor for rapid imaging of temperature and gas concentration. Opt Express 2015;23(17):4827–42. doi: [10.1364/OE.23.022494](https://doi.org/10.1364/OE.23.022494).
- [188] Wood MP, Ozanyan KB. Simultaneous temperature, concentration, and pressure imaging of water vapor in a turbine engine. IEEE Sens J 2015;15(1):545–51. doi: [10.1109/JSEN.2014.2349796](https://doi.org/10.1109/JSEN.2014.2349796).
- [189] Cai W, Kaminski CF. A tomographic technique for the simultaneous imaging of temperature, chemical species, and pressure in reactive flows using absorption spectroscopy with frequency-agile lasers. Appl Phys Lett 2014;104(3). doi: [10.1063/1.4862754](https://doi.org/10.1063/1.4862754).
- [190] McCann H, Wright P, Daun K. Chemical species tomography. In: Wang M, editor. Industrial tomography: systems and applications; chap. 5. Elsevier; 2015.
- [191] Daun KJ, Grauer SJ, Hadwin PJ. Chemical species tomography of turbulent flows: discrete ill-posed and rank deficient problems and the use of prior information. J Quant Spectrosc Radiat Transf 2016;172:58–74. doi: [10.1016/j.jqsrt.2015.09.011](https://doi.org/10.1016/j.jqsrt.2015.09.011). <http://www.sciencedirect.com/science/article/pii/S0022407315003040>.
- [192] Cai W, Kaminski CF. Tomographic absorption spectroscopy for the study of gas dynamics and reactive flows. Prog Energy Combust Sci 2017;59:1–42. doi: [10.1016/j.pecs.2016.11.002](https://doi.org/10.1016/j.pecs.2016.11.002). <http://dx.doi.org/10.1016/j.pecs.2016.11.002>.
- [193] Gordon R, Bender R, Herman GT. Algebraic reconstruction techniques (ART) for three-dimensional electron microscopy and x-ray photography. J Theor Biol 1970;29(3):471–81. doi: [10.1016/0022-5193\(70\)90109-8](https://doi.org/10.1016/0022-5193(70)90109-8).
- [194] Kak AC, Slaney M. Principles of computerized tomographic imaging. IEEE Press; 1988.
- [195] Andersen AH, Kak AC. Simultaneous algebraic reconstruction technique (SART): a superior implementation of the ART algorithm. Ultrason Imaging 1984;6:81–94. doi: [10.1016/0161-7346\(84\)90008-7](https://doi.org/10.1016/0161-7346(84)90008-7).
- [196] Rockmore AJ, Macovski A. A maximum likelihood approach to emission image reconstruction from projections. IEEE Trans Nucl Sci 1976;23(4):1428–32. doi: [10.1109/TNS.1976.4328496](https://doi.org/10.1109/TNS.1976.4328496).
- [197] Sidky EY, Pan X. Image reconstruction in circular cone-beam computed tomography by constrained, total-variation minimization. Phys Med Biol 2008;53(17):4777–807. doi: [10.1088/0031-9155/53/17/021](https://doi.org/10.1088/0031-9155/53/17/021)?key=crossref.3610c169110f92910d46d3a1-f79aa788.
- [198] Tang J, Nett BE, Chen G-H. Performance comparison between total variation (TV)-based compressed sensing and statistical iterative reconstruction algorithms.. Phys Med Biol 2009;54(19):5781–804. doi: [10.1088/0031-9155/54/19/008](https://doi.org/10.1088/0031-9155/54/19/008). NIHMS150003
- [199] Hansen PC. Rank-Deficient and discrete ill-Posed problems: numerical aspects of linear inversion. 1998.
- [200] Cai W, Ewing DJ, Ma L. Application of simulated annealing for multispectral tomography. Comput Phys Commun 2008;179(4):250–5. doi: [10.1016/j.cpc.2008.02.012](https://doi.org/10.1016/j.cpc.2008.02.012). <http://www.sciencedirect.com/science/article/pii/S0010465508000982>.
- [201] Ma L, Li X, Cai W, Roy S, Gord JR, Sanders ST. Selection of multiple optimal absorption transitions for nonuniform temperature sensing. Appl Spectrosc 2010;64(11):1274–82. doi: [10.1366/00037021079335052](https://doi.org/10.1366/00037021079335052). <http://www.ncbi.nlm.nih.gov/pubmed/21073797>.
- [202] Rein KD, Roy S, Sell B, Hoke JL, Caswell AW, Schauer FR, et al. Time-resolved *in situ* absorption spectroscopy of a hydrogen-air rotating detonation engine using a fiber-coupled tunable laser system. In: Proceedings of the 54th aerospace sciences meeting AIAA SciTech; 2016/AIAA2016–1199.
- [203] Goldenstein CS, Spearin RM, Jeffries JB, Hanson RK. Wavelength-modulation spectroscopy near 2.5 μm for h_2o and temperature in high-pressure and -temperature gases. Appl Phys B 2014;116:705–16. doi: [10.1007/s00340-013-5754-1](https://doi.org/10.1007/s00340-013-5754-1).
- [204] Petersen EL. A shock tube and diagnostics for chemistry measurements at elevated pressures with application to methane ignition. Stanford University Ph.D. thesis; 1998.
- [205] Kranendonk LA, Sanders ST. Optical design in beam steering environments with emphasis on laser transmission measurements. Appl Opt 2005;44(31):6762–72. doi: [10.1364/AO.44.006762](https://doi.org/10.1364/AO.44.006762). <http://www.osapublishing.org/viewmedia.cfm?uri=ao-44-31-6762&seq=0&html=true>.
- [206] Whitney JM, Takami K, Sanders ST, Okura Y. Design of system for rugged, low-noise fiber-optic access to high-temperature, high-pressure environments. IEEE Sens J 2011;11(12):3295–302. doi: [10.1109/JSEN.2011.2156780](https://doi.org/10.1109/JSEN.2011.2156780).
- [207] Strand CL. Scanned wavelength-modulation absorption spectroscopy with application to hypersonic impulse flow facilities. Stanford University Ph.D. thesis; 2014.
- [208] An X, Caswell AW, Lipor JJ, Sanders ST. Determining the optimum wavelength pairs to use for molecular absorption thermometry based on the continuous-spectral lower-state energy. J Quant Spectrosc Radiat Transf 2011;112(14):2355–62. doi: [10.1016/j.jqsrt.2011.05.002](https://doi.org/10.1016/j.jqsrt.2011.05.002). <http://linkinghub.elsevier.com/retrieve/pii/S0022407311001749>.
- [209] An X, Caswell AW, Sanders ST. Quantifying the temperature sensitivity of practical spectra using a new spectroscopic quantity: frequency-dependent lower-state energy. J Quant Spectrosc Radiat Transf 2011;112(5):779–85. doi: [10.1016/j.jqsrt.2010.10.014](https://doi.org/10.1016/j.jqsrt.2010.10.014). <http://linkinghub.elsevier.com/retrieve/pii/S0022407310004000>.
- [210] Goldenstein CS, Spearin RM, Schultz IA, Jeffries JB, Hanson RK. Wavelength-modulation spectroscopy near 1.4 μm for measurements of h_2o and temperature in high-pressure and -temperature gases. Meas Sci Technol 2014;25(5):055101. doi: [10.1088/0957-0233/25/5/055101](https://doi.org/10.1088/0957-0233/25/5/055101). <http://stacks.iop.org/0957-0233/25/i=5/a=055101?key=crossref.5ca24c189e3cc37c22001a9ddf0dc452>.
- [211] Brittelle MS, Simms JM, Sanders ST, Gord JR, Roy S. Fixed-wavelength h_2o absorption spectroscopy system enhanced by an on-board external-cavity diode laser. Meas Sci Technol 2016;27(3):035501. doi: [10.1088/0957-0233/27/3/035501](https://doi.org/10.1088/0957-0233/27/3/035501). <http://iopscience.iop.org/article/10.1088/0957-0233/27/3/035501>.
- [212] Caswell AW, Roy S, An X, Sanders ST, Schauer FR, Gord JR. Measurements of multiple gas parameters in a pulsed-detonation combustor using time-mode-locked lasers. Appl Opt 2013;52(12):2893–904.
- [213] Witzel O, Klein A, Meffert C, Wagner S, Kaiser S, Schulz C, et al. VCSEL-Based, high-speed, *in situ* TDLAS for *in-cylinder* water vapor measurements in IC engines. Opt Express 2013;21(17):8057–67. doi: [10.1364/OE.21.019951](https://doi.org/10.1364/OE.21.019951).
- [214] Kranendonk LA, Caswell AW, Sanders ST. Robust method for calculating temperature, pressure, and absorber mole fraction from broadband spectra. Appl Opt 2007;46(19):4117–24. doi: [10.1364/OE.46.004117](https://doi.org/10.1364/OE.46.004117). <http://www.osapublishing.org/viewmedia.cfm?uri=ao-46-19-4117&seq=0&html=true>.
- [215] Simms JM, An X, Brittelle MS, Ramesh V, Ghandhi JB, Sanders ST. Simultaneous optimization method for absorption spectroscopy postprocessing. Appl Opt 2015;54(14):4403. doi: [10.1364/OE.54.004403](https://doi.org/10.1364/OE.54.004403). <https://www.osapublishing.org/ao/abstract.cfm?uri=ao-54-14-4403>.
- [216] Rieker GB, Li H, Liu X, Jeffries JB, Hanson RK, Allen MG, et al. A diode laser sensor for rapid, sensitive measurements of gas temperature and water vapour concentration at high temperatures and pressures. Meas Sci Technol 2007;18(5):1195–204. doi: [10.1088/0957-0233/18/5/005](https://doi.org/10.1088/0957-0233/18/5/005). <http://stacks.iop.org/0957-0233/18/i=5/a=005?key=crossref.5ffe8b40f523928f-be0961cf37575d>.
- [217] Farooq A, Jeffries JB, Hanson RK. Measurements of CO_2 concentration and temperature at high pressures using 1/ f -normalized wavelength modulation spectroscopy with second harmonic detection near 2.7 μm . Appl Opt 2009;48(35):6740–53. <http://www.ncbi.nlm.nih.gov/pubmed/20011014>.

- [218] Pyun SH, Porter JM, Jeffries JB, Hanson RK, Montoya JC, Allen MG, et al. Two-color-absorption sensor for time-resolved measurements of gasoline concentration and temperature. *Appl Opt* 2009;48(33):6492–500. doi: [10.1364/AO.48.006492](https://doi.org/10.1364/AO.48.006492).
- [219] Kluczynski P, Gustafsson J, Lindberg AM, Axner O. Wavelength modulation absorption spectrometry an extensive scrutiny of the generation of signals. *Spectrochim Acta, Part B* 2001;56(8):1277–354. doi: [10.1016/S0584-8547\(01\)00248-8](https://doi.org/10.1016/S0584-8547(01)00248-8). <http://www.sciencedirect.com/science/article/pii/S0584854701002488>.
- [220] Silver JA, Stanton AC. Optical interference fringe reduction in laser absorption experiments. *Appl Opt* 1988;27(10):1914–6. doi: [10.1364/AO.27.001914](https://doi.org/10.1364/AO.27.001914). <http://ao.osa.org/abstract.cfm?URL=ao-27-10-1914>.
- [221] Zhou X, Jeffries JB, Hanson RK. Development of a fast temperature sensor for combustion gases using a single tunable diode laser. *Appl Phys B* 2005;81:711–22. doi: [10.1007/s00340-005-1934-y](https://doi.org/10.1007/s00340-005-1934-y). <http://www.springerlink.com/index/10.1007/s00340-005-1934-y>.
- [222] Lytkine JA, Jäger W, Tulip J. Gas phase chemical analysis using long-wavelength vertical-cavity surface-emitting lasers. *Opt Eng* 2006;45(4):044301. doi: [10.1117/1.2190662](https://doi.org/10.1117/1.2190662). <http://opticalengineering.spiedigitallibrary.org/article.aspx?doi=10.1117/1.2190662>.
- [223] Chen J, Hangauer A, Strzoda R, Amann MC. VCSEL-Based calibration-free carbon monoxide sensor at 2.3 μm with in-line reference cell. *Appl Phys B* 2011;102(2):381–9. doi: [10.1007/s00340-010-4011-0](https://doi.org/10.1007/s00340-010-4011-0).
- [224] Stein BA, Jayaraman V, Jiang JY, Cable A, Sanders ST. Doppler-limited H₂O and HF absorption spectroscopy by sweeping the 1,321–1,354 nm range at 55 khz repetition rate using a single-mode MEMS-tunable VCSEL. *Appl Phys B: Lasers Opt* 2012;108(4):721–5. doi: [10.1007/s00340-012-5135-1](https://doi.org/10.1007/s00340-012-5135-1).
- [225] Huber R, Wojtkowski M, Taira K, Fujimoto J, Hsu K. Amplified, frequency swept lasers for frequency domain reflectometry and OCT imaging: design and scaling principles. *Opt Express* 2005;13(9):3513–28. doi: [10.1364/OE.13.003513](https://doi.org/10.1364/OE.13.003513).
- [226] Huber RA, Wojtkowski M, Fujimoto JG. Fourier domain mode locking (FDML): a new laser operating regime and applications for optical coherence tomography. *Opt Express* 2006;14(8):3225–37. doi: [10.1364/OE.14.003225](https://doi.org/10.1364/OE.14.003225). <http://www.ncbi.nlm.nih.gov/pubmed/16916464>.
- [227] Caswell AW. Water vapor absorption thermometry for practical combustion applications. University of Wisconsin Ph.D. thesis; 2009.
- [228] Kelkar PV, Coppinger F, Bhushan AS, Jalali B. Time domain optical sensing. In: Proceedings of 12th annual meeting IEEE lasers and electro-optics society 1999, vol. 1; 19991999.
- [229] Walewski JW, Sanders ST. High-resolution wavelength-agile laser source based on pulsed super-continua. *Appl Phys B* 2004;79(4):415–8. doi: [10.1007/s00340-004-1587-2](https://doi.org/10.1007/s00340-004-1587-2).
- [230] Hagen C, Sanders ST. Application of a novel white laser sensor to an HCCI engine. Society of automotive engines; 2006.
- [231] Hult J, Watt RS, Kaminski CF. High bandwidth absorption spectroscopy with a dispersed supercontinuum source.. *Opt Express* 2007;15(18):11385–95. doi: [10.1364/OE.15.011385](https://doi.org/10.1364/OE.15.011385).
- [232] Kaminski CF, Watt RS, Elder AD, Frank JH, Hult J. Supercontinuum radiation for applications in chemical sensing and microscopy. *Appl Phys B* 2008;92(3 SPECIAL ISSUE):367–78. doi: [10.1007/s00340-008-3132-1](https://doi.org/10.1007/s00340-008-3132-1).
- [233] Werblinski T, Mittmann F, Altenhoff M, Seeger T, Zigan L, Will S. Temperature and water mole fraction measurements by time-domain-based supercontinuum absorption spectroscopy in a flame. *Appl Phys B: Lasers Opt* 2014;118(1):153–8. doi: [10.1007/s00340-014-5964-1](https://doi.org/10.1007/s00340-014-5964-1).
- [234] Blume NC, Ebert V, Dreizler A, Wagner S. Broadband fitting approach for the application of supercontinuum broadband laser absorption spectroscopy to combustion environments. *Meas Sci Technol* 2016;27(1):015501. doi: [10.1088/0957-0233/27/1/015501](https://doi.org/10.1088/0957-0233/27/1/015501). <http://stacks.iop.org/0957-0233/27/i=1/a=015501?key=crossref.3d9a35853327387beb8d4542c3f2042>.
- [235] Dupont S, Qu Z, Kiwanuka SS, Hooper LE, Knight JC, Keiding SR, et al. Ultra-high repetition rate absorption spectroscopy with low noise supercontinuum radiation generated in an all-normal dispersion fibre. *Laser Phys Lett* 2014;11(7):75601. doi: [10.1088/1612-2011/11/7/075601](https://doi.org/10.1088/1612-2011/11/7/075601). <http://iopscience.iop.org/1612-202X/11/7/075601>.
- [236] Spearrin RM, Goldenstein CS, Schultz IA, Jeffries JB, Hanson RK. Simultaneous sensing of temperature, CO, and CO₂ in a scramjet combustor using quantum cascade laser absorption spectroscopy. *Appl Phys B* 2014;117:689–98. doi: [10.1007/s00340-014-5884-0](https://doi.org/10.1007/s00340-014-5884-0).
- [237] Goldenstein CS, Spearrin RM, Jeffries JB, Hanson RK. Infrared laser absorption sensors for multiple performance parameters in a detonation combustor. *Proc Combust Inst* 2015;35(3):3739–47. doi: [10.1016/j.proci.2014.05.027](https://doi.org/10.1016/j.proci.2014.05.027). <http://dx.doi.org/10.1016/j.proci.2014.05.027>.
- [238] Rein KD, Roy S, Sanders ST, Caswell AW, Schauer FR, Gord JR. Multispecies absorption spectroscopy of detonation events at 100 khz using a fiber-coupled time-division-multiplexed quantum-cascade-laser system. *Appl Opt* 2016;55(23):6256–62.
- [239] Faist J, Capasso F, Sivco DL, Sirtori C, Hutchinson AL, Cho AY. Quantum cascade laser. *Science* 1994;264(5158):553–6. doi: [10.1126/science.264.5158.553](https://doi.org/10.1126/science.264.5158.553). <http://science.sciencemag.org.ezproxy.lib.purdue.edu/content/264/5158/553.abstract>.
- [240] Faist J, Gmachl C, Capasso F, Sirtori C, Sivco DL, Baillargeon JN, et al. Distributed feedback quantum cascade lasers. *Appl Phys Lett* 1997;70(20):2670. doi: [10.1103/119208](https://doi.org/10.1103/119208). <http://scitation.aip.org.ezproxy.lib.purdue.edu/content/aip/journal/api/70/20/10.1103/119208>.
- [241] Curl RF, Capasso F, Gmachl C, Kosterev AA, McManus B, Lewicki R, et al. Quantum cascade lasers in chemical physics. *Chem Phys Lett* 2010;487(1–3):1–18. doi: [10.1016/j.cplett.2009.12.073](https://doi.org/10.1016/j.cplett.2009.12.073). <http://www.sciencedirect.com/science/article/pii/S0009261409016200>.
- [242] Willians BS. Terahertz quantum-cascade lasers. *Nat Photonics* 2007;1(9):517–25. doi: [10.1038/nphoton.2007.166](https://doi.org/10.1038/nphoton.2007.166). <http://www.nature.com.ezproxy.lib.purdue.edu/nphoton/journal/v1/n9/abs/nphoton.2007.166.html>.
- [243] Vurgaftman I, Weih R, Kamp M, Meyer JR, Canedy CL, Kim CS, et al. Interband cascade lasers. *J Phys D Appl Phys* 2015;48(12):123001. doi: [10.1088/0022-3727/48/12/123001](https://doi.org/10.1088/0022-3727/48/12/123001). <http://iopscience.iop.org.ezproxy.lib.purdue.edu/article/10.1088/0022-3727/48/12/123001>.
- [244] Yang RQ. Infrared laser based on intersubband transitions in quantum wells. *Superlattices Microstruct* 1995;17(1):77–83. doi: [10.1006/spmi.1995.1017](https://doi.org/10.1006/spmi.1995.1017). <http://www.sciencedirect.com/science/article/pii/S0749603685710178>.
- [245] Kim M, Canedy CL, Bewley WW, Kim CS, Lindle JR, Abell J, et al. Interband cascade laser emitting at λ=3.75 μm in continuous wave above room temperature. *Appl Phys Lett* 2008;92(19):191110. doi: [10.1063/1.2930685](https://doi.org/10.1063/1.2930685). <http://scitation.aip.org.ezproxy.lib.purdue.edu/content/aip/journal/api/92/19/10.1063/1.2930685>.
- [246] Vurgaftman I, Bewley WW, Canedy CL, Merritt CD, Abell J, Meyer JR. Interband cascade lasers with low threshold powers and high output powers. *IEEE J Sel Top Quantum Electron* 2013;19(4). doi: [10.1109/JSTQE.2012.2237017](https://doi.org/10.1109/JSTQE.2012.2237017). <http://ieeexplore.ieee.org/lpdocs/epic03/wrapper.htm?arnumber=6415976>.
- [247] Bauer A. Shortened injector interband cascade lasers for 3.3- to 3.6-μm emission. *Opt Eng* 2010;49(11):111117. doi: [10.1117/1.3505831](https://doi.org/10.1117/1.3505831). <http://opticalengineering.spiedigitallibrary.org.ezproxy.lib.purdue.edu/article.aspx?articleid=1096494>.
- [248] Saad M. Indium fluoride glass fibers. In: Epstein RI, Sheik-Bahae M, editors. *Proceedings of SPIE 8275, laser refrigeration of solids V*. International society for optics and photonics; 2012. p. 82750D.
- [249] Kriesel JM, Gat N, Bernacki BE, Erikson RL, Cannon BD, Myers TL, et al. Hollow core fiber optics for mid-wave and long-wave infrared spectroscopy. *SPIE defense, security, and sensing*. International society for optics and photonics; 2011. p. 80180V.
- [250] Kanamori T, Terunuma Y, Takahashi S, Miyashita T. Chalcogenide glass fibers for mid-infrared transmission. *J Lightwave Technol* 1984;2(5):607–13. doi: [10.1109/JLT.1984.1073657](https://doi.org/10.1109/JLT.1984.1073657). <http://ieeexplore.ieee.org/lpdocs/epic03/wrapper.htm?arnumber=1073657>.
- [251] Thomas ME, Joseph RI, Tropp WJ. Infrared transmission properties of sapphire, spinel, yttria, and ALON as a function of temperature and frequency. *Appl Opt* 1988;27(2):239–45. doi: [10.1364/AO.27.000239](https://doi.org/10.1364/AO.27.000239). <http://www.osapublishing.org/viewmedia.cfm?url=ao-27-2-239&seq=0&html=true>.
- [252] Harris TR. Optical properties of si, ge, gaas, gasb, inas, and inp at elevated temperatures. *Air Force Institute of Technology Ph.D. thesis*; 2010.
- [253] Beyer T, Braun M, Lambrecht A. Fast gas spectroscopy using pulsed quantum cascade lasers. *J Appl Phys* 2003;93(6):3158–60. doi: [10.1063/1.1555271](https://doi.org/10.1063/1.1555271).
- [254] Hancock G, Horrocks SJ, Ritchie GAD, Van Helden JH, Walker RJ. Time-resolved detection of the CF₃ photofragment using chirped QCL radiation. *J Phys Chem A* 2008;112(40):9751–7. doi: [10.1021/jp804849m](https://doi.org/10.1021/jp804849m).
- [255] Quine ZR, Mcnnesby KL. Acetylene measurement in flames by chirp-based quantum cascade laser spectrometry. *Appl Opt* 2009;48(16):3075–83.
- [256] Chrystie RSM, Nasir EF, Farooq A. Towards simultaneous calibration-free and ultra-fast sensing of temperature and species in the intrapulse mode. *Proc Combust Inst* 2014;35(3):3757–64. doi: [10.1016/j.proci.2014.06.069](https://doi.org/10.1016/j.proci.2014.06.069). <http://dx.doi.org/10.1016/j.proci.2014.06.069>.
- [257] Schroeder P, Wright R, Coburn S, Sodergren B, Cossel K, Drosté S, et al. Dual frequency comb laser absorption spectroscopy in a 16 MW gas turbine exhaust. *Proc Combust Inst* 2016. doi: [10.1016/j.proci.2016.06.032](https://doi.org/10.1016/j.proci.2016.06.032). In Press, <http://linkinghub.elsevier.com/retrieve/pii/S1540748916300906>.
- [258] Wehe SD, Baert DS, Hanson RK. Tunable diode-laser absorption measurements of temperature, velocity, and H₂O in hypervelocity flows. In: *Proceedings of 33rd joint propulsion conference and exhibit*; 1997AIAA97–3267.
- [259] Wehe SD, Baert DS, Hanson RK. Measurements of gas temperature and velocity in hypervelocity flows using diode-laser sensors. In: *Proceedings of 20th AIAA advanced measurement and ground testing technology conference AIAA*; 1998. AIAA-98-2699.
- [260] Jeffries JB, Porter JM, Sung HP, Hanson RK, Sholes KR, Kiyotaka S, et al. An in-cylinder laser absorption sensor for crank-angle-resolved measurements of gasoline concentration and temperature. *SAE Int J Engines* 2010;3(2):373–82. <http://saeng.saejournals.org/content/3/2/373.short>.
- [261] Rein KD, Sanders ST. Fourier-transform absorption spectroscopy in reciprocating engines. *Appl Opt* 2010;49(25):4728–34.
- [262] Schultz IA, Goldenstein CS, Strand CL, Jeffries JB, Hanson RK, Goyne CP. Hypersonic scramjet testing via diode laser absorption in a reflected shock tunnel. *Propulsion Power* 2014;30(6):1586–94. doi: [10.2514/1.B35220](https://doi.org/10.2514/1.B35220).
- [263] Strand CL, Hanson RK. Quantification of supersonic impulse flow conditions via high-bandwidth wavelength modulation absorption spectroscopy. *AIAA J* 2015;53(10):2978–87. doi: [10.2514/1.J053842](https://doi.org/10.2514/1.J053842). <http://arc.aiaa.org/doi/10.2514/1.J053842>.
- [264] Wang Z, Sanders ST. Toward single ended absorption spectroscopy probes based on backscattering from rough surfaces: H₂O vapor measurements near 1350 nm. *Appl Phys B* 2015;121:187–92. doi: [10.1007/s00340-015-6216-8](https://doi.org/10.1007/s00340-015-6216-8). <http://dx.doi.org/10.1007/s00340-015-6216-8>.
- [265] Goldenstein CS, Spearrin RM, Hanson RK. Fiber-coupled diode-laser sensors for calibration-free stand-off measurements of gas temperature, pressure, and composition. *Appl Opt* 2016;55(3):479–84.

- [266] Witzel O, Klein A, Meffert C, Schulz C, Kaiser S, Ebert V. Calibration-free, high-speed, in-cylinder laser absorption sensor for cycle-resolved, absolute H_2O measurements in a production IC engine. Proc Combust Inst 2015;35(3):3653–61. doi: 10.1016/j.proci.2014.06.038. <http://www.sciencedirect.com/science/article/pii/S1540748914001965>.
- [267] Hall MJ, Koenig M. A fiber-optic probe to measure precombustion in-cylinder fuel-air ratio fluctuations in production engines. Symp (Int) Combust 1996;26(2):2613–8. doi: 10.1016/S0082-0784(96)80095-6. <http://www.sciencedirect.com/science/article/pii/S0082078496800956>.
- [268] Tomita E, Kawahara N, Shigenaga M, Nishiyama A, Dibble RW. *In situ* measurement of hydrocarbon fuel concentration near a spark plug in an engine cylinder using the 3.392 m infrared laser absorption method: discussion of applicability with a homogeneous methane-air mixture. Meas Sci Technol 2003;14(8):1350–6. doi: 10.1088/0957-0233/14/8/321. <http://iopscience.iop.org/article/10.1088/0957-0233/14/8/321>.
- [269] Cundy M, Schucht T, Thiele O, Sick V. High-speed laser-induced fluorescence and spark plug absorption sensor diagnostics for mixing and combustion studies in engines. Appl Opt 2008;48(48):B94. doi: 10.1364/AO.48.000B94. <http://www.osapublishing.org.ezproxy.stanford.edu/viewmedia.cfm?uri=ao-48-4-B94&seq=0&html=true>.
- [270] Peng WY, Goldenstein CS, Spearrin RM, Jeffries JB, Hanson RK. A single-ended mid-infrared laser-absorption sensor for simultaneous *in-situ* measurements of HO, CO, CO₂, and temperature in combustion flows. Appl Opt 2016;55(33):9347–59.
- [271] Wang H. A high-temperature chemical kinetic model of n-alkane (up to n-dodecane), cyclohexane, and methyl-, ethyl-, n-propyl and n-butyl-cyclohexane oxidation at high temperatures, JetSurF version 2.0.2010. <http://melchior.usc.edu/JetSurF>.
- [272] Ren W, Farooq A, Davidson DF, Hanson RK. CO Concentration and temperature sensor for combustion gases using quantum-cascade laser absorption near 4.7 μm . Appl Phys B 2012;107(3):849–60. doi: 10.1007/s00340-012-5046-1. <http://link.springer.com/10.1007/s00340-012-5046-1>.
- [273] Farooq A, Jeffries JB, Hanson RK. *In situ* combustion measurements of H_2O and temperature near 2.5 μm using tunable diode laser absorption. Meas Sci Technol 2008;19(7):075604. doi: 10.1088/0957-0233/19/7/075604.
- [274] Farooq A, Jeffries JB, Hanson RK. Sensitive detection of temperature behind reflected shock waves using wavelength modulation spectroscopy of CO₂ near 2.7 μm . Appl Phys B 2009;86(1):161–73. doi: 10.1007/s00340-009-3446-7. <http://link.springer.com/10.1007/s00340-009-3446-7>.
- [275] Ren W, Jeffries JB, Hanson RK. Temperature sensing in shock-heated evaporating aerosol using wavelength-modulation absorption spectroscopy of CO₂ near 2.7 μm . Meas Sci Technol 2010;21(10):105603. doi: 10.1088/0957-0233/21/10/105603. <http://stacks.iop.org/0957-0233/21/i=10/a=105603?key=crossref.9a0c46da93c19ea09367f47c5ef80fe1>.
- [276] Campbell MF, Parise T, Tulgestke AM, Spearrin RM, Davidson DF, Hanson RK. Strategies for obtaining long constant-pressure test times in shock tubes. Shock Waves 2015;25(6):651–65. doi: 10.1007/s00193-015-0596-x. <http://link.springer.com/10.1007/s00193-015-0596-x>.
- [277] Uddi M, Das AK, Sung C-J. Temperature measurements in a rapid compression machine using mid-infrared H_2O absorption spectroscopy near 76 μm . Appl Opt 2012;51(22):5464. doi: 10.1364/AO.51.005464.
- [278] MacDonald ME, Ren W, Zhu Y, Davidson DF, Hanson RK. Fuel and ethylene measurements during n-dodecane, methylcyclohexane, and isooctane pyrolysis in shock tubes. Fuel 2013;103:1060–8. doi: 10.1016/j.fuel.2012.09.068.
- [279] Zhu Y, Davidson D, Hanson R. Pyrolysis and oxidation of decalin at elevated pressures: a shock-tube study. Combust Flame 2014;161(2):371–83. doi: 10.1016/j.combustflame.2013.09.005.
- [280] Ren W, Davidson DF, Hanson RK. IR Laser absorption diagnostic for C_2H_4 in shock tube kinetics studies. Int J Chem Kinet 2012;44(6):423–32. doi: 10.1002/kin.20599. <http://doi.wiley.com/10.1002/kin.20599>.
- [281] Pilla GL, Davidson DF, Hanson RK. Shock tube/laser absorption measurements of ethylene time-histories during ethylene and n-heptane pyrolysis. Proc Combust Inst 2011;33(1):333–40. doi: 10.1016/j.proci.2010.06.146.
- [282] Pyun SH, Cho J, Davidson DF, Hanson RK. Interference-free mid-IR laser absorption detection of methane. Meas Sci Technol 2011;22(2):025303. doi: 10.1088/0957-0233/22/2/025303. <http://stacks.iop.org/0957-0233/22/i=2/a=025303?key=crossref.20b622841a32877fb82cdda62fe5652>.
- [283] Wang S, Davidson DF, Hanson RK. High-temperature laser absorption diagnostics for CH₂O and CH₃CHO and their application to shock tube kinetic studies. Combust Flame 2013;160(10):1930–8. doi: 10.1016/j.combustflame.2013.05.004. <http://dx.doi.org/10.1016/j.combustflame.2013.05.004>.
- [284] Sajid MB, Javed T, Farooq A. Shock tube/laser absorption measurements of methane, acetylene and ethylene during the pyrolysis of n-pentane and isopentane. Combust Flame 2016;164:1–9. doi: 10.1016/j.combustflame.2015.10.021.
- [285] Stranic I, Hanson RK. Laser absorption diagnostic for measuring acetylene concentrations in shock tubes. J Quant Spectrosc Radiat Transfer 2014;142:58–65. doi: 10.1016/j.jqsrt.2014.03.024.
- [286] KC U, Nasir EF, Farooq A. A mid-infrared absorption diagnostic for acetylene detection. Appl Phys B 2015;120(2):223–32. doi: 10.1007/s00340-015-6125-x. <http://link.springer.com/10.1007/s00340-015-6125-x>.
- [287] Nations M, Wang S, Goldenstein CS, Sun K, Davidson DF, Jeffries JB, et al. Shock-tube measurements of excited oxygen atoms using cavity-enhanced absorption spectroscopy. Appl Opt 2015;54(29):8766–75.
- [288] Alquatty ABS, Es-sebbar E-t, Farooq A. Sensitive and ultra-fast species detection using pulsed cavity ringdown spectroscopy. Opt Expr 2015;23(6):7217. doi: 10.1364/OE.23.007217. <https://www.osapublishing.org/oe/abstract.cfm?uri=oe-23-6-7217>.
- [289] Fjodorow P, Fikri M, Schulz C, Hellmig O, Baev VM. Time-resolved detection of temperature, concentration, and pressure in a shock tube by intracavity absorption spectroscopy. Appl Phys B 2016;122(6):159. doi: 10.1007/s00340-016-6434-8. <http://link.springer.com/10.1007/s00340-016-6434-8>.
- [290] Li S, Farooq A, Hanson RK. H_2O temperature sensor for low-pressure flames using tunable diode laser absorption near 2.9 μm . Meas Sci Technol 2011;22(12):125301. doi: 10.1088/0957-0233/22/12/125301. <http://stacks.iop.org/0957-0233/22/i=12/a=125301?key=crossref.8794fa85d2528f01e12c-ce2c79bc460>.
- [291] Wagner S, Fisher BT, Fleming JW, Ebert V. TDLAS-Based *in situ* measurement of absolute acetylene concentrations in laminar 2D diffusion flames. Proc Combust Inst 2009;32(1):839–46. doi: 10.1016/j.proci.2008.05.087. <http://dx.doi.org/10.1016/j.proci.2008.05.087>.
- [292] Wagner S, Klein M, Kathrotia T, Riedel U, Kissel T, Dreizler A, et al. *In situ* TDLAS measurement of absolute acetylene concentration profiles in a non-premixed laminar counter-flow flame. Appl Phys B: Lasers Opt 2012;107(3):585–9. doi: 10.1007/s00340-012-4953-5.
- [293] Nau P, Koppmann J, Lackner A, Kohse-Höinghaus K, Brockhinke A. Quantum cascade laser-based MIR spectrometer for the determination of CO and CO₂ concentrations and temperature in flames. Appl Phys B 2015;118(3):361–8. doi: 10.1007/s00340-014-5992-x. <http://link.springer.com/10.1007/s00340-014-5992-x>.
- [294] Girard J, Spearrin R, Goldenstein C, Hanson R. Compact optical probe for flame temperature and carbon dioxide using interband cascade laser absorption near 4.2 μm . Combust Flame 2016. In Press.
- [295] Sur R, Sun K, Jeffries JB, Socha JG, Hanson RK. Scanned-wavelength-modulation-spectroscopy sensor for CO, CO₂, CH₄ and H_2O in a high-pressure engineering-scale transport-reactor coal gasifier. Fuel 2015;150:102–11. doi: 10.1016/j.fuel.2015.02.003. <http://www.sciencedirect.com/science/article/pii/S001623611500143X>.
- [296] Ebert V, Fitzer J, Gerstenberg I, Pleban K-U, Pitz H, Wolfrum J, et al. Simultaneous laser-based *in-situ* detection of oxygen and water in a waste incinerator for active combustion control purposes. Proc Combust Inst 1998;27:1301–8.
- [297] Ebert V, Fernholz T, Giesemann C, Pitz H, Teichert H, Wolfrum J, et al. Simultaneous diode-laser-based *in situ* detection of multiple species and temperature in a gas-fired power plant. Proc Combust Inst 2000;28(1):423–9. doi: 10.1016/S0082-0784(00)80239-8.
- [298] Teichert H, Fernholz T, Ebert V. Simultaneous *in situ* measurement of CO, H_2O , and gas temperatures in a full-sized coal-fired power plant by near-infrared diode lasers. Appl Opt 2003;42(12):2043–51. doi: 10.1364/AO.42.002043. <http://www.ncbi.nlm.nih.gov/pubmed/12716144>.
- [299] Ebert V, Teichert H, Strauch P, Kolb T, Seifert H, Wolfrum J. Sensitive *in situ* detection of CO and O₂ in a rotary kiln-based hazardous waste incinerator using 760 nm and new 2.3 μm diode lasers. Proc Combust Inst 2005;30(1):1611–8. doi: 10.1016/j.proci.2004.08.224. <http://linkinghub.elsevier.com/retrieve/pii/S0082078404002930>.
- [300] Ortwein P, Woiwode W, Fleck S, Eberhard M, Kolb T, Wagner S, et al. Absolute diode laser-based *in situ* detection of HCl in gasification processes. Exp Fluids 2010;49(4):961–8. doi: 10.1007/s00348-010-0904-2.
- [301] Sappey AD. Wavelength-multiplexed diode laser spectroscopy for closed loop combustion control and optimization. In: Proceedings of the American-Japanese flame research committees international symposium. Waialoa; 2007.
- [302] Chao X, Jeffries JB, Hanson RK. *In situ* absorption sensor for NO in combustion gases with a 5.2 μm quantum-cascade laser. Proc Combust Inst 2011;33(1):725–33. doi: 10.1016/j.proci.2010.05.014. <http://linkinghub.elsevier.com/retrieve/pii/S1540748910000441>.
- [303] Chao X, Jeffries JB, Hanson RK. Real-time, *in situ*, continuous monitoring of CO in a pulverized-coal-fired power plant with a 2.3 μm laser absorption sensor. Appl Phys B 2013;110(3):359–65. doi: 10.1007/s00340-012-5262-8.
- [304] Jenkins TP, Bergmans J. Diode laser temperature measurements. In: Charles E. Baukal J, editor. Industrial combustion testing; chap. 14. CRC Press Technology and engineering; 2010. p. 311–36.
- [305] Sun K, Sur R, Chao X, Jeffries JB, Hanson RK, Pummill RJ, et al. TDL Absorption sensors for gas temperature and concentrations in a high-pressure entrained-flow coal gasifier. Proc Combust Inst 2013;34(2):3593–601. doi: 10.1016/j.proci.2012.05.018. <http://linkinghub.elsevier.com/retrieve/pii/S1540748912000193>.
- [306] Liu X, Jeffries JB, Hanson RK, Hinckley KM, Woodmansee MA. Development of a tunable diode laser sensor for measurements of gas turbine exhaust temperature. Appl Phys B 2006;82(3):469–78. doi: 10.1007/s00340-005-2078-9.
- [307] Meyer TR, Roy S, Anderson TN, Lucht RP, Barron-Jimenez R, Gord JR. 10 Khz detection of CO₂ at 4.5 μm by using tunable diode-laser-based difference-frequency generation. Opt Lett 2005;30(22):3087–9. doi: 10.1364/OL.30.003087. <http://www.opticsinfobase.org/abstract.cfm?URI=OL-30-22-3087>.
- [308] Zhou X, Jeffries JB, Hanson RK, Li G, Gutmark E. Wavelength-scanned tunable diode laser temperature measurements in a model gas turbine combustor. AIAA J 2007;45(2):420–5. doi: 10.2514/1.26624.
- [309] Li H, Zhou X, Jeffries JB, Hanson RK. Active control of lean blowout in a swirl-stabilized combustor using a tunable diode laser. Proc Combust Inst 2007;31:3215–23. doi: 10.1016/j.proci.2006.07.006.
- [310] Li H, Zhou X, Jeffries JB, Hanson RK. Sensing and control of combustion instabilities in swirl-Stabilized combustors using diode-Laser absorption. AIAA Journal 2007;45(2):390–8. doi: 10.2514/1.24774.

- [311] Li H, Wehe SD, McManus KR. Real-time equivalence ratio measurements in gas turbine combustors with a near-infrared diode laser sensor. *Proc Combust Inst* 2011;33(1):717–24. doi: [10.1016/j.proci.2010.05.114](https://doi.org/10.1016/j.proci.2010.05.114). <http://linkinghub.elsevier.com/retrieve/pii/S1540748910002889>.
- [312] Caswell AW, Kraetschmer T, Rein K, Sanders ST, Roy S, Shouse DT, et al. Application of time-division-multiplexed lasers for measurements of gas temperature and CH₄ and H₂O concentrations at 30 kHz in a high-pressure combustor. *Appl Opt* 2010;49(26):4963–72. <http://www.ncbi.nlm.nih.gov/pubmed/20830185>.
- [313] Wright P, Terzija N, Davidson JL, Garcia-Castillo S, Garcia-Stewart C, Pegrum S, et al. High-speed chemical species tomography in a multi-cylinder automotive engine. *Chem Eng J* 2010;158(1):2–10. doi: [10.1016/j.cej.2008.10.026](https://doi.org/10.1016/j.cej.2008.10.026).
- [314] Terzija N, Karagiannopoulos S, Begg S, Wright P, Ozanyan K, McCann H. Tomographic imaging of the liquid and vapour fuel distributions in a single-cylinder direct-injection gasoline engine. *Int J Engine Res* 2015;16(4):565–79. doi: [10.1177/1468087414544178](https://doi.org/10.1177/1468087414544178). <http://jер.sagepub.com/lookup/doi/10.1177/1468087414544178>.
- [315] Witzel O, Klein A, Wagner S, Meffert C, Schulz C, Ebert V. High-speed tunable diode laser absorption spectroscopy for sampling-free in-cylinder water vapor concentration measurements in an optical IC engine. *Appl Phys B* 2012;109(3):521–32. doi: [10.1007/s00340-012-5225-0](https://doi.org/10.1007/s00340-012-5225-0). <http://link.springer.com/10.1007/s00340-012-5225-0>.
- [316] Jatana GS, Naik SV, Shaver GM, Lucht RP. High-speed diode laser measurements of temperature and water vapor concentration in the intake manifold of a diesel engine. *Int J Engine Res* 2014;15(7):773–88. doi: [10.1177/1468087413517107](https://doi.org/10.1177/1468087413517107). <http://jер.sagepub.com/content/early/2014/01/29/1468087413517107.abstract>.
- [317] Griffiths AD, Houwing APP. Diode laser absorption spectroscopy of water vapor in a scramjet combustor. *Appl Opt* 2005;44(31):6653–9. <http://www.ncbi.nlm.nih.gov/pubmed/16270554>.
- [318] Rieker GB, Liu JTC, Jeffries JB, Hanson RK, Mathur T, Gruber MR, et al. Diode laser sensor for gas temperature and H₂O concentration in a scramjet combustor using wavelength modulation spectroscopy. In: Proceedings of 41st AIAA/ASME/SAE/ASEE joint propulsion conference & exhibit; 2005AIAA2005–3710.
- [319] Li F, Yu X, Gu H, Li Z, Zhao Y, Ma L, et al. Simultaneous measurements of multiple flow parameters for scramjet characterization using tunable diode-laser sensors. *Appl Opt* 2011;50(36):6697–707. doi: [10.1364/AO.50.006697](https://doi.org/10.1364/AO.50.006697). <http://www.osapublishing.org/viewmedia.cfm?uri=ao-50-36-6697&seq=0&html=true>.
- [320] Schultz IA, Goldenstein CS, Spearin RM, Jeffries JB, Hanson RK, Rockwell RD, et al. Multispecies midinfrared absorption measurements in a hydrocarbon-fueled scramjet combustor. *J Propul Power* 2014;30(6):1595–604. doi: [10.2514/1.B35261](https://doi.org/10.2514/1.B35261).
- [321] Meyers JM, Fletcher D. Diode laser absorption sensor design and qualification for CO₂ hypersonic flows. *J Thermophys Heat Transfer* 2011;25(2):193–200. doi: [10.2514/1.49270](https://doi.org/10.2514/1.49270).
- [322] Schultz IA, Goldenstein CS, Jeffries JB, Hanson RK, Rockwell RD, Goyne CP. Spatially resolved water measurements in a scramjet combustor using diode laser absorption. *J Propul Power* 2014;30(6):1551–8. doi: [10.2514/1.B35219](https://doi.org/10.2514/1.B35219).
- [323] Schultz IA, Goldenstein CS, Jeffries JB, Hanson RK, Rockwell RD, Goyne CP. Diode laser absorption sensor for combustion progress in a model scramjet. *J Propul Power* 2014;30(3):550–7. doi: [10.2514/1.B34905](https://doi.org/10.2514/1.B34905).
- [324] Jackson KR, Gruber MR, Buccellato S. Mach 68+ hydrocarbon-fueled scramjet flight experiment: the HiFire flight 2 project. *J Propul Power* 2015;31(1):36–53. doi: [10.2514/1.B35350](https://doi.org/10.2514/1.B35350). <http://www.scopus.com/inward/record.url?eid=2-s2.0-84930462281&partnerID=tOtx3y1>.
- [325] Strand CL, Hanson RK. Thermometry and velocimetry in supersonic flows via scanned wavelength-modulation absorption spectroscopy. In: Proceedings of 47th AIAA/ASME/SAE/ASEE joint propulsion conference & exhibit. San Diego; 2011. p. AIAA2011–5600.
- [326] Schwer DA, Kailasanath K. Modeling exhaust effects in rotating detonation engines. In: Proceedings of the 48th AIAA/ASME/SAE/ASEE joint propulsion conference and exhibit; 2012AIAA2012–3943.
- [327] Mattison DW, Brophy CM, Sanders ST, Ma L, Hinckley KM, Jeffries JB, et al. Pulse detonation engine characterization and control using tunable diode-laser sensors. *J Propul Power* 2003;19(4):568–72.
- [328] Caswell AW, Roy S, An X, Sanders ST. High-bandwidth H₂O absorption sensor for measuring pressure, enthalpy, and mass flux in a pulsed-detonation combustor. In: Proceedings of the 50th AIAA aerospace sciences meeting including the new horizons forum and aerospace exposition; 2012AIAA2012–0471.
- [329] Goldenstein CS, Schultz IA, Spearin RM, Jeffries JB, Hanson RK. Diode laser measurements of temperature and H₂O for monitoring pulse detonation combustor performance. In: Proceedings of the 24th international colloquium on the dynamics of explosions and reactive systems. Taipei; 2013. p. 1–6.
- [330] Spearin RM, Goldenstein CS, Jeffries JB, Hanson RK. Mid-infrared laser absorption diagnostics for detonation studies. In: Proceedings of the 29th international symposium on shock waves. Madison; 2013.
- [331] Cheng J, Pedersen MEV, Wang K, Xu C, Grüner-Nielsen L, Jakobsen D. Time-domain multimode dispersion measurement in a higher-order-mode fiber. *Opt Lett* 2012;37(3):347. doi: [10.1364/OL.37.000347](https://doi.org/10.1364/OL.37.000347). <https://www.osapublishing.org/abstract.cfm?URL=ol-37-3-347>.
- [332] McGahan CJ, Tom BA, Caswell AW, Gord JR, Schauer FR, Hoke JL. Exhaust gas analysis of a rotating detonation engine using tunable diode laser absorption spectroscopy. In: Proceedings of the 52nd aerospace sciences meeting AIAA Sci-Tech.; 2014AIAA2014–0391.
- [333] Rankin BA, Richardson DR, Caswell AW, Naples A. Imaging of OH* chemiluminescence in an optically accessible rotating detonation engine. In: Proceedings of 53rd AIAA aerospace sciences meeting; 2015AIAA. doi: [10.2514/6.2015-1604](https://doi.org/10.2514/6.2015-1604).